Effects of Surface Chemistry on Kinetics of Coagulation of Submicron Iron Oxide Particles (α–Fe_2O_3) in Water

Thesis by

Liyuan Liang

In Partial Fulfillment of the Requirements

for the Degree of

Doctor of Philosophy

California Institute of Technology

Pasadena, California

1988

Submitted May 20, 1988

Acknowledgements

I would like to express my appreciation for the help and fellowship I have received from my friends and colleagues during the course of my research. I am particularly grateful to Professor J. J. Morgan for his guidance, help and tolerance, and for introducing me to the world of surface chemistry. I would also like to thank Professor Norman Brooks for his encouragement, and the other members of my examination committee: Professors M. Hoffmann, R. Flagan, and G. Rossman.

Professor J. Westall of Oregon State University and Professor F. M. M. Morel of MIT provided helpful insights into the application of surface chemical models. Professors W. Stumm of EAWAG, P. Gschwend of MIT, and C. O'Melia of John Hopkins University also gave useful suggestions.

I would like to thank the following people. Simon Davies for helping me to start my laboratory work; Sue Larson for introducing me to the use of Mie theory; Bill Munger for assisting me in using the IC and TOC instruments; Scott Northrop and Ranajit Sahu for making the BET measurements. Elton Daly, Joe Fontana and Rich Eastvedt played an invaluable role in making effective instruments according to the vaguest specifications.

Rueen-Fang Wang helped me get familiar with the idiosyncrasies of the Keck computers, and made numerous helpful suggestions throughout my research. Her kindness and friendship provided vital support throughout the many vicissitudes of

my work.

The following people have aided my research, either by giving specific help, or by generally improving the quality of life in Keck Laboratory, and are much appreciated: Elaine Granger, Joan Matthews, Rayma Harison, Gunilla Hastrup, Bob Koh, Sandy Brooks, Chi Kin Ting, Imad Hannoun, Pratim Biswas, Dennis Lyn, Kit Yin Ng, David James, Terri Olson and Michael Scott.

I am grateful for the financial support provided by a fellowship from Jessie Smith Noyes, Inc., and for funding from the Mellon Foundation.

I would like to thank my parents whose spiritual support was always apparent in spite of the great distance separating us across the Pacific Ocean.

Finally, I would like to dedicate this thesis to my husband, David, who has supported me with love, patience, and good humor throughout my work.

Table of Contents

Abstract

Particles in the colloidal size range, i.e. smaller than 10^{-6} meter, are of interest in environmental science and many other fields of science and engineering. Since aqueous oxide particles have high specific surface areas they adsorb ions and molecules from water, and may remain stable in the aqueous phase with respect to coagulation. Submicron particles collide as a result of their thermal energy, and the effective collision rate is slowed by electric repulsion forces. A key to understanding particle stability and coagulation is the role of simple chemical changes in the water altering the electrostatic repulsion forces between particles.

Experiments using hematite particles ($\alpha-Fe_2O_3$, 70nm in diameter) reveal important features of coagulation dynamics. Three experimental techniques are employed: (1) Light scattering measurements to yield quantitative information on the rate of the initial coagulation process; (2) electrokinetic measurements to provide information about the sign and magnitude of the electrical charge on the aqueous oxide particles; (3) acid-base titration and equilibrium adsorption to obtain the intrinsic equilibrium constants for surface species.

The acid-base titration data indicate that the pH_{zpc} of the synthesized hematite colloid is 8.5. This is also supported by the electrophoretic mobility measurements. In the presence of non–specific adsorbing ions (such as Na^+ and Ca^{2+}, etc.), the coagulation of a hematite colloid is achieved mainly by the compression of diffuse layer and Schulze–Hardy Rule is exhibited for non-specific electrolytes. Specifically adsorbed counter ions (such as phosphate) are able to reduce the surface charge of

aqueous oxide particles, and the critical coagulation concentrations are dependent on the value of the pH, and are much less than those predicted by DLVO theory. In inorganic media, we found that the order of the effectiveness in causing hematite particles to coagulate is:

$$\text{phosphate} > \text{sulfate} > \text{chloride} \quad \text{at } pH < pH_{zpc}$$

and

$$\text{magnesium} > \text{calcium} > \text{sodium} \sim \text{potassium} \quad \text{at } pH > pH_{zpc}$$

The adsorption study reveals that phthalate ions specifically adsorb on hematite particles. The process is most likely due to carboxylic group bonding to the surface. The hematite coagulation rates in the presence of poly-aspartic acid (PAA) demonstrate that the polyelectrolyte is very effective in causing the colloid to coagulate. When the PAA concentration is increased beyond the critical coagulation concentration, the particles are stabilized; this is attributed to the reversal of surface potential as a result of the adsorption of PAA. Similar features are observed in the initial coagulation rates when naturally occurring organics (fulvic and humic acid from Suwannee River) are used.

The adsorption of lauric acid on hematite was investigated and the results interpreted in terms of the energy contributed by the specific chemical, electrostatic and hydrophobic interactions. The initial coagulation rates of hematite particles and the electrophoretic mobilities with respect to fatty acid concentration both show systematic variations as a function of the numbers of carbons in the acid. Hydrophobic interaction may account for these observations since the specific chemical energy appears to be the same for all the fatty acids studied, and the electrostatic contribution is also similar at the same extent of adsorption.

List of Plates

List of Tables

List of Figures

1. INTRODUCTION

1.0 Introduction

The primary purpose of this research is to gain a better understanding of the chemical interactions between aqueous species and suspended particles in water, and of the influence of surface chemistry on particle coagulation kinetics. A hematite particle suspension has been chosen as a model system for this purpose. Experimental results are interpreted in terms of surface chemical models and colloid stability models to gain an understanding of the relationship of adsorption, particle electrokinetic behavior, and coagulation rates of particles.

1.1 The Influence of Surface Chemistry on Colloid Stability

Naturally occurring particles include metal oxides/hydroxides, metal carbonates, clays, bacteria and algae (Stumm and Morgan, 1981). These particles have a broad size distribution (Fig. 1.1). The colloidal particles in the lower part of the size spectrum, from 1 nm to 10 μm, possess appreciable specific surface areas. Due to the high surface energy of these particles, and the strong chemical affinities between surface sites and various aqueous species, many physical chemical processes readily take place at the aqueous/solid interface. For example, Schindler et al. (1976) showed that metal ions, such as those of Pb(II), Cu(II) and Cd(II), specifically adsorb at the silica/water interface through surface complex formation. Sigg and Stumm (1981) studied the adsorption of anions on the surface of goethite particles, and concluded

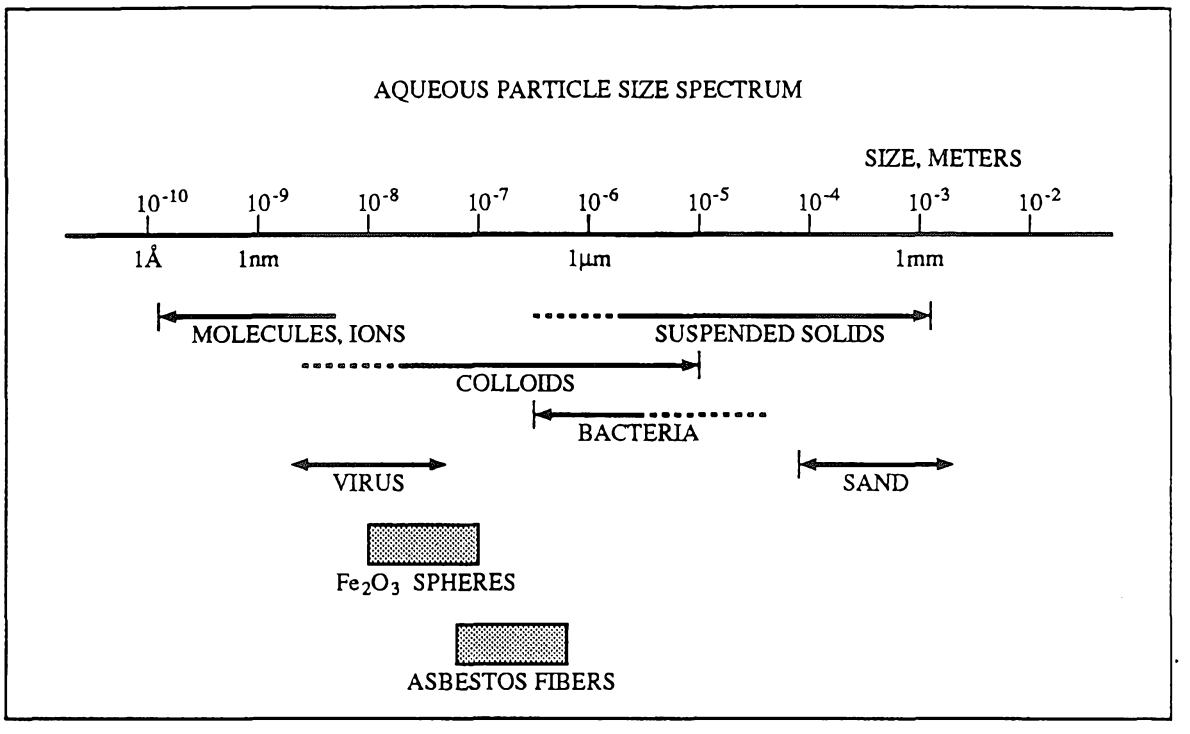

Figure 1.1: Size spectrum for aqueous particles.

that the stability of surface complexes follows the same trend as that of the corresponding complex formation reactions in the aqueous phase.

The adsorption of aqueous species by suspended particles changes the surface properties of the particles. The presence of negatively charged iron oxide particles in lake and river environments has been attributed to the adsorption of dissolved organic matter (Tipping, 1981). Using adsorption equilibrium models Sigg (1985) estimated that phosphate and silicate in a lake environment determine the negative surface charge of α-FeOOH at the pH of the natural water. Consequently, colloid stability, which depends on surface properties and solution chemistry, is directly affected by the adsorption process. Stumm and Morgan (1962) were among the first to emphasize the importance of specific chemical aspects of coagulation. Hahn and Stumm (1968) studied the coagulation kinetics of silica particles in the presence of hydrolyzed Al(III), and concluded that the specific adsorption of aluminum cations was primarily responsible for destabilizing silica particles by lowering the negative surface potential.

Gaudin and Fuerstenau (1955), Somasundaran et al. (1964), and Fuerstenau (1981) investigated the flotation of several minerals in the presence of surfactants, and concluded that the reversal of particle zeta potentials was the consequence of adsorption of surfactants on the surface of particles. In one of the studies (1964), they observed that the surfactant concentration necessary to reduce the particle zeta potential to zero increased as the hydrocarbon chain length decreased.

1.2 Coagulation in Natural Water Environments

An understanding of the chemical aspects of coagulation can have wide application in natural water environments. Suspended particles exist in lake and river water as a result of weathering and biological processes. The adsorption of dissolved organic material on metal oxides changes the particle surface characteristics (Tipping, 1981), and the aggregation process is affected by the chemical interaction of bivalent ions with surface-adsorbed humics (Tipping and Ohnstad, 1984). Ali et al. (1984) showed that dissolved organic matter increases the stability of lake particles while magnesium and calcium decrease the stability. In estuarine waters the river-borne particles experience increased salt concentration as they move toward the sea. This can cause particle destabilization by means of electrostatic interaction. In addition to this, however, particle stability also depends on the surface chemical properties of the particles, and the solution phase chemistry in the mixing zone, which is largely determined by the chemical content of the inflowing river. Sholkovitz (1976) observed that "dissolved" iron in rivers can be stabilized by dissolved organic matter. These iron containing organic colloids are destabilized in estuaries by sea water cations through both general electrostatic forces ("double layer compression") and specific chemical reactions with the humic material. Further evidence of the importance of adsorption on coagulation kinetics comes from Gibbs (1983) who studied the coagulation of river-borne particles and the same type of particles with the organic coating removed. Gibbs observed that the naturally coated particles coagulate significantly

more slowly than the uncoated ones. Knowledge of particle-particle interactions is helpful in assessing the geochemical cycle of metals, such as iron and manganese, and the material transport in lakes, rivers, estuaries, and the oceans.

1.3 Coaglation in Water and Wastewater Treatment

Suspended particles in water and waste water not only result in a non-aesthetic appearance (turbidity, color), but also carry potentially harmful components, such as toxic trace metals and organics. Thus the removal of suspended particles is necessary in water and wastewater. An understanding of the role of chemistry in particle-particle interactions may serve in the better selection of the type and concentration of the chemicals to cause effective coagulation and removal of suspended solids. The use of ocean outfalls has become a common practice in the discharge of wastewater effluent around the world. A knowledge of the interaction of the discharged particles with the ambient sea water will help in understanding the coagulation behavior of discharged particles.

1.4 Motivation to Study Hematite

Iron ranks second in abundance among the metals (aluminum is first), and fourth among all elements in the Earth's crust (4.7%). Iron is chemically combined in oxides, carbonates, silicates and sulfides. It is believed that in nature, dissolution of minerals which contain Fe(II) followed by oxidation results in the formation of Fe(III), which is subsequently precipitated as oxide or hydroxide due to its extremely low solubility in the pH conditions of the natural environment (Schwertmann and Taylor, 1977). Hematite is one of the iron minerals found in nature. Iron is used as a coagulant in water treatment processes, in which colloidal iron oxides are produced. In oxic conditions iron exists as ferric iron oxides/hydroxides in lake, river and estuarine waters. In field studies of contaminated groundwater, ferrous phosphate colloids have been found (Gschwend and Reynolds, 1987). Gschwend speculated that these colloids, formed by sewage-derived phosphate combining with iron from soil, are able

to transform to ferric oxides at oxic interfaces.

Hematite can be synthesized under laboratory conditions by hydrolysis of ferric iron salts (Matijević and Scheiner, 1978). The use of hematite particles as a model system serves well in understanding some of the surface properties of iron oxides, adsorption behavior and coagulation consequences. Hematite particles have zero point of charge (pH_{zpc}) at 8.5 (Chap. 3). This allows the study of chemical interactions on positive as well as negative surfaces. Iron(III) has a strong affinity to many aqueous ions, and forms aqueous complexes. Studies have shown the adsorption of phosphate, sulfate, and some cations on iron oxide surfaces (Breeuwsma, 1973; and Sigg, 1979). Order of magnitude estimates deduced from these studies have been useful in designing the adsorption and coagulation experiments of this thesis.

1.5 Scope and Objectives

Early theoretical and experimental studies of systems in which particles interact only through Van der Waals' attraction and electrostatic repulsion led to the development of Derjaguin-Landau-Verwey-Overbeek theory (DLVO theory). This theory has been successful in providing a quantitative understanding of the relationship between critical coagulation concentration and the valence of simple electrolytes. It is expected that multivalent ions will prove more effective in causing coagulation than monovalent ions, and that polymeric species will prove more effective than monomeric species. It is also expected that the specifically adsorbed species will be more effective than non-specifically adsorbed species in causing particles to coagulate.

However, DLVO theory and experiments do not agree satisfactorily for slow coagulation (O'Melia, 1987). Surface chemistry influences the surface charge on particles and hence has an important effect on particle coagulation. An understanding of the relationship between surface chemistry and particle coagulation is therefore necessary. To gain a quantitative or semiquantitative understanding it is essential to combine adsorption and coagulation experiments with surface chemistry and coagulation models.

The objectives of this research are:

(1) To describe hematite surface protonation/deprotonation equilibrium properties, subsequently to model the surface charges as a function of pH, and to compare these results with electrokinetic measurements and hematite particle coagulation kinetics data.

(2) To determine the effect of various inorganic ions on hematite particle coagulation rates. The type of electrolytes to be studied include (i) chloride salts of sodium, magnesium, and calcium ions at pH greater than pH_{zpc}; (ii) sodium salts of chloride, sulfate, and phosphate at pH less than pH_{zpc}.

(3) To determine the influence of organic species on particle stability and understand the effects of hydrophobicity, configuration and size of the molecules on particle stability. The species to be studied include (i) fatty acids with different numbers of carbons in the hydrophobic chains; (ii) small molecules such as phthalic and oxalic acid; (iii) polymeric organic molecules such as polyaspartic acid; (iv) naturally occurring molecules, for example fulvic acid and humic acid.

(4) To perform adsorption measurements for selected systems and relate the extent of adsorption and surface charge to coagulation kinetics.

(5) To study the electrokinetic properties of hematite in the presence of both simple electrolytes and specifically adsorbed species, and to relate these properties to adsorption and coagulation.

(6) To interpret the experimental results in terms of surface chemical and colloid stability models.

2. BACKGROUND AND MODELS

2.0 Introduction

In a colloidal suspension particles constantly collide, and as a result of some of these collisions, subsequently attach to each other. Thermodynamically an aqueous oxide colloidal suspension is unstable because of the decrease of Gibbs free energy when particles aggregate into larger clusters and thereby reduce their surface energy. The term "stability" is used to characterize the degree to which the dispersed state can persist throughout the suspension. That is, it relates to the rate of change in particle size distribution by coagulation. Thus, by coagulation kinetics studies the stability of a colloid can be determined.

The coagulation of suspended particles can be described as two consecutive processes: collision and attachment. An understanding of the stability of a colloid toward coagulation requires an integration of chemical, physical-chemical, and physical factors (O'Melia, 1987). The chemical interactions between particle surface and aqueous species account for the origin of surface charges and the change of surface species distribution in the presence of specifically adsorbed metal ions, anions and polymeric species. Physical-chemical factors are important in determining the particle charge-potential relationship and the extent of the electric diffuse layer, and hence are important in models of the structure of solid/aqueous interface. Physical factors, such as diffusion, temperature, fluid mixing, particle size and shape, and Van der

Waals forces have direct influences on particle collision and attachment. In order to understand the chemical aspects of coagulation, it is important to choose colloidal systems in which the physical factors are well understood and readily controlled.

2.1 Smoluchowski's Equations for Brownian Coagulation

In an aqueous suspension, particles experience constant collisions. For particles smaller than 1μm, Brownian motion is the dominant cause of collisions (Hunt, 1980). Consider coagulation controlled by Brownian diffusion. The kinetic energy, which is proportional to kT (the product of Boltzmann's constant and the absolute temperature), is transferred to suspended particles by water molecules undergoing thermal motion. Let N_{ij} be the number of collisions occurring per unit time per unit volume between two types of particles of volume v_i and v_j, then,

$$N_{ij} = \beta(v_i, v_j) n_i n_j \tag{2.1}$$

where $\beta(v_i, v_j)$ is defined as the collision frequency function, which depends on particle size, temperature and pressure, and n_i is the number concentration of particles with volume v_i.

The rate of formation of particles of volume v_k by collisions between particles of volume v_i and v_j is given by $\frac{1}{2}\sum_{i+j=k} N_{ij}$. The notation $i + j = k$ indicates that the summation is taken over all collisions for which $v_i + v_j = v_k$.

The rate of loss of particles of volume v_k by collisions with all other particles is $\sum_{i=1}^{\infty} N_{ik}$. The equation which describes the rate of change in the number density of particles of volume v_k as a result of Brownian motion is:

$$\frac{dn_k}{dt} = \frac{1}{2}\sum_{i+j=k} N_{ij} - \sum_{i=1}^{\infty} N_{ik} \tag{2.2}$$

or,

$$\frac{dn_k}{dt} = \frac{1}{2}\sum_{i+j=k} \beta(v_i, v_j) n_i n_j - n_k \sum_{i=1}^{\infty} \beta(v_i, v_k) n_i \tag{2.3}$$

The collision frequency function can be obtained by solving the steady state particle diffusion equation. The result is,

$$\beta(v_i, v_j) = 4\pi(D_i + D_j)(a_i + a_j) \tag{2.4}$$

where D denotes the diffusion coefficient and a the particles' radius. The solution of Eq. (2.3) for an initially monodisperse system was obtained by Smoluchowski (1917). Applying the Einstein-Stokes relation,

$$D_i = \frac{\mathrm{kT}}{6\pi\mu a_i} \tag{2.5}$$

to a monodisperse system ($v_i = v_j$), the collision frequency function is reduced to

$$\beta(v_i = v_j) = \frac{8\mathrm{kT}}{3\mu} \tag{2.6}$$

where μ is the viscosity. Substituting equation (2.6) into (2.3), the rate of change in the number density of particles of volume v_k for an initially monodisperse system is given by,

$$\frac{dn_k}{dt} = \frac{1}{2}\beta \sum_{i+j=k} n_i n_j - \beta n_k \sum_{i=1}^{\infty} n_i \tag{2.7}$$

Letting $N_\infty = \sum_{i=1}^{\infty} n_i$ be the total number of particles per unit volume of fluid, Smoluchowski showed that equation (2.7) is equivalent to

$$\frac{dN_\infty}{dt} = -\frac{1}{2}\beta N_\infty^2 \tag{2.8}$$

Writing $k_b = \beta/2 = 4\mathrm{kT}/3\mu$, where the subscript b here indicates that the process is Brownian diffusion, equation (2.8) can be rewritten as

$$\frac{dN_\infty}{dt} = -k_b N_\infty^2 \tag{2.9}$$

The solution to (2.9) is

$$N_\infty = \frac{N_\infty(0)}{1 + k_b N_\infty(0) t} \tag{2.10}$$

or

$$N_\infty = \frac{N_\infty(0)}{1 + t/\tau_b} \tag{2.11}$$

where $\tau_b = 1/k_b N_\infty(0)$. The physical significance of τ_b is that it represents the time at which the initial total number of particles is reduced by a half, and is therefore a time scale for coagulation.

The concentration of singlets during coagulation can be evaluated by solving,

$$\frac{dn_1}{dt} = -2k_b n_1 N_\infty \tag{2.12}$$

to give,

$$n_1 = \frac{N_\infty(0)}{(1 + t/\tau_b)^2} \tag{2.13}$$

Similarly, the solution for the concentration of doublets during coagulation can be shown to be

$$n_2 = \frac{N_\infty(0)(t/\tau_b)}{(1 + t/\tau_b)^3} \tag{2.14}$$

In general, the concentration of k^{th} aggregates is represented by

$$n_k = \frac{N_\infty(0)(t/\tau_b)^{k-1}}{(1 + t/\tau_b)^{k+1}} \tag{2.15}$$

Figure (2.1) shows the change of the total number concentration with normalized time, (t/τ_b), and the number concentration of singlets, doublets, triplets and so on. It is clear from Figure (2.1) that singlets and doublets are dominant in the initial coagulation stage. This is an important result, which provides justification for the light scattering calculations presented in Chapter 3.

2.2 Fuchs' Treatment

In the previous section, the discussion is focused on coagulation controlled by Brownian diffusion. In reality, particles in a suspension may be subjected to other forces in addition to the forces exerted by fluid molecules in Brownian motion. Van der Waals forces, for example, are always operative between particles. Charged particles experience electrostatic interactions upon approaching each other. The presence of a force field can ultimately affect the rate of particle coagulation. The quantitative influence of a force field on particle coagulation was dealt with by Fuchs (1934). He

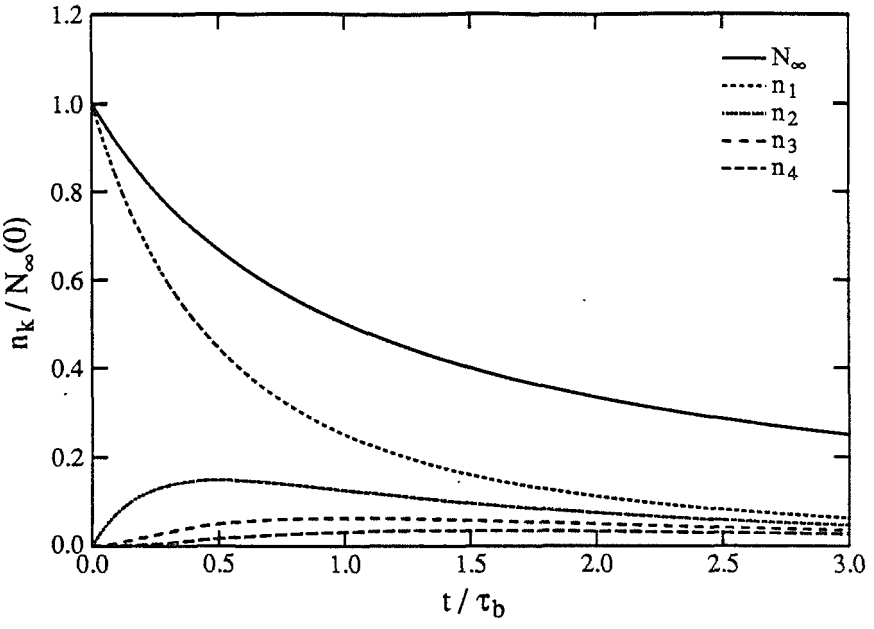

Figure 2.1: The variation of the total number concentration, N_∞, with normalized time, t/τ_b, for an initially mono-dispersed system undergoing coagulation. The dashed curves show the relative number concentrations of singlets, doublets, triplets, and so on.

treated the problem as diffusion in a force field, and showed that if $V(R)$ is the interaction energy due to the force between the centers of two particles separated by a distance R, then the particle coagulation rate is reduced by a factor, W, given by:

$$W = 2a \int_{2a}^{\infty} \frac{1}{R^2} \exp\left(V(R)/\mathrm{kT}\right) dR \tag{2.16}$$

In experimental terms, W represents the ratio of the diffusion-controlled coagulation rate to the actual coagulation rate in the presence of the force field. An expression similar to Eq. (2.9) can be used to give the observed coagulation rate,

$$\frac{dN_\infty}{dt} = -k_a N_\infty^2 \tag{2.17}$$

Hence, $W = k_b/k_a$. W is defined as the *stability ratio*, which describes how stable a colloidal suspension is with respect to diffusion-controlled coagulation.

2.3 DLVO Theory of Colloid Stability

To explain the stability of a hydrophobic colloidal suspension, Derjaguin and Landau and Verwey and Overbeek independently developed a quantitative theory (DLVO theory) to calculate the stability. In the formulation of the theory, Van der Waals attraction and electrostatic repulsion are taken into consideration. A detailed description of the interaction between charged particles in electrolytic media is given by Verwey and Overbeek (1948).

2.3.1 The Electrical Double Layer

Colloidal particles, such as hematite, acquire electrical charges on their surfaces when they are in contact with water. Since the colloidal suspension as a whole is electrically neutral, the aqueous medium surrounding the particles must develop an equivalent charge of opposite sign. The electrical double layer is formed as a result of an unequal distribution of ions at the interfaces; there is a layer of fixed charges on the solid surfaces and a diffuse layer with an excess of oppositely charged ions distributed in the aqueous phase.

The charge distribution, and the corresponding electric potential function, in the diffuse layer is given by the Gouy-Chapman theory, which is derived by solving Poisson's equation for a charged interface, assuming the diffuse layer of ionic charge is described by a Boltzmann distribution. The fundamental differential equation for a single double layer is:

$$\nabla^2\Psi = \kappa^2 \frac{\sinh(zF\Psi/\mathrm{RT})}{(zF/\mathrm{RT})} \tag{2.18}$$

Where κ^{-1} is the Debye-Hückel length, and defines the diffuse layer thickness. It is given by:

$$\kappa = \left(\frac{F^2 \sum n_i z_i^2}{\epsilon\epsilon_0 \mathrm{RT}} \right)^{\frac{1}{2}} \tag{2.19}$$

where n_i is concentration of ion i in moles/cm^3, z_i is the valence of ions of the i^{th} component, F is the Faraday constant, ϵ is the relative permittivity, ϵ_0 is the

permittivity in vacuum.

Other assumptions involved in equation (2.18) are that the surface charges are homogeneous and that the ions in solution can be represented as point charges of negligible dimensions. The solution to (2.18) is discussed in detail by Verwey and Overbeek (1948).

2.3.2 Electrostatic Repulsion Energy

Electrostatic repulsion arises when two particles of the same charge approach each other and their diffuse layers of ions overlap. In calculating the interaction energy between spherical particles, there is no general analytical solution. For particle radii much larger than the Debye-Hückel length ($\kappa a \gg 2.5$), and small surface potential ($\Psi < 25mV$), the interaction energy can be calculated from the corresponding flat plate interactions. Imagining that the interaction energy of two particles was contributed by infinitesimal parallel rings on the surface of the particles, Verwey and Overbeek obtained an approximate analytical expression by integrating the contributions over the entire surface to obtain,

$$V_R = 2\pi\epsilon\epsilon_0 a\Psi_0^2 \ln(1 + e^{-\kappa H}) \tag{2.20}$$

where $H = R - 2a$, and R is the distance between the centers of the particles. Equation (2.20) is applicable for small separations, i.e., $H < 2a$. Improvements to this equation were made by McCartney and Levine (1969). They expressed the potential in terms of a distribution of electric dipoles on the surface of the particles, and developed an integral equation, from which a better approximation was derived,

$$V_R = 4\pi\epsilon\epsilon_0 a\Psi_0^2 \frac{(R-a)}{R} \ln\left(1 + \frac{a}{R-a} e^{-\kappa(R-2a)}\right) \tag{2.21}$$

This equation is applicable over all separations, provided that the surface potential is low, and $\kappa a > 5$ is satisfied. The error compared with the numerical solution is less than 3%.

For somewhat larger potential values, an extension of the last formula was given by Bell et al. (1970),

$$V_R = 4\pi\epsilon\epsilon_0 a \left(\frac{\mathrm{RT}}{F}\right)^2 Y^2 \left(\frac{R-a}{R}\right) \ln\left\{1 + \frac{a}{R-a}\exp\left[-\kappa(R-2a)\right]\right\} \tag{2.22}$$

where Y is defined as follows,

$$Y = 4\tanh\left(\frac{zF\Psi_0}{4\mathrm{RT}}\right) \tag{2.23}$$

The formula is quite accurate for $\Psi = 100mV$ and $\kappa a = 10$ compared with the numerical solution, as long as $\kappa(R-2a) > 1$.

For small particles, or larger κ^{-1} (corresponding to the freshwater environment), $\kappa a \sim 1$. A solution in this case is available only for small potential ($\Psi < 25mV$),

$$V_R = \frac{4\pi\epsilon\epsilon_0\Psi_0^2 a \exp(-\kappa H)}{2 + H/a} \tag{2.24}$$

2.3.3 London-Van der Waals Attraction Energy

In addition to the repulsive energy arising from electrostatic interaction, there is also a short range attraction energy acting between particles due to London-Van der Waals forces. These forces are produced as a result of the polarization of one atom by the fluctuation of charge distribution in a second atom, and vice versa. In calculating the total attraction energy, it is assumed that the forces acting on each atom are independent of the presence of other atoms and hence that the forces are purely additive. The attractive energy between spherical particles is given by the equation,

$$V_A = -\frac{A}{6}\left[\frac{2}{s^2-4} + \frac{2}{s^2} + \ln\left(\frac{s^2-4}{s^2}\right)\right] \tag{2.25}$$

where $s = R/a$ and A is the Hamaker constant of the particle (Hamaker, 1937), which can be evaluated theoretically from particle atomic properties. Hamaker showed that the value of A can range from 3.0×10^{-12} erg to 0.7×10^{-14} erg. Experimentally, the Hamaker constant can be estimated from coagulation kinetics (Watillon and Joseph-Petit, 1966), or surface tension measurements (Fowkes, 1965).

With expressions for V_R and V_A, the total interaction energy V_T is attainable ($V_T = V_R + V_A$), and the stability of a colloid in the presence of electrostatic and Van der Waals forces can be calculated.

2.3.4 Applications of DLVO Theory

DLVO theory has played an important role in modern colloid science. It has been successful in explaining the empirical Schulze-Hardy Rule, which states that the electrolyte concentration at which a hydrophobic colloid can be completely destablized depends strongly on the valency of the electrolyte. In a "static" treatment of colloidal stability vs. instability, the critical coagulation concentration (c.c.c.) corresponds to a zero interaction energy and force, i.e., $V_T = 0$, $dV_T/dR = 0$. Under these conditions, the electrolyte concentration is given by (for plates, or large particles, where $\kappa a > 5$ at 25°C in water),

$$c.c.c. = \frac{8.0 \times 10^{-36}}{A^2 z^6} \gamma^4 \tag{2.26}$$

where $\gamma = \tanh(zF\Psi_0/4\mathrm{RT})$. If $\gamma = 1$,

$$c.c.c. \propto \frac{1}{z^6} \tag{2.27}$$

Hence, from the theory the critical coagulation concentration for monovalent, bivalent and trivalent electrolytes are predicted to be directly related by

$$c(1) : c(2) : c(3) = \frac{1}{1^6} : \frac{1}{2^6} : \frac{1}{3^6} \tag{2.28}$$

For example, if the concentration of monovalent ions needed to coagulate a colloid is 150mM, the concentration required for bivalent ions will be about 2mM, whereas only 0.2mM trivalent ions will be sufficient to achieve destabilization.

DLVO theory not only yields a qualitative description of two states of a colloid (stable vs. unstable) in an ionic medium, it also helps to explain the kinetic behavior of coagulation of colloids. Following Fuchs' approach, Verwey and Overbeek showed that the stability ratio of a colloid can be predicted in a quantitative way. Replacing

$V(R)$ with V_T in Eq. (2.16), and substituting an appropriate expression for V_T, the stability ratio, W, is obtained by integration of Eq. (2.16).

Efforts have been made to compare DLVO theory with the results of coagulation kinetic experiments. There is a detailed review by Napper and Hunter (1972). Assuming DLVO theory to be generally valid, early researchers have tried to find agreement between the theoretically calculated Hamaker constant for several colloids and those derived from kinetic experiments. In the case of AgI suspensions, the experimentally and theoretically determined values of A agree to within a factor of 3. In other cases, such as polystyrene latex suspensions, the agreement between theory and experiment, and between the experimental results of different investigators, is not so good. The experimental values obtained by various workers are widely spread over a range of $0.1\text{–}22\times10^{-20}$ Joules.

It appears that when the particle interaction energy is favorable for *rapid* coagulation, the experimental results follow theoretical predictions. In contrast, when theory predicts *slow* coagulation because of unfavorable interaction energies, the stability ratios derived from kinetic measurements are orders of magnitude smaller than theoretical values. These are the conclusions from experimental studies such as the deposition of polystyrene latex particles onto a disc by Hull and Kitchener (1969) and packed bed filtration experiments by Gregory and Wishart (1980). Furthermore, kinetic experiments have not confirmed the increase in the stability ratio with particle size predicted by DLVO theory (Penners and Koopal, 1987; and Ottewill and Shaw, 1966). The discrepancy is largely due to certain limitations in the theory and unrealistic assumptions. In the first place, the assumption that ions act as point charges is not valid at high ionic strength. To overcome this difficulty, the Stern correction can be applied.

The Stern model takes both finite ion size and the possibility of specific adsorption into consideration. The result is that the potential in the aqueous phase adjacent to a

particle surface can be viewed as being composed of two parts. Next to the interface there is a region in which the potential varies linearly from Ψ_0 at the surface to Ψ_δ in the solution phase, where δ is the Stern thickness. The second region of the potential profile is similar to that of the Gouy-Chapman diffuse layer with the initial value at Ψ_δ. Other variables associated with this model are the inner layer dielectric constant ϵ_1, the total number of adsorption surface sites, N, and the specific adsorption energy Φ. Difficulties in using the Stern model lie in uncertainties in model parameters. The value of δ has been estimated to lie between 3 and 10Å, depending on the size of the adsorbing ions (e.g. 5.4 Å for potassium ions, estimated by Lyklema, 1978). The local dielectric constant, ϵ_1, is assumed to be less than the bulk value, and the inner layer capacitance, $\epsilon_1\epsilon_0/\delta$, has been estimated from electrocapillarity measurements and related studies for mercury surfaces (Adamson, 1982). The value of N is related to the surface area occupied by adsorbing ions, and the range of surface area for different kinds of ions is from 10 to 100Å^2 per ion. The adsorption energy is obtained from the chemical interaction of adsorbed ions with surfaces, e.g., from surface chemistry experiments or from correlations with analogous reactions in solution.

With the Stern layer correction, the surface potential can be replaced by the Stern potential when calculating the total interaction energy. This is justified because the Stern layer thickness is comparable with atomic dimensions, and within the Stern layer, the total interaction energy is dominated by the Van der Waals attraction energy. In calculating the stability ratio, integration of $\exp(V_T/RT)$ in the Stern layer yields a negligible contribution. The diffuse layer interaction between particles contributes primarily to the total repulsion. Applying the Stern correction to Eq. (2.22),

$$V_R = 4\pi\epsilon\epsilon_0 a' \left(\frac{\mathrm{RT}}{F}\right)^2 \left(\frac{R-a'}{R}\right) Y^2 \ln\left[1 + \frac{a'}{R-a'}\exp\left(-\kappa(R-2a')\right)\right] \qquad (2.29)$$

where $a' = a + \delta$, and $Y = 4\tanh(zF\Psi_\delta/4RT)$.

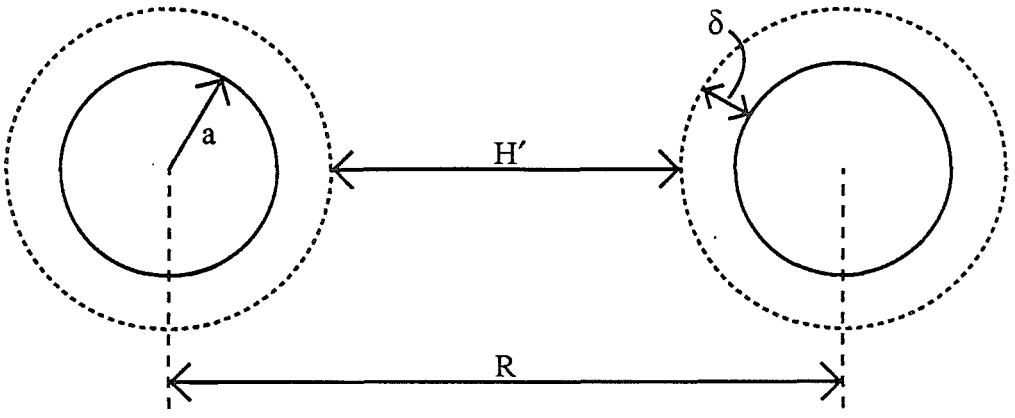

Figure 2.2: The geometry of two interacting spheres.

Discrepancies between DLVO theory and experiments has led to a re-examination of other aspects of the theory, including hydrodynamic interaction. Spielman (1970) considered viscous interactions for two neighboring particles and quantitatively incorporated them into colloid stability calculations. The viscous effect can be calculated quantitatively by estimating the diffusion coefficient along the line interconnecting the center of the particles as a function of separation distance, R. Honig et al. (1971) gave a useful approximation in the form of a rational function,

$$\frac{D_0}{D(u)} = \beta(u) = \frac{6u^2 + 13u + 2}{6u^2 + 4u} \tag{2.30}$$

where $u = H/a$. Incorporating this expression into equation (2.16),

$$W = \int_0^\infty \frac{\beta(u')}{(2+u')^2} \exp\left(V_T/\mathrm{kT}\right) du' \Big/ \int_0^\infty \frac{\beta(u')}{(2+u')^2} \exp\left(V_A/\mathrm{kT}\right) du' \tag{2.31}$$

In the last expression, $u' = H'/(\delta + a)$, and $H' = H - 2\delta$. The physical meaning of the distances in Eqs. (2.20) - (2.31) is illustrated in Fig. 2.2.

2.4 Hematite Surface Speciation

2.4.1 Surface Chemical Model

2.4.1.1 The Origin of the Surface Hydroxyl Group

When hematite particles come into contact with water, the surface metal ions coordinate with water molecules because of their reduced coordination number at

the interface. Subsequently, water molecules dissociate and react with the surface iron, thereby producing surface hydroxyl groups. This chemisorption process can be described using the schematic pictures of Schindler (1981) shown in Fig. (2.3).

The presence of hydroxyl groups on the hematite surface is evidenced by infrared spectroscopy measurements (Peck et al., 1966). If hematite surface iron ions are completely hydroxylated, the number density of hydroxyl groups (which is denoted by Sd) can be 9 OH groups per 100Å^2, based on crystal structure calculations. The value reported from various adsorption measurements ranges from 4.5 to 9 OH groups per 100Å^2 (Jurinak, 1966; Breeuwsma, 1973; Micale et al., 1985).

From Fig. 2.3 it appears that OH^- ions may be in one of two coordinations with respect to iron ions in the hematite particle surface. There may be a distribution of energies corresponding to different modes of hydroxyl group coordination. Parfitt (1978) obtained infrared spectra for goethite after exchanging the surface OH with heavy water, D_2O. The spectra clearly revealed three types of surface OD (OH) vibrations, which indicates three types of surface OH sites. Nevertheless, assuming just one type of site on the iron oxide surface, Davies (1985) was able to model Mn(II) oxidation in the presence of surface catalysts. Wehrli and Stumm (1987) found that in the presence of metal oxides the oxygenation of vanadyl (IV) was consistent with coordination reaction between surface hydroxyl groups and vanadyl, followed by oxidation reaction. Therefore, for simplicity, it is assumed in this study that the surface hydroxyl groups are identical and possess the same level of energy. Furthermore, it is assumed that all the sites are evenly distributed.

2.4.1.2 Development of Chemical Speciation Model

Surface complexation models proposed by Schindler et al. (1976) have been used to describe accurately the results of potentiometric and adsorption experiments. These models require a description of surface chemical reactions (which are incorporated into mass and charge balance equations) and a description of interfacial

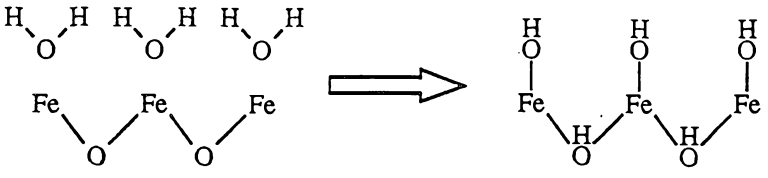

Figure 2.3: Schematic representation of the adsorption of water on a hematite surface.

structures. On the basis of the surface chemical model, the acid–base reactions on hematite surfaces are expressed as follows:

$$\begin{aligned} \equiv\mathrm{FeOH}_2^+ &\rightleftharpoons \equiv\mathrm{FeOH} + \mathrm{H}^+ \qquad K_{a1}^{int} \\ \equiv\mathrm{FeOH} &\rightleftharpoons \equiv\mathrm{FeO}^- + \mathrm{H}^+ \qquad K_{a2}^{int} \end{aligned} \tag{2.32}$$

The equilibrium constants are defined as:

$$\begin{aligned} K_{a1}^{int} &= \frac{(\equiv\mathrm{FeOH})(\mathrm{H}^+)}{(\equiv\mathrm{FeOH}_2^+)} = \frac{[\equiv\mathrm{FeOH}](\mathrm{H}^+)}{[\equiv\mathrm{FeOH}_2^+]} \frac{\gamma_{\equiv\mathrm{FeOH}}}{\gamma_{\equiv\mathrm{FeOH}_2^+}} \\ K_{a2}^{int} &= \frac{(\equiv\mathrm{FeO}^-)(\mathrm{H}^+)}{(\equiv\mathrm{FeOH})} = \frac{[\equiv\mathrm{FeO}^-](\mathrm{H}^+)}{[\equiv\mathrm{FeOH}]} \frac{\gamma_{\equiv\mathrm{FeO}^-}}{\gamma_{\equiv\mathrm{FeOH}}} \end{aligned} \tag{2.33}$$

where [ ] represent concentration (e.g., in mole/liter) and ( ) represents activity. The superscript "int" indicates an intrinsic constant. The quantity γ_i is the activity coefficient for species i.

The surface charge and potential are a consequence of the charged species, $\equiv\mathrm{FeO}^-$ and $\equiv\mathrm{FeOH}_2^+$, and the surface charge density can be evaluated by applying a proton material balance relationship to titration data:

$$\begin{aligned} \sigma &= \Big([\equiv\mathrm{FeOH}_2^+] - [\equiv\mathrm{FeO}^-]\Big) \frac{F}{Sa \cdot Sc} \\ &= \Big(C_A - C_B + [\mathrm{OH}^-] - [\mathrm{H}^+]\Big) \end{aligned} \tag{2.34}$$

where Sc is the concentration of solid in g/liter, F is the Faraday constant, C_A and C_B are the resulting concentrations of acid and base, respectively, added to the system. Sa is the specific surface area of the solid. It can be determined by BET adsorption or negative adsorption in solution (Breeuwsma, 1973). When the solid

phase is composed of regularly shaped particles, the surface area can be estimated from their geometry (e.g., for spherical particles with a uniform diameter, Sa can be determined from Eq. (3.2), see Sec. 3.2.1).

The mass conservation for iron species on the surface is expressed by

$$Fe_T = [\equiv \mathrm{FeOH}_2^+] + [\equiv \mathrm{FeOH}] + [\equiv \mathrm{FeO}^-] \tag{2.35}$$

Fe_T denotes the total concentration of surface species, and is usually independently estimated by $Fe_T = Sd \cdot Sa \cdot Sc$, where Sd is the site density, and Sc is the solid concentration. The product of Sd and Sa can be experimentally determined and yields the maximum exchange capacity in moles/g (see Sec. 3.2.2).

Equation (2.34) relates surface charge to solution pH. The pH value at which the surface proton adsorption density equals that of hydroxide ions, i.e., where proton–derived surface charge is zero, is defined as $\mathrm{pH_{zpc}}$. The $\mathrm{pH_{zpc}}$ found for hematite is 8.5, which is in the range of 8 to 9, found by other workers (James and Parks, 1982).

2.4.2 Models of the Solid/Aqueous Interface

To model the adsorption of protons on hematite surfaces it is necessary to have a description of surface chemical reactions. In addition, an electrostatic model is required to account for surface species activity corrections in the presence of charged surfaces. Under charged conditions, the activity quotients in Eq. (2.33) can be assumed to be related to surface potential (Sposito, 1983) and asymptotically approach 1 as the surface charge goes to zero. The equilibrium constants are rewritten as,

$$\begin{aligned} K_{a1}^{int} &= K_{a1}^{app} \exp\left(-\frac{F\Psi}{RT}\right) \\ K_{a2}^{int} &= K_{a2}^{app} \exp\left(-\frac{F\Psi}{RT}\right) \end{aligned} \tag{2.36}$$

where,

$$\begin{aligned} K_{a1}^{app} &= \frac{[\equiv \mathrm{FeOH}](\mathrm{H}^+)}{[\equiv \mathrm{FeOH}_2^+]} \\ K_{a2}^{app} &= \frac{[\equiv \mathrm{FeO}^-](\mathrm{H}^+)}{[\equiv \mathrm{FeOH}]} \end{aligned} \tag{2.37}$$

The superscription "app" denotes apparent constants which can be determined by experiment, and which vary with surface charge and actual pH. The intrinsic constants are obtained by extrapolating the apparent constants to zero surface charge. Equilibrium calculations of surface speciation are readily made by using a surface chemical equilibrium computer code, e.g., MINEQL (Westall et al., 1976) implemented later as SURFEQL (Faughnan, 1981). The agreement of model calculations and titration data determines the optimum values of the equilibrium constants (equilibrium constants are usually treated as fitting parameters). In addition to the intrinsic surface equilibrium constants, a computer model requires an electrostatic model to describe the surface-solution interface. The choice of the electrostatic model gives rise to a number of additional fitting parameters.

The commonly used surface complexation models are the diffuse layer model, the Stern layer model, and the constant capacitance model, and the triple layer model. These models have similar mass–balance equations, and they are distinguished by ways of formulating the electrostatic energy associated with adsorption on charged surfaces. The diffuse layer model assumes a layer of fixed charge on the surface of the particles and next to the surface a diffuse layer of opposite charges distributed in solution according to the Boltzmann distribution. The potential, Ψ, in Eq. (2.36) is replaced by Ψ_0, the surface potential. Other parameters, such as the diffuse layer capacitance, are governed by Gouy–Chapman theory, hence the electrostatic description of the diffuse layer model yields no "extra" fitting parameters apart from K_{a1}^{int} and K_{a2}^{int}. (The total exchange capacity can be a model fitting parameter as well if no independent and reliable value is obtained through experiment.)

Westall and Hohl (1980) compared different surface models and concluded that these models are equivalent in their ability to fit the same titration or adsorption results, although they have different numbers of fitting parameters, and yield large differences in the numerical values of the fitting parameters, such as the equilibrium

constants. The diffuse layer model is chosen for this work because (1) the simple physical presentation of the interface gives rise to the least number of fitting parameters, and (2) the description of a diffuse layer is essential in model calculations of hematite stability because two diffuse layers overlap when particles approach each other.

Figure 2.4 shows experimental results for acid-base titration of hematite in NaCl ionic media. Using the FITEQL (Westall, 1982) and SURFEQL equilibrium computer codes, the titration data were simulated by the diffuse layer model, as shown in Fig. 2.5. The parameters used in the model are as follows. pK_{a1}^{int}=7.25, pK_{a2}^{int}=9.75, total exchange capacity, $Sd \cdot Sa = 3.16 \times 10^{-4}$ mole/g (Section 3.2.2). Taking the specific surface area to be 80 m^2/g, the modeled results in Fig. 2.5 provide good fits to the titration data in Fig. 2.4.

2.4.3 Adsorption of Anions on Hematite.

The adsorption of inorganic and organic ions alters the hematite surface charge and potential characteristics. Consequently, the stability of hematite is expected to depend on these adsorption processes. In this study, the following anions are investigated: phosphate , sulfate, chloride, and anions of carboxylic groups associated with naturally occurring organic matter. The heterogeneous properties of natural organic matter make it difficult to interpret and model the adsorption on hematite. As a first approximation, it is assumed that the adsorption characteristics of low molecular weight carboxylic acids resemble those of natural organic matter. Results from the analysis of carboxylic acid adsorption are applied to interpret the extent of adsorption of natural organic matter on hematite particles.

The complex formation constants of different anions with surface groups are found to follow the same trend as those for the formation of anion–metal complexes in solution (Sigg and Stumm, 1980). Assuming that a similar analogy applies to hematite surfaces, the equilibrium constants for an anion surface complex can be estimated

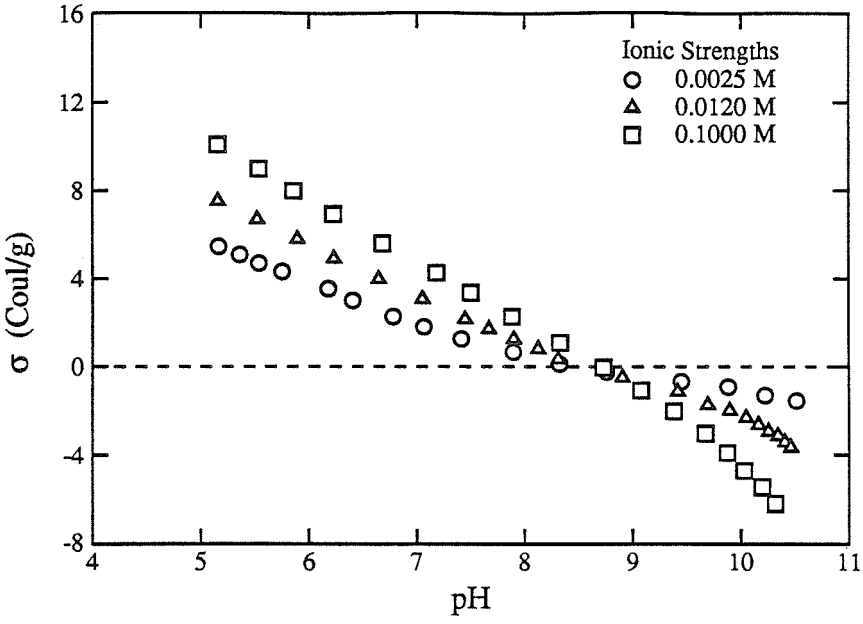

Figure 2.4: The surface charge, σ_0, on hematite particles plotted as a function of pH for differing ionic strengths.

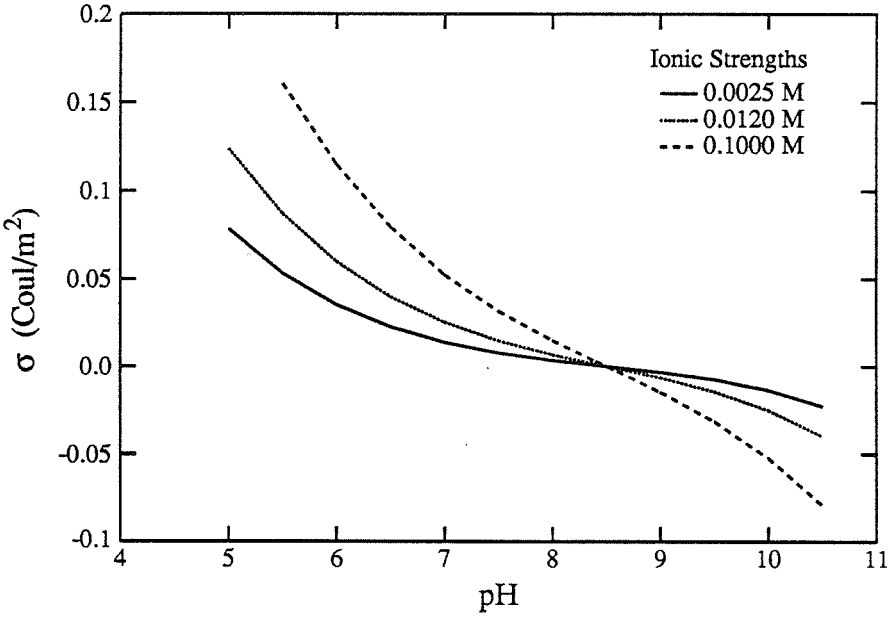

Figure 2.5: Hematite surface density as a function of pH as determined by a surface equilibrium model. The model parameters are given in the text.

from the equilibrium constants for solution complexes. If the equilibrium reaction for solution complexes is written as

$$FeOH^{2+} + HL \rightleftharpoons FeL^{2+} + H_2O \tag{2.38}$$

The corresponding surface complex formation is represented by

$$\equiv FeOH + HL \rightleftharpoons \equiv FeL + H_2O \tag{2.39}$$

Table 2-1 is a list of published equilibrium constants for iron complexes of various anions in solution. The reactions are of the following form

$$Fe^{3+} + H_mL^{m-n} \rightleftharpoons FeH_mL^{3+m-n} \tag{2.40}$$

This equation can be transformed to

$$FeOH^{2+} + H_nL \rightleftharpoons FeH_mL^{3+m-n} + (n-m)H^+ + H_2O \tag{2.41}$$

For example, complex formation of iron and $H_2PO_4^-$ has an equilibrium constant $10^{3.65}$,

$$Fe^{3+} + H_2PO_4^- \rightleftharpoons FeH_2PO_4{}^{2+} \qquad \mathrm{Log}K = 3.65 \tag{2.42}$$

To obtain the equilibrium constant for reactions of the form of Eq. (2.39) the following equilibrium reactions are used,

$$\begin{aligned} Fe^{3+} + H_2PO_4^- &\rightleftharpoons FeH_2PO_4{}^{2+} && \mathrm{Log}K = 3.65 \\ FeOH^{2+} &\rightleftharpoons Fe^{3+} + OH^- && -11.81 \\ H_3PO_4 &\rightleftharpoons H_2PO_4{}^- + H^+ && -2.15 \\ H^+ + OH^- &\rightleftharpoons H_2O && 14.0 \end{aligned} \tag{2.43}$$

Summing the above equations yields

$$FeOH^{2+} + H_3PO_4 \rightleftharpoons FeH_2PO_4{}^{2+} + H_2O \qquad \mathrm{Log}K = 3.69 \tag{2.44}$$

The corresponding surface complex reaction is:

$$\equiv FeOH + H_3PO_4 \rightleftharpoons \equiv FePO_4H_2 + H_2O \tag{2.45}$$

(a) Iron Complexes.

Anions (L)	Equilibrium Constant, K	Log K
Nitrate (NO_3^-)	$FeL/Fe \cdot L$	0.76
Perchlorate (ClO_4^-)	$FeL/Fe \cdot L$	1.15
Chloride (Cl^-)	$FeL/Fe \cdot L$	1.48
Acetate (CH_3COO^-)	$FeL/Fe \cdot L$	4.00*
Sulfate (SO_4^{2-})	$FeL/Fe \cdot L$	4.04
Propionate ($CH_3CH_2COO^-$)	$FeL/Fe \cdot L$	4.29*
Oxalate ($C_2O_4^{2-}$)	$FeHL/Fe \cdot HL$	4.35*
	$FeL/Fe \cdot L$	7.74*
Phthalate ($C_8H_6O_4^{2-}$)	$FeL/Fe \cdot L$	N/A
Salicylate ($C_7H_6O_3^{2-}$)	$FeHL/Fe \cdot HL$	5.06*
	$FeL/Fe \cdot L$	17.57
Fluoride (F^-)	$FeL/Fe \cdot L$	6.00*
Phosphate (PO_4^{3-})	$FeH_2L/Fe \cdot H_2L$	3.65*
	$FeHL/Fe \cdot HL$	10.15*

(b) Other Metals and Hydroxide Ions (OH^-).

Sodium (Na^+)	$NaOH/Na \cdot OH$	-0.20
Potassium (K^+)	$KOH/K \cdot OH$	-0.50
Calcium (Ca^{2+})	$Ca(OH)/Ca \cdot OH$	1.30
Magnesium (Mg^{2+})	$Mg(OH)/Mg \cdot OH$	2.58
Iron (Fe^{3+})	$Fe(OH)/Fe \cdot OH$	11.81

(c) Acidity Constants of Organic Ligands.

Acetic acid	$pK_a = 4.75$
Propionic acid	$pK_a = 4.87$
Caprylic acid	$pK_a = 4.89$
Capric acid	$pK_a = 4.85$
Aspartic acid	pK_1=2.0, pK_2=3.9, pK_3=10.0
Oxalic acid	pK_1=1.25, pK_2=4.27
Phthalic acid	pK_1=2.95, pK_2=5.41
Salicylic acid	pK_1=2.97, pK_2=13.74

* Constants are extrapolated to I=0 M using the Davies equation.

Table 2.1: Equilibrium constants for the formation of aqueous complexes from metals and ligands (from Smith and Martel (1976), and Perrin (1979)).

Assuming the surface complex formation constant for $\equiv FePO_4H_2$ has a similar order of magnitude as the aqueous formation constant ($\mathrm{Log}K$=3.69) for $FeH_2PO_4^{2+}$, the equilibrium constant in terms of $\mathrm{Log}K$ is of the order of 4. According to Table 2-1, the strength of complex formation between iron(III) and negatively-charged ions is ordered as follows: $HPO_4^{2-} > F^- >$ Salicylate $> H_2PO_4^- >$ Propionate $\sim$ Acetate $> SO_4^{2-} > Cl^- \sim ClO_4^- > NO_3^-$.

Equilibrium constant information is not available for phthalate-iron complexes. To estimate the complex formation constant, it is assumed that the strength of the iron-phthalate complex lies between those of iron with oxalate and salicylate ions. The estimated value for the iron-phthalate complex is thus approximately 10^6.

Chloride ions form a very weak aqueous complex with iron(III) ($\mathrm{Log}K \sim 1.5$). It is possible that chloride ions have a weak specific interaction with hematite surface hydroxyl groups. Experimental results by Breeuwsma (1973), however, did not show specific interaction of chloride on hematite surfaces. Data in Fig. 2.4 of the current research also indicate that the chloride ion is non-specific, as the three data sets all intersect at the same point, and no shift of pH_{zpc} occurs with a change in electrolyte concentration of near three orders of magnitude. Hence, it is expected that chloride is not adsorbed on hematite through specific chemical interaction.

Phosphate forms the strongest complex among all the anions considered here. Electrophoretic mobility data show that concentrations of phosphate as small as 10μM are capable of shifting the isoelectric pH point of a hematite suspension ($\sim$30 mg/l) from 8.5 to 6.5 (see Fig. 4.20).

The equilibrium adsorption of phosphate was calculated with a diffuse layer model using the SURFEQL computer code. Fig. 4.26 illustrates the predicted total adsorption of phosphate in the pH range of 4 to 10; the total adsorption of phosphate is compared with the experimental results.

In the model calculations, the surface acid-base equilibrium constants, K_{a1}^{int} and K_{a2}^{int}, are taken to be the same as in Fig. 2.5, without phosphate present. Additional constants for phosphate complexation with the surface are estimated based on the values given in Sigg (1979) and constants for the corresponding solution complexes. The reactions considered are

$$\equiv FeOH + H_3PO_4 \rightleftharpoons \equiv FeH_2PO_4 + H_2O \tag{2.46}$$

$$\equiv FeOH + H_3PO_4 \rightleftharpoons \equiv FeHPO_4^- + H^+ + H_2O \tag{2.47}$$

$$\equiv FeOH + H_3PO_4 \rightleftharpoons \equiv FePO_4^{2-} + 2H^+ + H_2O \tag{2.48}$$

The equilibrium constants for acetate-iron and propionate-iron solution complexes indicate that the aqueous carboxylate ions specifically interact with iron and form strong complexes in solution. Complex formation constants are not available for fatty acids whose carbon chains contain more than three carbon atoms. Since the $-CH_2$ group has hydrophobic characteristics, and the interaction of each $-CH_2$ group involves an energy of about RT (~2500 Joules/mole or ~600 cal/mole), it is expected that an increase in the number of carbons has a direct influence on complex formation. The surface complex formation constants for these fatty acids are estimated from those of the simple acids (namely, acetic and propionic acids), accounting for the additional contribution of the hydrophobic tails.

3. MATERIALS AND METHODS

3.0 General Remarks

Deionized distilled water was used to prepare all solutions. All reagents were analytical grade and were used without further treatment. Fatty acids were obtained from SIGMA^{TM} and were at least 99% pure. Fulvic and humic acids were supplied by the International Humic Substances Society. All solutions were filtered through 0.2 μm Nuclepore to remove possible particle contaminants.

Pyrex glassware was used in general, but in certain experiments, such as the fluoride adsorption experiment described in Sec. 3.2.2, teflon beakers were used instead. The glassware was first cleaned in a detergent solution (Linbro^{TM}), soaked in concentrated hydrochloric acid, rinsed with deionized distilled water, and finally oven dried. A suction pump was used to facilitate the cleaning of syringes and electrophoresis cells.

The pH of solution was monitored in all coagulation, titration, electrophoresis and adsorption experiments. These measurements were made using a Radiometer glass combination electrode (GK2401C) and a pH meter (Radiometer Model PHM84 research pH meter). The electrode was calibrated by NBS buffers and, if frequent measurements were made, was checked against buffers every two hours.

3.1 Particle Preparation and Characterization

3.1.1 Preparation of Hematite Particles

Hematite particles were synthesized according to the method of Matijević and Scheiner (1978), with some modification. Matijević and Scheiner discuss at length the dependence of the shape and crystal structure of the synthesized particles on the solution pH, the concentration of ferric ions and the nature of the anions present. To prepare hematite particles, a concentrated aqueous solution of $Fe(ClO_4)_3/HClO_4$ was quickly mixed in deionized distilled water pre-heated to 100°C. The dilution ratio was kept at 1 to 20. The solution final concentrations of H^+ and Fe(III) were 0.05M and 0.035M, respectively. The mixture was covered and kept in an oven at 100°C for 24 hours. The forced hydrolysis process can be described by,

$$2Fe^{3+} + 3H_2O = Fe_2O_3(s) + 6H^+ \tag{3.1}$$

After heating, the suspension was cooled to room temperature. The suspension containing iron oxide particles was decanted and the remaining particles were soaked in 0.01M $HClO_4$ for 24 hours. The procedure was repeated at least three times to minimize amorphous iron oxide coatings that might be present in the suspension (Faust, 1985). The final suspension was stored at pH$\sim$3 as stock.

3.1.2 Particle Characterization

To analyze the particles by X-ray crystallography a sample was first withdrawn from the stock suspension and dialyzed to remove electrolytes (Spectrapor^{TM} dialysis membrane tubings were used). The conductivity of the water in which the dialysis bags were placed was monitored by a conductance meter (YSI Scientific model 35). The process was terminated when the conductivity was about the same as that of deionized water. The resulting suspension was centrifuged at 3000 rpm for 30 minutes, followed by decantation to separate the particles from the supernatant. The particles collected were dried at 100°C, and then kept in a desiccator. Debye-Scherrer X-

ray diffraction patterns were obtained using Co(Kα) radiation. As may be seen from comparing Plates Ia and Ib, the observed diffraction pattern for the synthesized particles is very similar to that of standard hematite particles, confirming that the bulk material is hematite. X-ray crystallography revealed some impurities in some samples. The presence of these impurities was confirmed by IR spectroscopy, and identified as β-FeOOH. Since the surface properties of hematite and β-FeOOH are similar, the presence of these impurities does not significantly affect the results of the experiments or their interpretation.

Scanning electromicrographs were taken for each batch of suspensions. The particles (see Plate II) were approximately spherical in shape. Particle sizes are dependent on the chemical and heating conditions of each synthesis (Matijević and Scheiner, 1978).

Three batches of synthesized particles were used in the experiments. The batch 1 particles, which have an average diameter of about 30 nm, were used in the adsorption experiments. The particles in batches 2 and 3 have an average diameter of 70 nm, as may be seen in Plate II. The batch 2 particles were mainly used in the coagulation and electrophoretic mobility measurements. The batch 3 particles were used only in preliminary experiments. Titration experiments yielded the same pH_{zpc} for the three batches, showing that the surface acid-base properties of the particles in the three batches are the same. Table 3.1 summarizes the properties of the hematite particles used in this and other studies.

Scanning electromicrographs of the particles taken one year after their synthesis showed that the shape and size of the particles had not changed in this time. Titration and mobility measurements made every few months after particle synthesis yielded a constant value of pH_{zpc}. It may be concluded, therefore, that the surface chemical properties of the synthesized hematite particles do not vary over the time interval in which the experiments were conducted.

Plate Ia: Debye-Scherrer X-ray diffraction pattern of synthesized hematite particles.

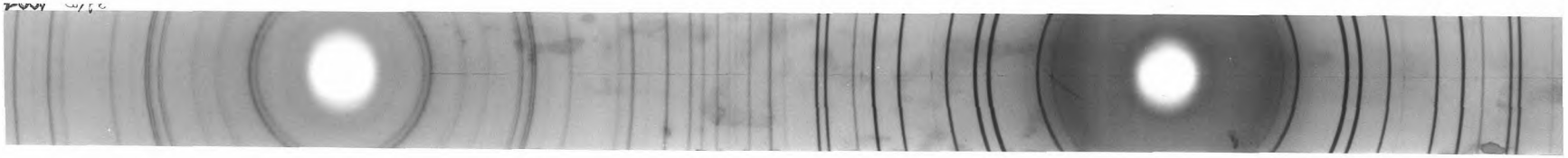

Plate Ib: Debye-Scherrer X-ray diffraction pattern of standard hematite particles.

Reference	Sample Preparation	pH_{zpc}	Electrolyte	Specific Surface Area
Parks and deBruyn (1962)	Hydrolysis of $Fe(NO_3)_3$ at boiling point	8.50	KNO_3	BET: $15 m^2/g$ Postulated: $60 m^2/g$
Breeuwsma (1973)	Hydrolysis of $Fe(NO_3)_3$ at neutral pH (by adding KOH) at boiling point	8.50	KCl	BET: Batch A: $31 m^2/g$ Batch B: $18 m^2/g$ Batch C: $21 m^2/g$
Penners (1985)	Hydrolysis of $FeCl_3$ at 100°C, seeded growth	9.50	KCl	BET: $26.5 m^2/g$ Estimated from average diameter: $14.3 m^2/g$
Dumont et al. (1971)	Hydrolysis of $Fe(NO_3)_3$ at 100°C, pH 1.6	9.27 8.20	KCl $KClO_4$	$44.6 m^2/g$ $24.5\ m^2/g$
This work	Hydrolysis of $Fe(ClO_4)_3$ at 100°C	8.50	NaCl	BET: Batch 1: $40.0 m^2/g$ Estimated from averaged diameter: Batch 1: $38.3 m^2/g$ Batch 2: $16.3 m^2/g$

Table 3.1: Comparison of hematite properties.

Since the surface chemical properties of the particles in each batch are the same, the batch used need not be stated explicitly subsequently in this thesis. In the light scattering calculations the particle diameter, d, is taken as 70 nm since the coagulation experiments were made using batch 2 particles. Batch 1 particles were used in the adsorption experiments, so in interpreting these results a specific surface area of 40 m^2/g is used.

3.2 Surface Properties

3.2.1 Specific Surface Area

The specific surface area was determined for a batch of hematite particles according to the BET method (Brunauer, Emmett and Teller, 1938), and found to be $40 \pm 4\ m^2/g$ with negligible pore structure. The average diameter obtained from SEM for this particular sample of hematite was 30 nm. Assuming that the particles were

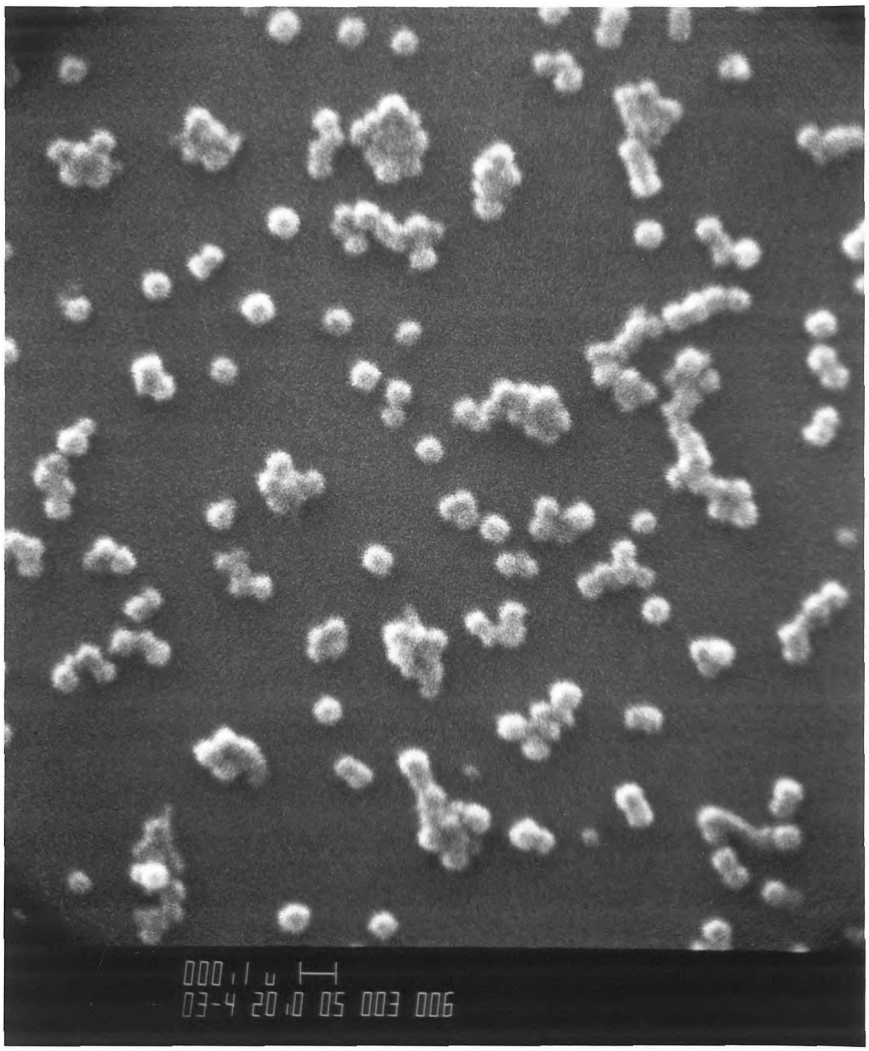

Plate II: Scanning electromicrograph of synthesized hematite particles.

perfect spheres, the specific surface area, Sa, was estimated to be 38.2 m^2/g using the following equation

$$Sa = \frac{1}{\rho}\left(\frac{\pi d^2}{\pi d^3/6}\right) = \frac{6}{\rho d} \tag{3.2}$$

where the density, ρ, is taken as 5.24 g/cm^3 and d is the diameter of the particles. The BET measurements and the theoretical calculation are in good agreement. Hence, for hematite samples for which BET measurements were not made, the specific surface area of the particles was estimated using Eq. (3.2).

3.2.2 Determination of Specific Surface Sites

The specific surface site measurement was carried out following the method described by Faust (1985). A suspension of 50 ml with 6.35 g/l of solids was added to 50 ml of 0.1M NaF solution. The pH of the mixture was adjusted to 3.6 using $HClO_4$. After an adsorption period of 3 hours the particles were filtered out. Subsequently, fluoride was desorbed from the hematite particles at pH$\sim$11. Following 2 hours of desorption the particles were removed by filtration and the filtrate was kept for fluoride determination. To provide a constant background ionic strength and adjust the solution pH, 10% of TISAB III (Orion 94-09-11) were present in all standards and samples. TISAB III complexes ions which may interfere with fluoride determination. Fluoride activity was measured by a specific ion electrode (Orion model 94-09 fluoride electrode and Orion model 901 ionalyzer). The total exchange capacity, $Sd \cdot Sa$, thus determined was $(3.16 \pm 0.32) \times 10^{-4}$ mol/g.

3.2.3 Acid-Base Titration

Acid-base titrations were performed in a 300ml double-walled beaker. The beaker was connected to a water bath (VWR refrigerated circulating bath model 1140) to keep the temperature at 25°C. N_2 gas was filtered and introduced to the reaction vessel after absorption of CO_2 in a column packed with Ascarite II.

Before each titration the particles were treated in the following way. An aliquot

of stock suspension containing about 1 gram of particles was brought to pH~4 by adding sodium hydroxide, and the total volume was adjusted to 200 ml. After being left overnight to equilibrate, the particles were coagulated at pH 8 to 9 by adding base. The supernatant was then sucked out very carefully with the aid of a water pump. Subsequently, the particles were washed with deionized distilled water several times, until the supernatant conductivity was about 2 μmho/cm, which is the same order of magnitude as that of deionized water. Particles were finally soaked in a medium of the desired ionic strength, and dispersed at pH~4 by adding a known amount of HCl. The total volume was again adjusted to 200 ml. The suspension was equilibrated for 24 hours, and was then ready for titration.

The suspension was titrated by adding 50 to 100 μl of 0.1M NaOH at intervals of from 15 to 60 minutes. During this interval the maximum pH change was less than 0.01.

3.3 Adsorption Measurements

3.3.1 Adsoption of Phosphate

Adsorption of phosphate was investigated at various pH values for a known initial total phosphate concentration. For direct comparison with the coagulation experiment results, the solid concentration used in the adsorption experiments was equivalent to that used in the coagulation experiments. First, an aliquot of hematite particles was placed in an Erlenmyer flask and phosphate was introduced as KH_2PO_4. Inorganic salt $KClO_4$, and acid ($HClO_4$) or base (KOH) were added to adjust the pH of the sample, and to obtain the desired electrolyte concentration. The final suspension volume was 50 to 100 ml and was stirred for 2 hours. After equilibrating for 24 hours, particles were separated from the liquid phase by filtration. The particles collected were resuspended in a 10 ml solution of pH 11.5 to desorb phosphate from the hematite particles. The amount of phosphate was measured by ion chromatography (model Dionex 2020i).

3.3.2 Adsorption of Organic Matter

Adsorption of organic matter, such as phthalic acid, lauric acid and Suwannee River fulvic acid, on hematite was studied using a total organic carbon analyzer. Adsorption isotherms at constant pH and adsorption as a function of pH at fixed acid concentration were both investigated. The samples were prepared as follows. An aliquot of hematite particles was placed in an Erlenmeyer flask. The desired pH and ionic strength were achieved by adding a small amount of NaOH or HCl and NaCl. Finally, an organic acid was introduced into the suspension and water was added to make the total volume between 200 to 1000 ml. The particle concentrations were similar as those in the coagulation experiments. The suspensions were stirred for 24 hours and pH measurements were taken. After an adsorption period of 24 hours, particles were filtered out of the suspension.

Since the solid concentration was low in the sample, the uptake of organic acid by particles was low and the difference between the initial organic concentration and the organic acid measurement in the filtrate was not an accurate measure of the amount of acid adsorbed by particles. Therefore, the amount of adsorbed organics was determined as follows. After filtration the particles were resuspended in a small volume (2-10 ml) of 0.02N H_2SO_4 solution. The carbon present in the last suspension was determined using a Dorhmann DC-80 Total Organic Carbon Analyzer. The method involves the oxidation of organic matter in persulfate and UV irradiation. The amount of CO_2 yielded in these processes was measured by an infra-red detector. The detection limit was between 0.5 ppm and 2 ppm, depending on whether a sample boat was used.

For one set of experiments, 2 g/l of hematite was used instead of a concentration of $\sim$20 mg/l. The organic acid adsorption was determined by the difference of the initial acid concentration and the amount left in the solution phase. A blank sample was prepared in the same way as the other samples, but with no solid present.

3.4 Electrophoretic Mobility Measurement

Hematite particle mobilities were investigated using a Mark II particle micro-electrophoresis apparatus (Rank Brothers, London). A thin-walled cylindrical cell and a 4 mW He:Ne laser (λ = 633 nm, 1304P, uniphase) were used to ensure a good view of particle movement. The particle concentration was chosen so that negligible coagulation occurred during an experiment. The ionic strength of the medium was adjusted using KCl. In each measurement at least 20 particles were timed in each direction of the movement. Although all data reported from the experiments were measured at the upper stationary point, frequent checks of the mobility at both stationary points agreed within experimental error. The cell was cleaned by soaking in 3M HCl and rinsing thoroughly in deionized distilled water. The mobility profile in a calibration was symmetric with respect to the axis of the cell. The electric field was kept between 2 and 10 Volt/cm, corresponding to a particle velocity of about 10 μm/sec. The range of distances used in the timing was 30 to 100 μm.

3.5 Coagulation Experiments

The turbidity of a colloidal suspension results from the light scattered by the dispersed particles. The amount of scattering depends on the size and shape of the particles, and the wavelength of the incident beam. Since the aggregation of particles causes a shift in the particle size distribution, the intensity of scattered light will change accordingly. Light scattering measurements have wide application in colloid sciences, such as in the estimation of particle size (Kerker, 1969) and in the kinetic study of colloid stability (Ottewill and Shaw, 1966).

3.5.1 Light Scattering Theory

For small particles ($d < \lambda/20$), Rayleigh theory of light scattering is applicable. When a light beam falls upon a particle, the electric field associated with the incident beam causes periodic oscillations of the electron clouds around the atoms of the particle. The induced dipoles act as secondary sources and radiate scattered light. In

the light scattering calculation, these particles are treated as point scatterers.

When the diameter of a particle is comparable to the wavelength of the incident light the particle can no longer be treated as a point scatterer and the interference between the light scattered from different locations in the same particle must be taken into consideration. For homogeneous isotropic spheres of arbitrary size and material, theoretical calculations can be made based on Mie theory, which was developed independently by Mie (1908) and Debye (1909). Detailed descriptions of solutions are given in van der Hulst (1981) and Kerker (1969).

To calculate the scattering properties of a spherical particle of radius, a, for radiation of wavelength, λ, the following parameters are relevant,

$$\alpha = \frac{2\pi a}{\lambda} \tag{3.3}$$

$$m = n - ki \tag{3.4}$$

where m is the complex refractive index and n, k are the refractive and absorptive indices, respectively. If the cross-section for the removal of incident energy from the forward beam by scattering and true absorption are denoted by C_{sca} and C_{abs}, respectively, then the efficiency factors are defined as follows

$$Q_{sca} = C_{sca}/\pi a^2 \tag{3.5}$$

$$Q_{abs} = C_{abs}/\pi a^2 \tag{3.6}$$

$$Q_{ext} = Q_{sca} + Q_{abs} \tag{3.7}$$

The quantities Q_{sca} and Q_{ext} can be computed from Mie theory,

$$Q_{sca} = \frac{2}{\alpha^2}\sum_{j=1}^{\infty}(2j+1)\left[|a_j|^2 + |b_j|^2\right] \tag{3.8}$$

$$Q_{ext} = \frac{2}{\alpha^2}\sum_{j=1}^{\infty}(2j+1)Re\,(a_j + b_j) \tag{3.9}$$

where $Re(x)$ denotes the real part of x. The values of a_j and b_j are given by the

following expressions,

$$a_j = \frac{\psi_j(\alpha)\psi_j'(m\alpha) - m\psi_j(m\alpha)\psi_j'(\alpha)}{\zeta_j(\alpha)\psi_j'(m\alpha) - m\psi_j(m\alpha)\zeta_j'(\alpha)} \tag{3.10}$$

$$b_j = \frac{m\psi_j(\alpha)\psi_j'(m\alpha) - \psi_j(m\alpha)\psi_j'(\alpha)}{m\zeta_j(\alpha)\psi_j'(m\alpha) - \psi_j(m\alpha)\zeta_j'(\alpha)} \tag{3.11}$$

The functions ψ_j and ζ_j are the Ricatti-Bessel functions and ψ_j' and ζ_j' are the derivatives of the corresponding functions with respect to their arguments.

The refractive indices of hematite with respect to water were taken from Kerker et al. (1979) and are plotted in Fig. 3.1. Since hematite particles are uniaxial monocrystalline particles (not isotropic) the reported real refractive indices are the average of the indices, n_ω and n_ε, for the ordinary and extraordinary rays. Thus,

$$n = \frac{n_0}{n_{\mathrm{w}}} = \frac{2n_\omega + n_\varepsilon}{3n_{\mathrm{w}}} \tag{3.12}$$

where n_0 is the real refractive index in vacuum and n_{w} is the refractive index of water. Thus, n is the relative refractive index and is used in Mie theory calculations for hematite dispersed in water. Kerker et al. defined the complex refractive index as $m = n(1 - i\kappa)$, where κn is equivalent to k in equation (3.4). For consistency, k is used throughout the calculation.

With the aid of a computer, Q_{ext} has been calculated as a function of radius, a, wavelength, λ and complex refractive index, m.

The total light extinction of a particle suspension as a result of absorption and light scattering was measured by a spectrophotometer (model HP-8451A). The total extinction, E_{tot}, (also known as the optical density) is related to Q_{ext} by the relationship (Hsu and Matejević, 1985),

$$E_{tot} = \frac{1}{\ln 10}\left(Q'_{ext} N \cdot l \cdot \pi a^2\right) \tag{3.13}$$

where N is the number concentration of particles and l is the optical path length. Q'_{ext} is the apparent extinction efficiency which differs from the true Q_{ext} by a correction

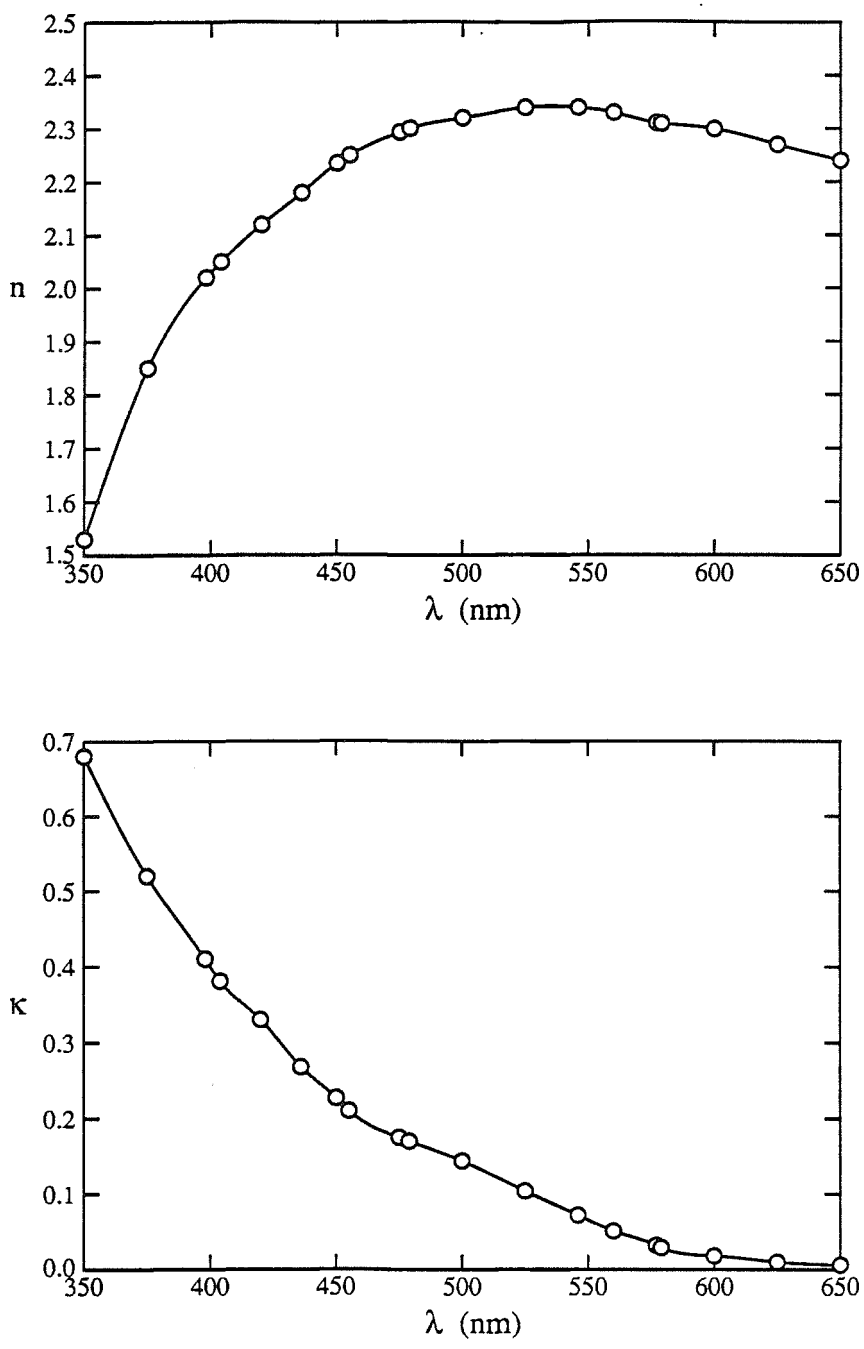

Figure 3.1: The complex refractive index, m, may be written $m = n(1 - i\kappa)$. In the above figures n and κ are plotted as a function of wavelength, λ. The open circles are experimental data taken from Kerker et al. (1979). The solid line is a cubic spline fit to the data.

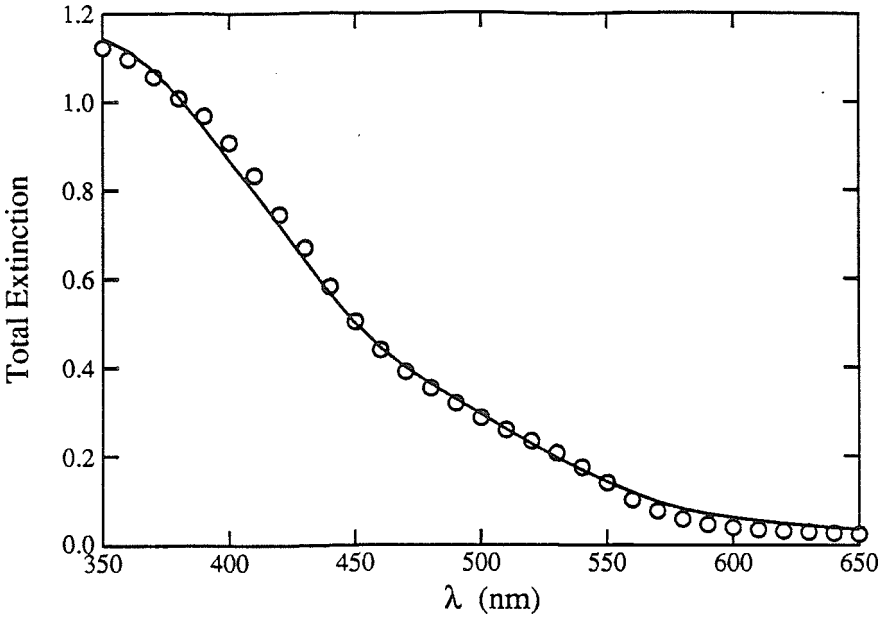

Figure 3.2: Total extinction, E_{tot}, plotted as a function of wavelength. The open circles represent experimental data. The solid line is the result of a Mie theory calculation for hematite particles of diameter 70nm in water.

factor necessary to account for light scattered in the forward direction which enters the finite aperture of the detector along with the direct radiation. Fig. 3.2 shows the experimental and calculated Mie total extinction for hematite particles as a function of the incident wavelength.

3.5.2 Total Light Extinction Measurement

An HP-8451A spectrophotometer was used to measure the total extinction of light for a particle suspension. Before each measurement, the colloidal suspension was subjected to ultrasonication to homogenize the system and set the initial condition. To avoid multiple scattering, the solid concentrations were kept between 5-100 mg/l, so the average spacing between particles was 35 to 100 times the particle diameter.

To perform a coagulation kinetics experiment, 3ml of colloidal suspension of desired pH and solid concentration was placed in a cell of 1cm light pathlength. 10 to

100μl of inorganic electrolytes or organic solutes were introduced to an adder-mixer (Ottewill and Sirs, 1957) by Hamilton syringes, and then mixed with the suspension by plunging the adder-mixer into the cell. Spectrophotometric measurements were begun immediately after the mixing time of approximately 0.4 seconds. Extinction as a function of time was measured (generally at $\lambda = 546$nm), and recorded by the spectrophotometer. Temperature control was achieved by employing a thermostattable cell holder (HP 89054A) connected to a thermostat-controlled water bath.

3.5.3 Interpretation of Light Scattering Data

As a result of coagulation, doublets, triplets and higher numbers of aggregated singlets form in an initially monodispersed system. The total extinction of light, E_{tot}, in a coagulating system results from the superposition of the extinction from all particle sizes. The total extinction is expressed similarly as in Eq. (3.13),

$$E_{tot} = \frac{1}{2.3} \sum_{i=1}^{\infty} Q_{ext,i} \cdot n_i \cdot l \cdot \pi a_i^2 \tag{3.14}$$

In the initial coagulation stage, when the normalized reaction time, t/τ_a, is much less than unity, singlets and doublets are dominant. Here τ_a denotes the actual coagulation characteristic time. Therefore, at this early stage of coagulation the total extinction can be approximated by,

$$E_{tot} = \frac{l}{2.3} \left(Q_{ext,1} \cdot n_1 \cdot \pi a_1^2 + Q_{ext,2} \cdot n_2 \cdot \pi a_2^2 \right) \tag{3.15}$$

Substituting Eqs. (2.13) and (2.14) for n_1 and n_2, the Eq. (3.15) becomes

$$E_{tot} = \frac{l}{2.3} \left[\pi a_1^2 \cdot Q_{ext,1} \frac{N_\infty(0)}{(1 + t/\tau_a)^2} + \pi a_2^2 \cdot Q_{ext,2} \frac{N_\infty(0)(t/\tau_a)}{(1 + t/\tau_a)^3} \right] \tag{3.16}$$

where the actual coagulation characteristic time, τ_a, is related to the initial reaction rate constant, k_a, by $\tau_a = 1/k_a N_\infty(0)$. The initial slope of the total extinction is derived from equation (3.16),

$$\left. \frac{dE_{tot}}{dt} \right|_{t=0} = \frac{N_\infty(0) \cdot l}{2.3\tau_a} \left(\pi a_2^2 \cdot Q_{ext,2} - 2\pi a_1^2 \cdot Q_{ext,1} \right) \tag{3.17}$$

or,

$$\left.\frac{dE_{tot}}{dt}\right|_{t=0} = \frac{N_\infty^2(0) \cdot l \cdot k_a}{2.3}\left(\pi a_2^2 \cdot Q_{ext,2} - 2\pi a_1^2 \cdot Q_{ext,1}\right) \tag{3.18}$$

Generally, dE_{tot}/dt is obtainable from light scattering data, and $Q_{ext,1}$, the extinction efficiency of a singlet, can be calculated by Mie theory. In order to evaluate the initial coagulation rate constant, k_a, the extinction coefficiency of a doublet (the unknown quantity $Q_{ext,2}$) needs to be modeled. If it is assumed that doublets are formed from coalesced spheres, the extinction efficiency of spheres is readily calculated by Mie theory. Two models are considered to derive the diameter of the coalesced spheres. Model 1 assumes that a coalesced particle has a volume equal to that of two singlets, whereas model 2 assumes that the diameter of a coalesced particle is twice that of a singlet. These models yield upper and lower limit on $Q_{ext,2}$, and the true value is expected to lie somewhere in between.

3.5.4 Experimental Conditions

In coagulation kinetic studies the concentrations of particles suitable for use are bounded by a upper limit, above which multiple scattering is significant, and a lower limit, below which the error in determining the extinction is large.

In addition to the restrictions on the concentration, the duration of the experiment is also limited in simple kinetic studies. The least time required for the experiment is determined by the complete mixing time, which is about 0.4 second with an adder-mixer (Ottewill and Sirs, 1957), and the upper time limit is such that the error introduced by instrument drift is small.

The concentration and time limitations have a direct influence on the range of initial coagulation rate constants and stability ratios. The relationship between the stability ratio, the colloid concentration and the experiment duration is illustrated in Fig. 3.3.

In Sec. 2.2, the experimentally defined stability ratio is,

$$W = \frac{k_b}{k_a} \tag{3.19}$$

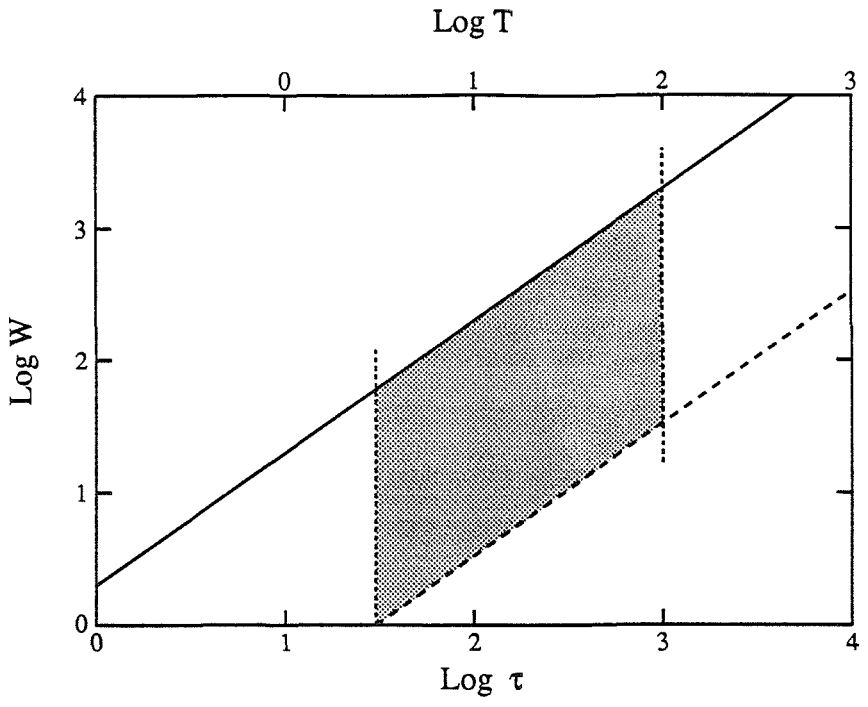

Figure 3.3: Stability ratio, W, plotted as a function of the characteristic time for coagulation, τ, for hematite particle number densities of $3{\times}10^{11}$ (upper solid line) and 5×10^{9} (lower dashed line). The vertical lines represent actual experiment durations of 3 and 100 seconds. The four lines define the experimental window shown shaded.

Recalling the expressions $\tau_a = 1/k_a N_\infty(0)$ and $\tau_b = 1/k_b N_\infty(0)$, W can be rewritten as

$$W = \frac{\tau_a}{\tau_b} = k_b N_\infty(0)\tau_a \tag{3.20}$$

Hence, $\log W = \log k_b N_\infty(0) + \log \tau_a$. The experiment duration has been chosen as $T = 0.1\tau_a$ for the reason that the total light scattering is mainly contributed by singlets and doublets and the simplified interpretation of light scattering data is valid.

Figure 3.3 illustrates the experimental window for coagulation kinetics studies. If an unstable colloid is expected after introducing electrolytes, a low concentration (in this case number concentration $\sim 5\times10^{9}$ cm^{-3} and mass concentration $\sim$ 5 mg/l) should be chosen in kinetic studies to obtain a fast coagulation rate. Similarly, if a

larger stability ratio is expected, a high particle concentration should be used when determining the coagulation rate.

4. EXPERIMENTAL RESULTS

4.0 Introduction

In this chapter experimental results are presented. These results are discussed in detail in Chapter 5. The primary objective of the experiments is to study the role of simple chemical changes in the aqueous phase on the kinetics of hematite coagulation. The effect of varying pH and temperature is investigated. At constant pH the influence of electrolyte concentration and valency are studied. The effects of organics (phthalate, oxalate, fatty acids and polyaspartic acid) on the coagulation rate are of importance, and the results of this study may help in understanding colloidal systems in which naturally occurring organics, such as fulvic and humic acid, are present. Adsorption experiments and electrokinetic mobility measurements were made to aid in the interpretation of the data.

4.1 Coagulation Rates

4.1.1 Effect of NaCl on Hematite Stability

The experimental procedure is described in Sec. 3.5.2. The pH of the stock electrolyte solutions was adjusted to be similar to that of the colloidal suspension; the pH measured after mixing typically differed by less than 0.05 from the initial value. The experiments were made at room temperature, which was about 21°C.

In this section data are presented to investigate the dependence of hematite particle stability on ionic strength. The initial coagulation rate is proportional to the

initial slope of the light extinction with respect to time (see Eq. (3.18)) and can be represented by:

$$\left.\frac{dE_{tot}}{dt}\right|_{t=0} \propto C \cdot N_{\infty}^{2}(0) k_a \tag{4.1}$$

where C is a constant, which only depends on the optical and geometric properties of the particles, and k_a is the rate constant for the reaction. Eq. (4.1) shows that the initial slope depends on the second power of initial number concentration (or mass concentration). This dependency is observed in the experimental results presented in Appendix A. The effect of pH, salt concentration and other chemical factors on hematite stability can only be compared at equal mass condition. Since the various coagulation experiments were not, in general, conducted using the same solid mass concentration (see Sec. 3.5.4 for experimental conditions), we normalize all initial slopes to a hematite solid concentration of 1 mg/l,

$$\left.\frac{dE}{dt}\right|_{t=0} = \frac{dE_{tot}/dt|_{t=0}}{m_0^2}$$

where m_0 is the initial mass concentration in mg/l. For fast coagulation, where the actual coagulation rate is just the fast Brownian coagulation rate (i.e., $k_a = k_b$), the initial slope of total light extinction with respect to time has a maximum value, $(dE/dt|_{t=0})_{max}$. Experimentally, the stability ratio, W_{exp}, is derived by,

$$W_{exp} = \frac{(dE/dt|_{t=0})_{max}}{dE/dt|_{t=0}} \tag{4.2}$$

which coincides with the definition in Sec. 2.2, i.e., W represents the ratio of the diffusion controlled coagulation rate to the actual coagulation rate.

Figure 4.1 shows the measured variation of light extinction with time of a hematite suspension to which NaCl has been added. It should be noted that as ionic strength increases the initial slope, $dE_{tot}/dt|_{t=0}$, also increases. In Fig. 4.1 the solid lines are fitted by rational approximations which are used to give the values of $dE/dt|_{t=0}$ plotted in Fig. 4.2 as a function of NaCl concentration. The values of the initial slope are

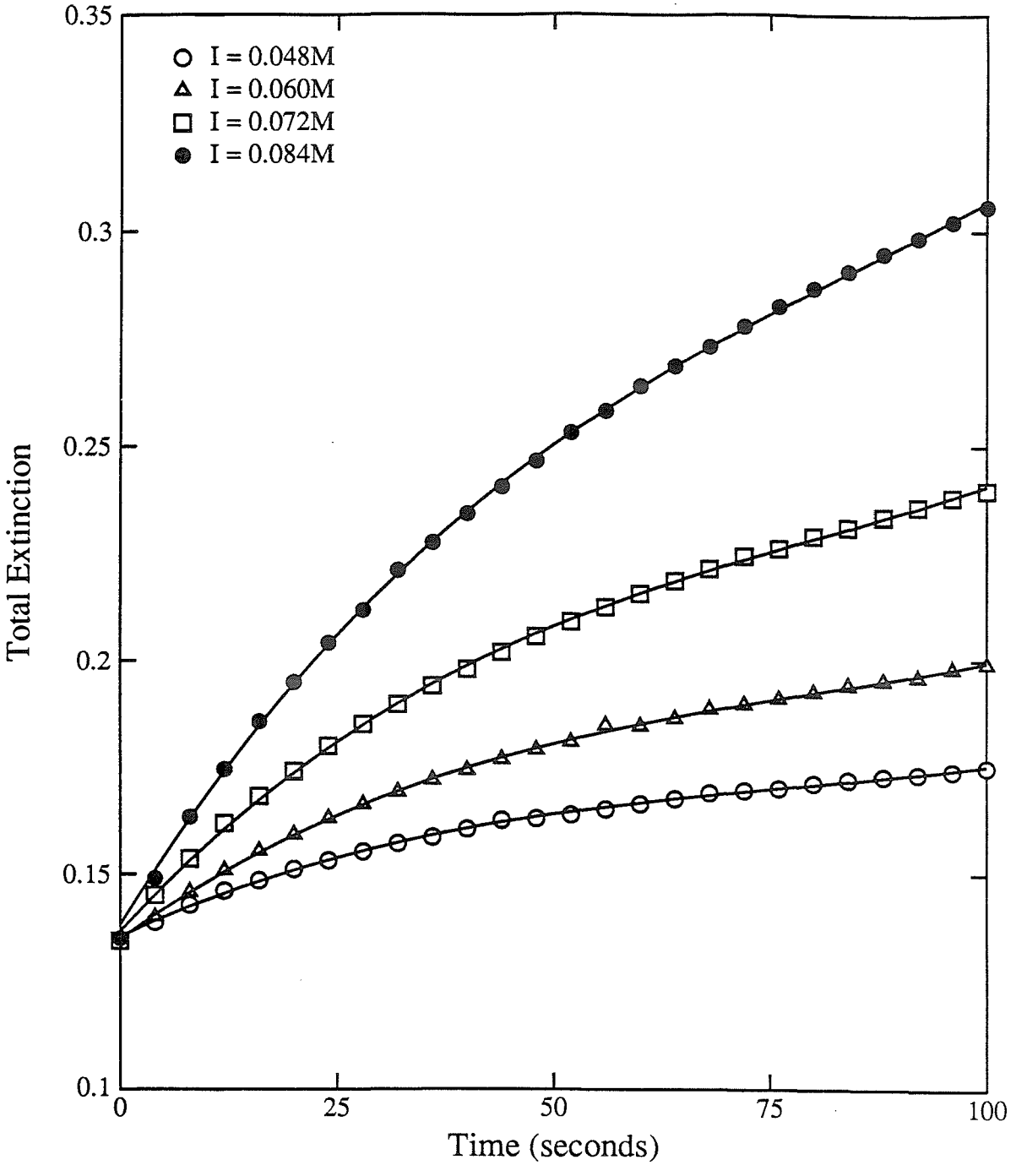

Figure 4.1: Total light extinction as a function of time for a hematite suspension at pH 4.7. The ionic strength, I, is adjusted with NaCl to lie in the range 0.048M to 0.084M. The hematite solid concentration is 33 mg/l, which corresponds to an initial particle number concentration of 3×10^{10} cm^{-3}.

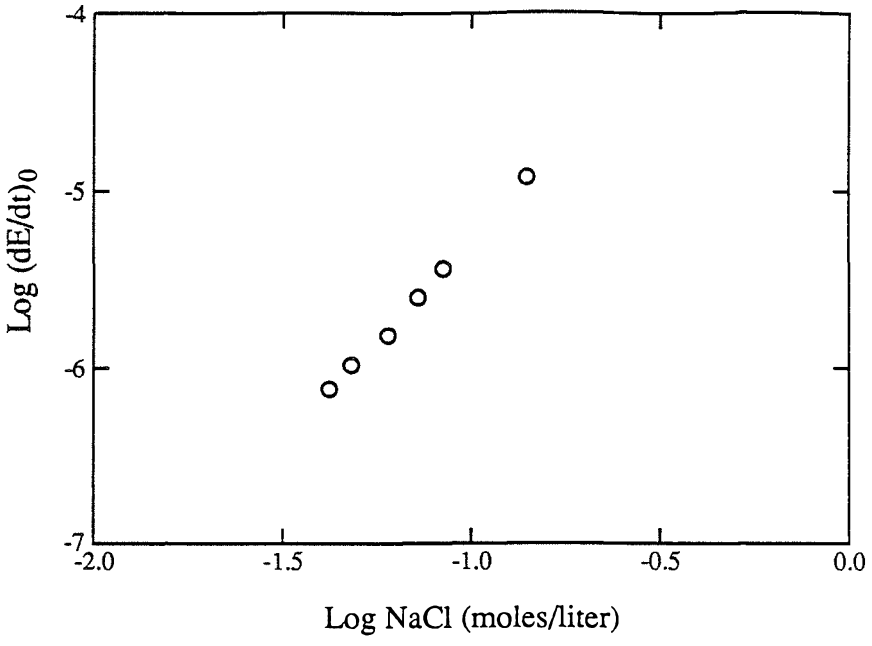

Figure 4.2: Initial slope of light extinction with respect to time, plotted as a function of NaCl concentration, for a hematite suspension at pH 4.7 and T=21°C.

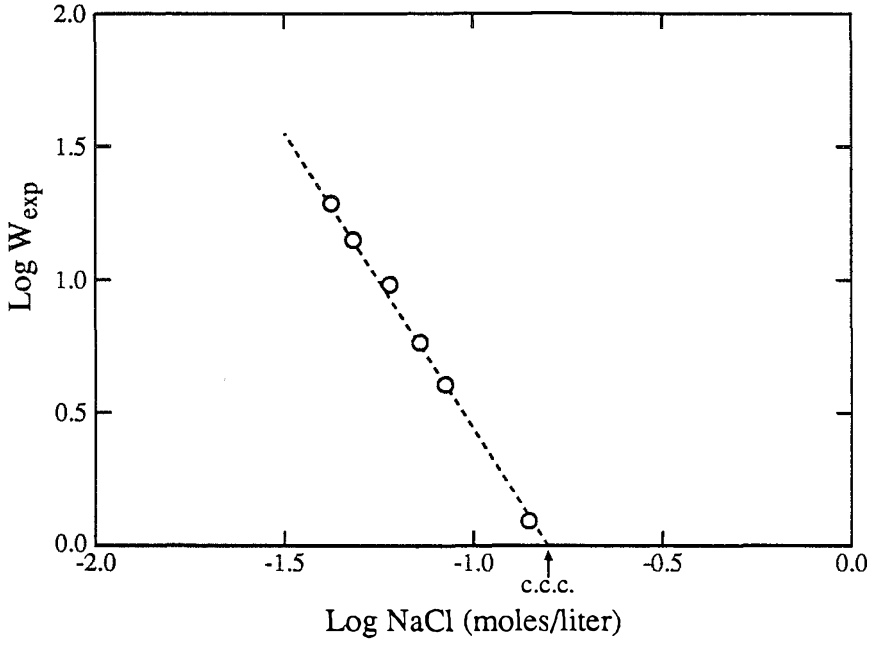

Figure 4.3: Experimentally derived stability ratio, W_{exp}, of a hematite suspension, plotted as a function of NaCl concentration. The values plotted were derived from the data shown in Fig. (4.2) using Eqs. (4.1) and (4.2). The critical coagulation concentration (c.c.c.) is indicated on the x-axis.

normalized to 1 mg/l solid concentration. Figure 4.3 shows experimentally obtained stability ratios over a range of NaCl concentration. The extrapolated concentration corresponding to $W_{exp} = 1$ is called the critical coagulation concentration (c.c.c.) and is the minimum concentration of NaCl needed to destabilize the system at a particular pH.

When calculating the initial coagulation rate constant, k_a, Mie theory of light scattering is used to determine the constant C in Eq. (4.1). The scattering coefficient for a dumb-bell doublet cannot be found analytically. Therefore, k_a has been estimated using two different assumptions for which Mie theory does provide analytic solutions. According to Model 1, $k_a(1)$ is based on the assumption that a doublet behaves like a coalesced particle having the same volume as two individual particles. Under Model 2, $k_a(2)$ is based on the assumption that the coalesced sphere has a diameter equal to twice that of a singlet. For the experimental conditions, Eqs. (3.9) and (3.18) show that $k_a(1)$ and $k_a(2)$ are given by:

$$k_a(1) = 1.93 \times 10^{-7} dE/dt|_{t=0} \tag{4.3}$$

$$k_a(2) = 5.34 \times 10^{-9} dE/dt|_{t=0} \tag{4.4}$$

where the rate constants are in cm^3/second. The correct solution for a doublet is expected to be bracketed by $k_a(1)$ and $k_a(2)$. $k_a(1)$ and $k_a(2)$ are plotted in Fig. 4.4 for the same experimental conditions as in Fig. 4.2 and Fig. 4.3. On the same plot, the diffusion controlled coagulation rate based on Smoluchowski's equation is shown as a horizontal dashed line. At the critical coagulation concentration, at which hematite particles are completely destabilized, a fast coagulation rate is expected. The extrapolated initial coagulation rate according to model (1) at c.c.c. (shown as a triangle in Fig. 4.4) agrees well with the theoretical value.

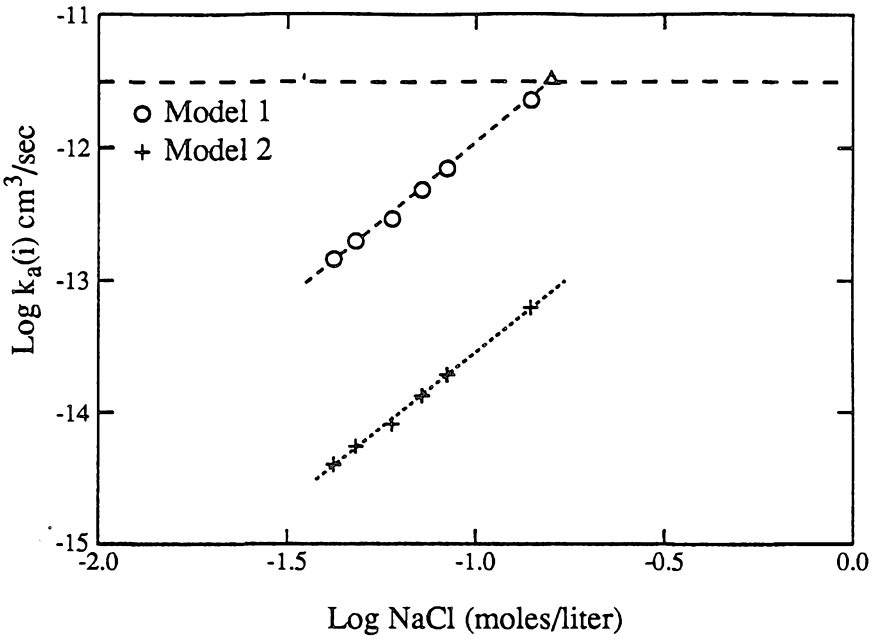

Figure 4.4: The initial coagulation rate constant of a hematite suspension at pH 4.7, plotted as a function of NaCl concentration for the two models described in the text. The dashed horizontal line indicates the diffusion controlled coagulation rate, corrected for hydrodynamic effects according to Spielman (1970). The triangle (△) is the extrapolated value of $k_a(1)$ at the critical coagulation concentration.

4.1.2 Effect of pH on Hematite Stability

Hematite stability was studied as a function of pH at room temperature for several ionic strengths. The initial slope of the light extinction data for each experimental point was estimated as outlined in Sec. 4.1.1 and is tabulated in Appendix A. The stability ratio, W_{exp}, is plotted in Fig. 4.5 as a function of pH for ionic strength ranging from 0.001 to 0.08 M. Dashed lines are drawn through the experimental points as a guide. The plot shows that as the pH differs from pH_{zpc}, the stability ratio is substantially increased. For low ionic strengths ($I \leq 0.01$ M) the data points are expected to lie on two straight lines which intersect at pH=pH_{zpc} and this appears to be the case in Fig. 4.5. At higher ionic strengths Fig. 4.5 shows there is a broad minimum in logW_{exp} centered on pH=pH_{zpc}. It should also be noted that at higher

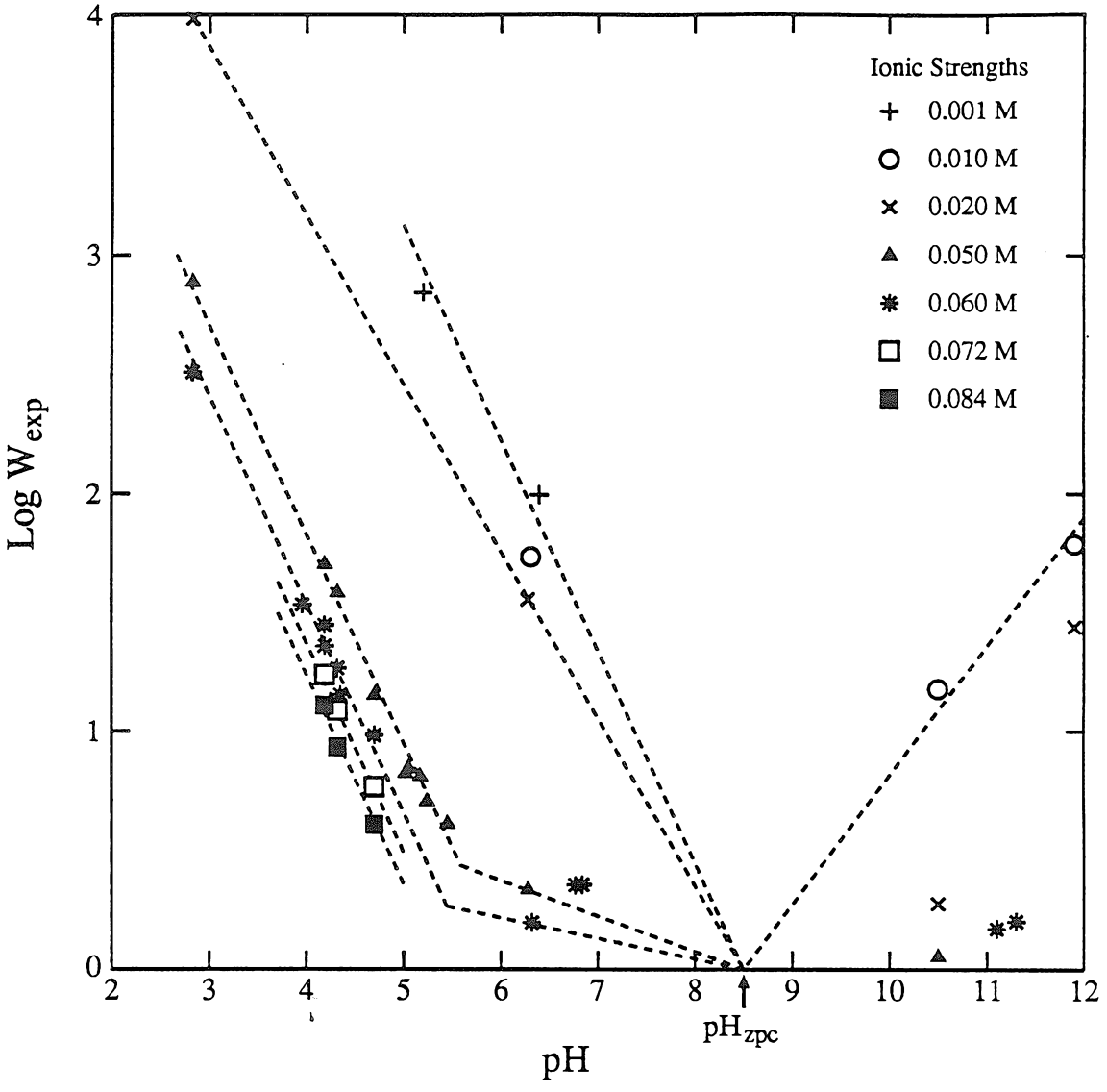

Figure 4.5: Experimentally derived stability ratio, W_{exp}, of a hematite suspension plotted as a function of pH for differing ionic strengths. The pH of zero proton condition is indicated. Dashed lines are drawn through the experimental points as a guide.

ionic strengths the dashed lines are parallel to each other when the pH is sufficiently far from pH_{zpc}, but this breaks down as the pH approaches pH_{zpc}.

4.1.3 Effect of Temperature on Hematite Stability

The effect of temperature on hematite stability was studied at moderate pH and ionic strength (pH 5.56, I=0.05M), since under these conditions hematite particles are relatively stable and any change in coagulation rate can be attributed to the temperature variation. In Appendix A, the initial coagulation rate constants are listed corresponding to the temperatures studied. These constants are derived from the initial slope of the total light extinction against time plots using the Mie theory calculations of Model (1). The fast coagulation rate constants given by Smoluchowski's equation, $k_b = 4kT/3\mu$, are also tabulated in Appendix A. The stability ratio, W, is not calculated as outlined in Sec 4.1.1 since the fast coagulation rate depends on temperature, and the temperature dependent $(dE/dt|_{t=0})_{max}$ is not available. Instead, W is obtained through the expression, $W = k_b/k_a$, where the subscript "exp" is now omitted since both k_a and k_b are not experimentally determined.

The initial slope of the light extinction with respect to time increases as temperature is increased, as shown in Fig. 4.6. However, the stability ratio W, is insensitive to variations in the temperature (Fig. 4.7). The average stability ratio is 5.65 with a standard deviation of 0.35. This observation is supported by Fig. 4.8 which shows the actual coagulation rate constant, $\ln k_a(1)$, and that of the fast coagulation, $\ln k_b$, as a function of $1/T(°K)$. The two data sets appear to be parallel to each other, so the difference between them ($\ln k_b - \ln k_a$) is approximately constant. By definition, $\ln k_b - \ln k_a = \ln(k_b/k_a) = \ln W$, which explains why the stability is relatively constant over the range of temperature studied.

4.1.4 Effect of Bivalent Ions on Hematite Stability

Bivalent ions were introduced into the hematite suspension in the form of sodium

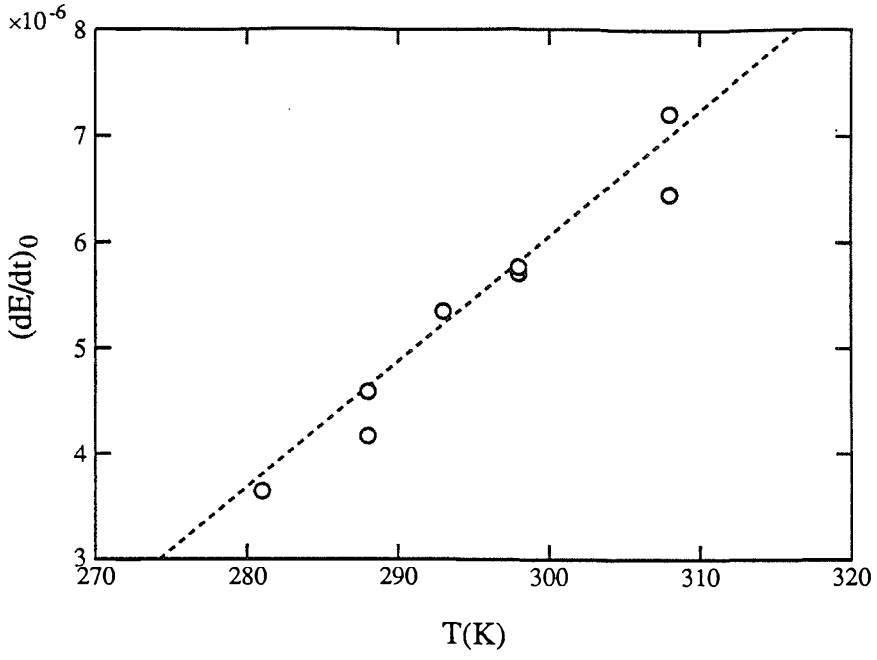

Figure 4.6: Initial slope of extinction with respect to time, plotted as a function of temperature. The suspension pH is 5.56 and the ionic strength is adjusted to 0.05M using NaCl.

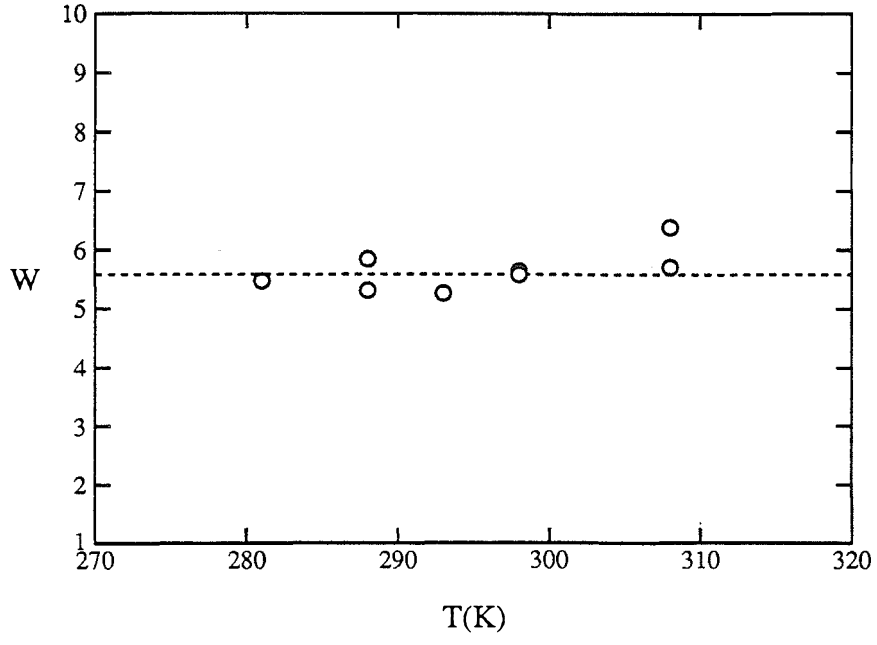

Figure 4.7: Stability ratio, W, evaluated using $W = k_b/k_a(1)$, plotted as a function of temperature. The suspension pH is 5.56 and the concentration of NaCl is 0.05M.

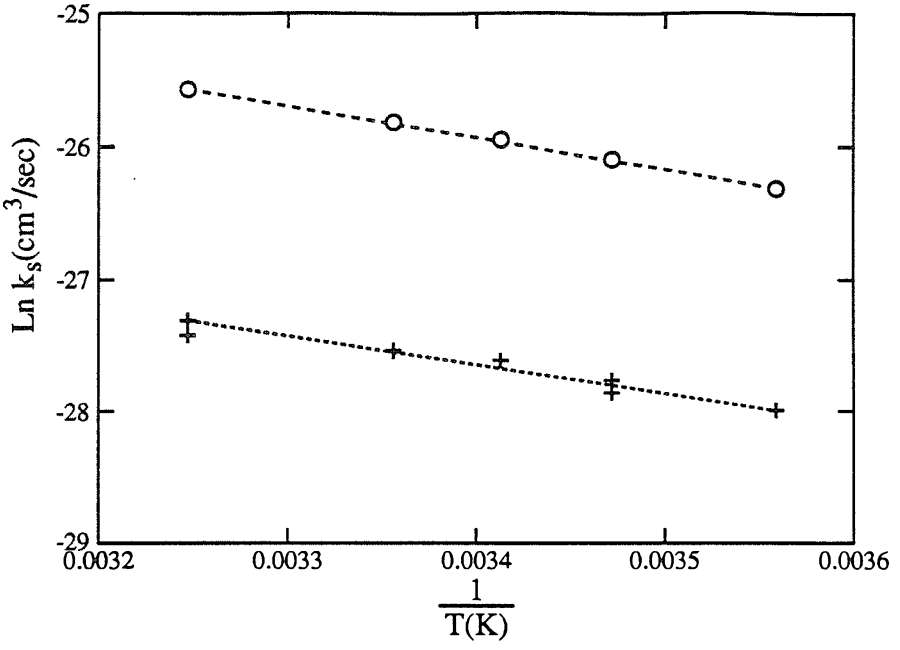

Figure 4.8: The lower set of data show the initial coagulation rate constant $k_a(1)$ plotted as a function of $1/T$. The upper set of data is for the case of diffusion controlled coagulation. The suspension pH is 5.56, and the concentration of NaCl is 0.05M.

or chloride salts, such as Na_2SO_4, $CaCl_2$ and $MgCl_2$. The effects of cations on hematite stability were studied at pH>pH_{zpc}, where the particles are negatively charged. Conversely, the influence of sulfate on hematite stability was investigated at pH<pH_{zpc}. In order to compare the overall results, the same ΔpH was selected, where ΔpH is operationally defined as the difference between the pH of the experiments and $pH_{zpc}$of the colloid. The initial coagulation rate constants, experimental light scattering data and parameters pertinent to the experimental conditions are summarized in Appendix A.

The stability of hematite under the influence of Na^+, Ca^{2+} and Mg^{2+} at a pH of 10.5 is plotted in Fig. 4.9. The slopes of the lines through the experimental points for the monovalent electrolytes differ slightly from those of the bivalent electrolytes, but little difference in slopes is observed among different kinds of bivalent ions. The

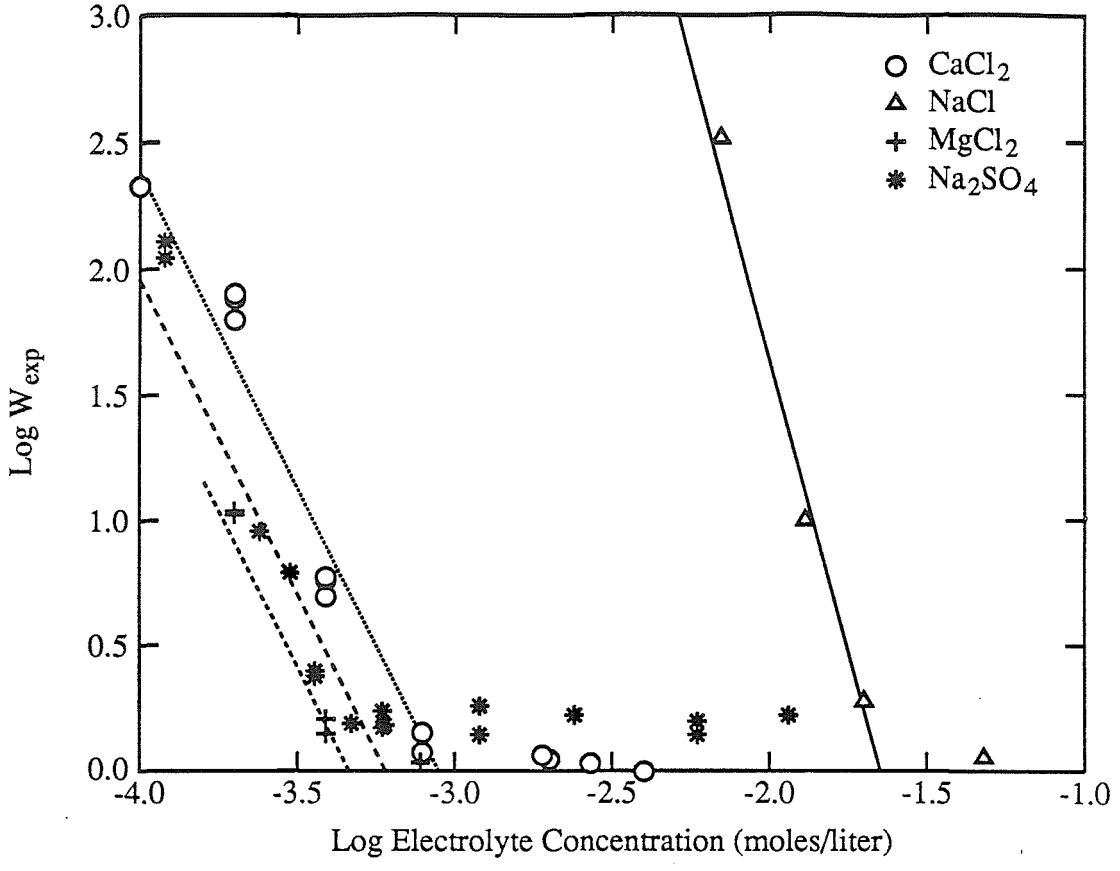

Figure 4.9: Experimentally derived values of the stability ratio, W_{exp}, plotted as a function of electrolyte concentration. The measurements for $CaCl_2$, $MgCl_2$, and NaCl were performed at pH 10.5, and those for Na_2SO_4 at pH 6.5. Lines are drawn through the experimental points as a guide.

extrapolated electrolyte concentrations at which the stability ratio reaches zero give the critical coagulation concentration, i.e., c.c.c. The c.c.c. values seem to follow the Schulze-Hardy Rule (see Sec. 2.3.4), with the c.c.c. for magnesium ions being somewhat less than that of calcium ions.

The effect of sulfate on hematite stability is also illustrated in Fig. 4.9. The working pH is 6.5, which makes the ΔpH identical to that of the other electrolytes. The c.c.c. of sulfate is comparable to calcium and magnesium ions and the slope of $\log W_{exp}$ versus $\log(SO_4^{2-})$ is also similar to that of the other bivalent ions.

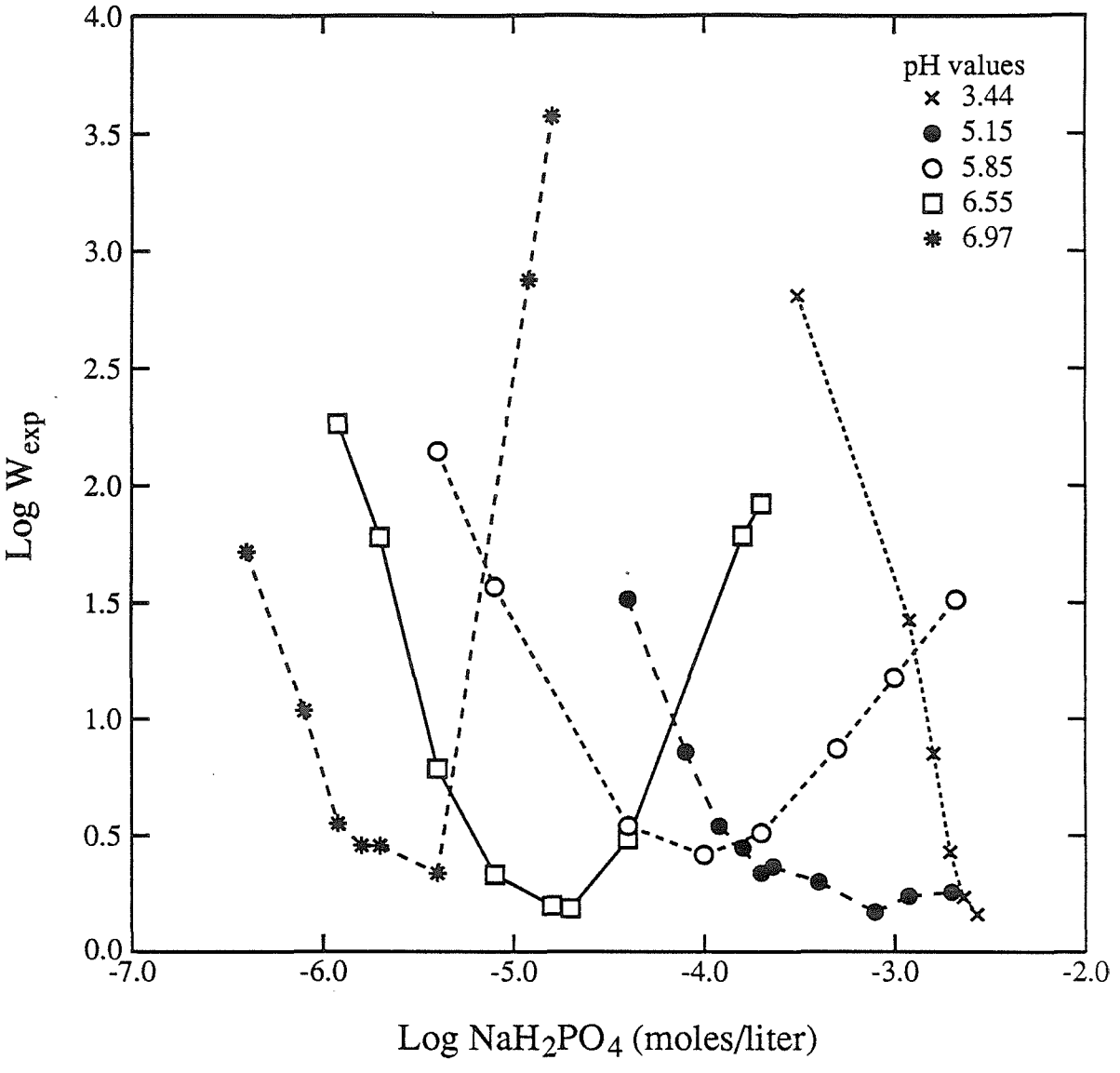

Figure 4.10: Experimentally derived values of the stability ratio, W_{exp}, plotted as a function of NaH_2PO_4 concentration at various pH values.

4.1.5 Effect of Phosphate on Hematite Stability

Phosphate has been proven to be specifically adsorbed on iron oxide surfaces through chemical reactions (Breeuwsma, 1973 and Sigg, 1979). Studies of coagulation in the presence of phosphate can yield important insights into the relationship between colloid stability and the adsorption of inorganic species on hematite particles. In Fig. 4.10, the stability ratio is plotted against phosphate concentration at constant pH. Several features are apparent. First, it appears that the critical coagulation concentration decreases as the pH is increased from 3 to 7. Second, the stability ratio decreases as phosphate concentration increases from zero to c.c.c. and then, depending on the pH studied, the stability ratio either remains low when the phosphate concentration is further increased (at pH<5), or else increases as more phosphate is added to the system.

At pH>7, a constant amount of phosphate was delivered to the hematite suspension. Subsequently, ionic strength was varied through the addition of NaCl. Figure 4.11 illustrates the dependency of hematite stability on the background electrolyte concentration in the presence of 0.5 millimolar phosphate at different pH values. At a constant pH, the stability decreases as ionic strength increases and the slope of each data set resembles one another, with the critical coagulation concentration slightly larger for higher pH than that for the lower pH condition.

4.1.6 Effect of Oxalate and Phthalate on Hematite Stability

Oxalate and phthalate ions were studied as model organic molecules. Adsorption experiments by Balistrieri and Murray (1987) on goethite surfaces indicate that these compounds specifically react with iron-hydroxyl groups. The coagulation experiments were conducted at pH 6.2, at which both oxalic and phthalic acid are in doubly deprotonated forms. The effects of oxalate and phthalate species on hematite stability are shown in Fig. 4.12. Both compounds reduce hematite stability to a minimum at concentrations around 0.2 millimolar. Hematite stability in the presence of phthalate

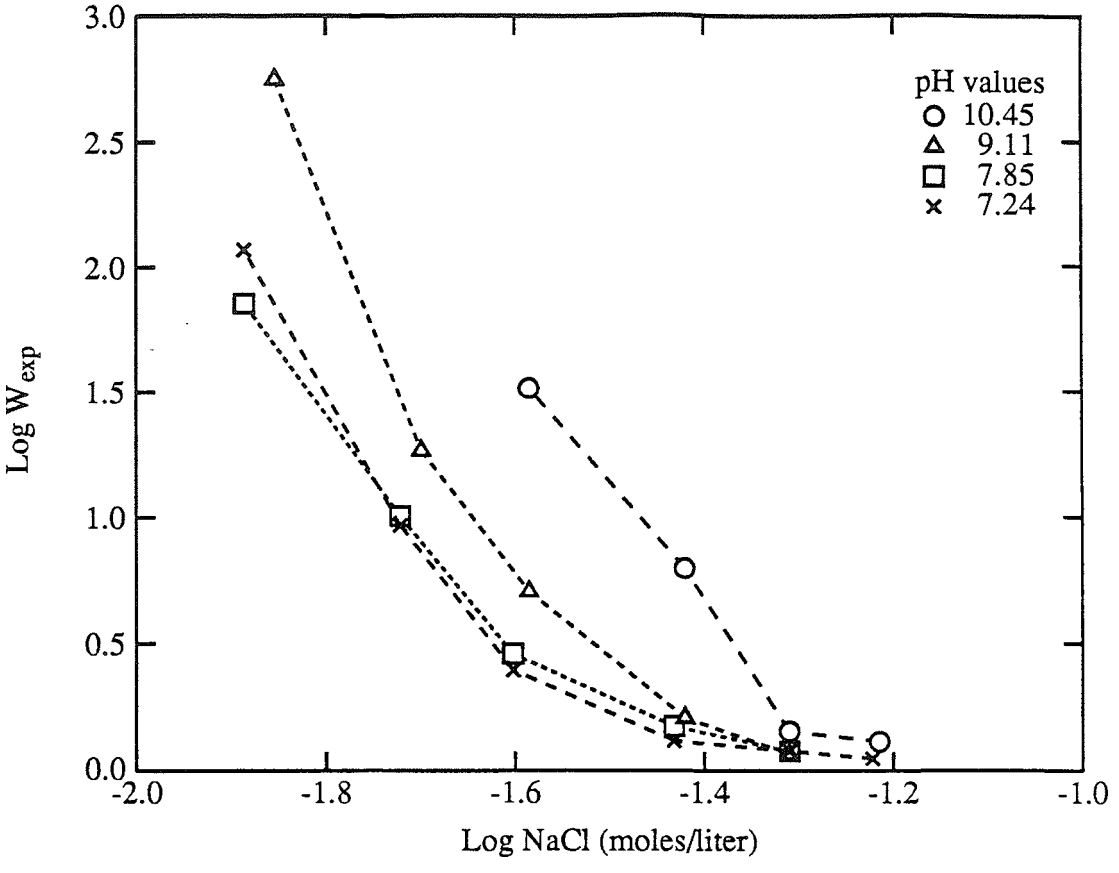

Figure 4.11: Experimentally derived stability ratio, W_{exp}, plotted as a function of NaCl concentration in the presence of 0.5 millimolar phosphate at various pH values.

ions tends to increase as the phthalate concentration is raised above 0.2 millimolar, whereas in the case of oxalate, the stability ratio fluctuates around the minimum.

The dependence of hematite stability on pH in the presence of 0.1 millimolar phthalate ions is plotted in Fig. 4.13. The supporting electrolyte concentration was kept at 5 millimolar. Figure 4.13 shows that at the extremes of pH, hematite particles are relatively stable, and that the lowest stability occurs at a pH of about 6.5. Compared with Fig. 4.5, the pH value at which the particle stability reaches a minimum is shifted from 8.5 (in the absence of phthalic acid) to 6.5 (with phthalic acid).

4.1.7 Effect of Polymeric Organic Compounds on Hematite Stability

Polyaspartic acid (PAA) was studied as a model compound for polymeric, high-

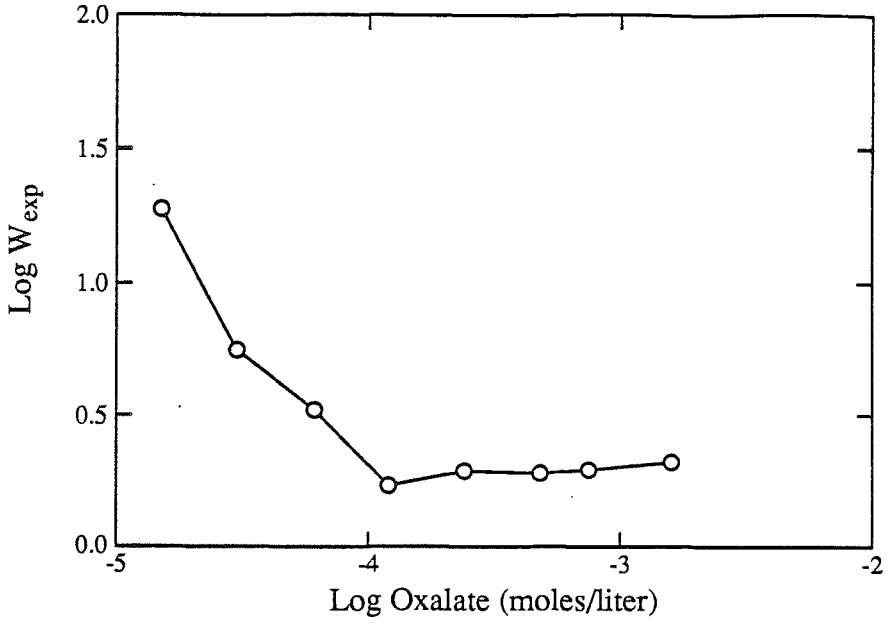

Figure 4.12(a): Experimentally derived stability ratio, W_{exp}, of a hematite suspension, plotted as a function of oxalate concentration at pH 6.2 in the presence of 1 millimolar NaCl.

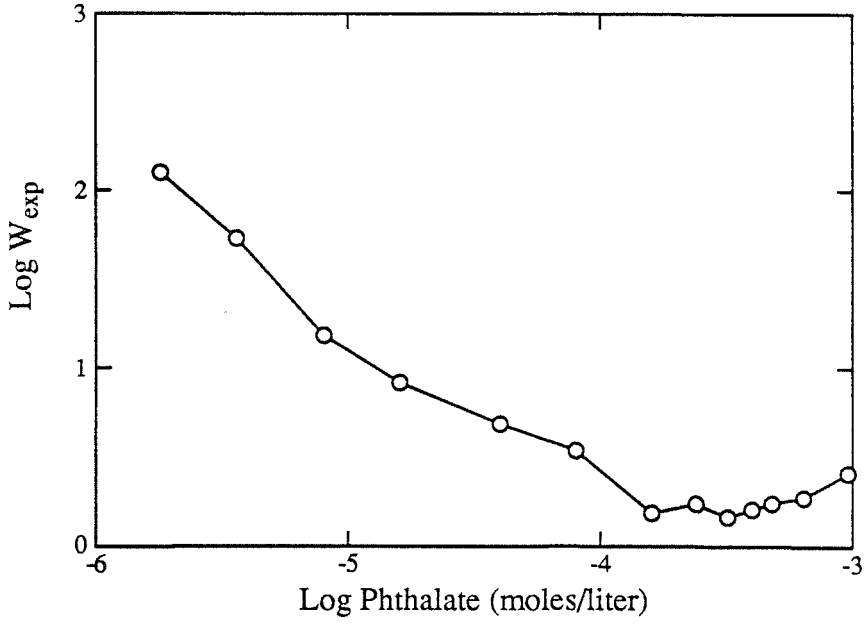

Figure 4.12(b): Experimentally derived stability ratio, W_{exp}, of a hematite suspension, plotted as a function of phthalate concentration at pH 6.2 in the presence of 1 millimolar NaCl.

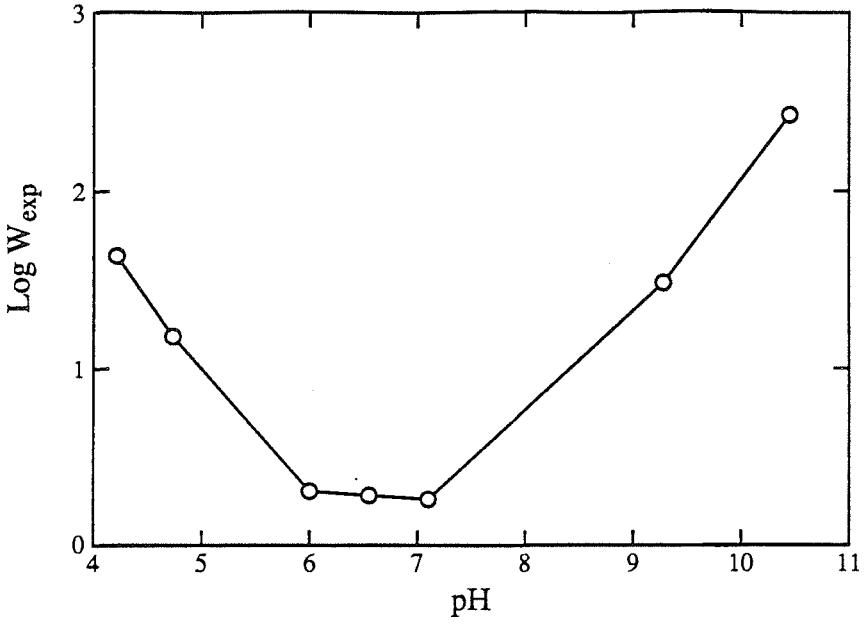

Figure 4.13: Experimentally derived stability ratio, W_{exp}, of a hematite suspension, plotted as a function of pH in the presence of 0.1 millimolar of phthalate ions. The ionic strength is 5 millimolar of NaCl.

molecular weight organic compounds. Naturally occurring organic substances, e.g., fulvic acid (FA) and humic acid (HA) were also used in the coagulation experiments. The results are compared in Fig. 4.14. The pH values of these experiments differ by less than 0.3 units. The evident features of these data are: (1) there is a sharp decrease of stability (100 times) within a factor of 10 increase in organic concentration, (2) the organic concentration for minimum colloid stability is between 10^{-5} and 10^{-4} g/l, (3) the slope of particle stability versus the concentration of organics is positive after the organic concentration is increased beyond the critical coagulation concentration (restabilization).

4.1.7.1 pH Variation

The stability of hematite particles as a function of pH was studied in the presence of fulvic acid (0.1 mg/l FA in ~17 mg/l hematite). The background ionic strength was kept at 5 millimolar with NaCl . Colloidal hematite of the desired solid concentration

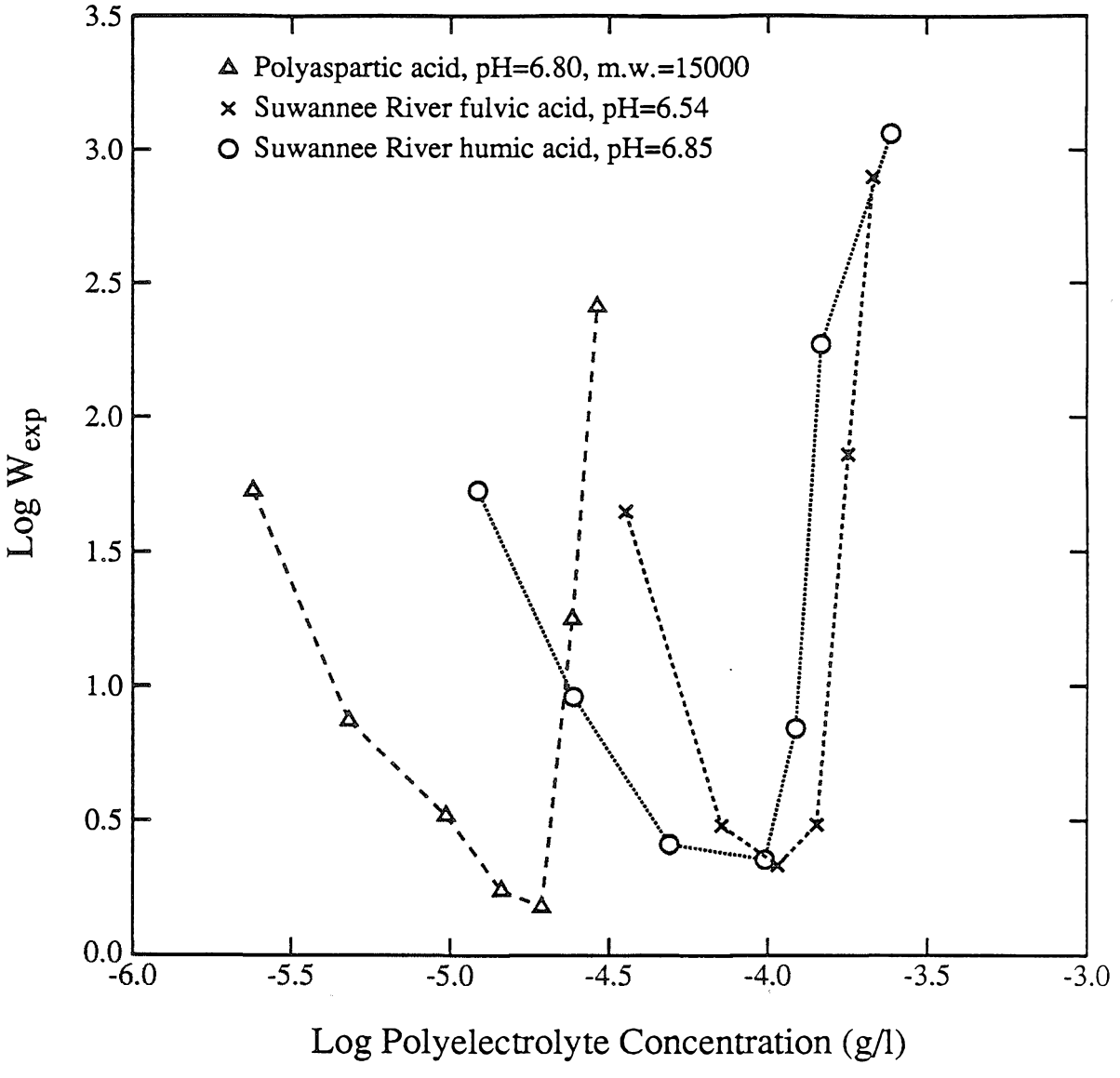

Figure 4.14: Experimentally derived stability ratio, W_{exp}, of a hematite suspension, plotted as a function of polyelectrolyte concentration in the presence of 1 millimolar NaCl.

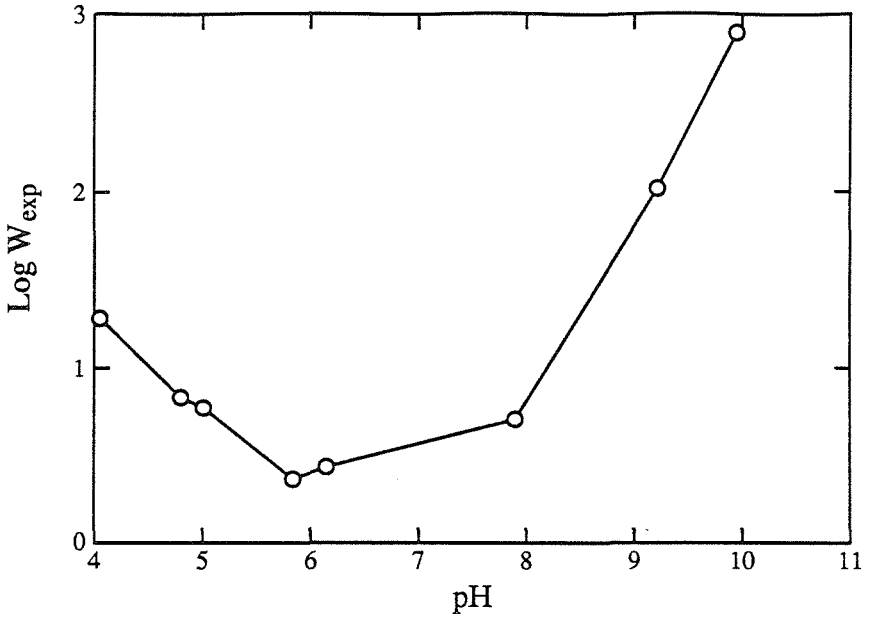

Figure 4.15: Experimentally derived stability ratio, W_{exp}, of a hematite suspension, plotted as a function of pH in the presence of 0.1 mg/l of fulvic acid. The ionic strength is 5 millimolar of NaCl.

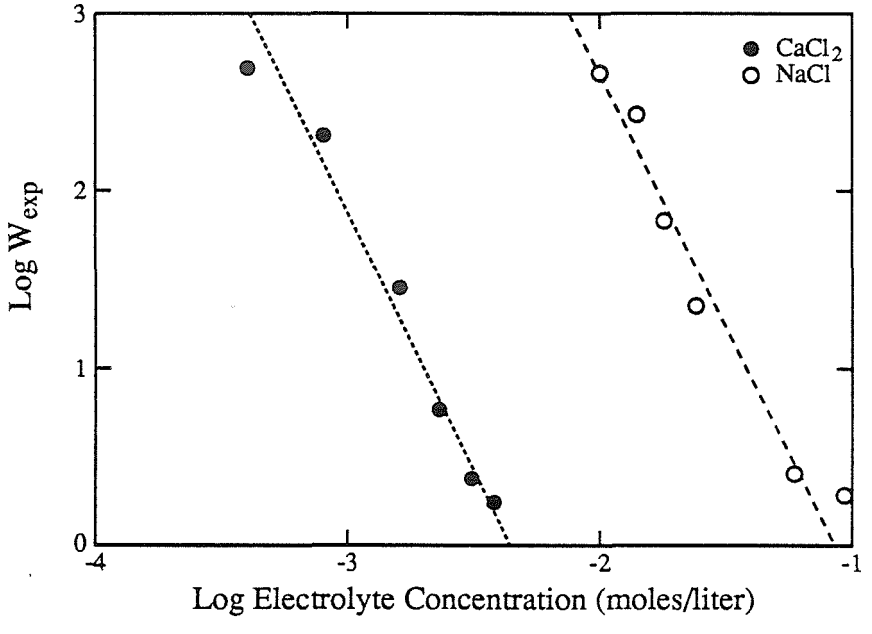

Figure 4.16: Experimentally derived stability ratio, W_{exp}, of a hematite suspension, plotted as a function of electrolyte concentration, after allowing 0.3 mg/l of humic acid to equilibrate with 17 mg/l of hematite particles at pH 6.3.

was prepared from stock, and pH values were adjusted to between 4 and 11. The results are presented in Fig. 4.15, which shows that the pH of minimum stability is approximately 7, compared with 8.5 in the absence of naturally occurring organic matter.

4.1.7.2 Variation of Electrolyte Concentration

Following the studies presented in Fig. 4.14, 0.3 mg/l of HA was added to hematite particles at pH$\sim$6.3. This amount of HA is sufficient to reverse the surface potential of the hematite particles from positive to negative (see discussion in Sec. 5.3.2). Thus it is expected that cations of different valency, such as Na^+ and Ca^{2+}, will not have the same effect on hematite stability. Figure 4.16 compares the effects of Ca^{2+} and Na^+ on hematite particle stability. The electrolyte concentration required to reach minimum stability is 30 times lower for $CaCl_2$ than that for NaCl.

4.1.8 Effect of Fatty Acids on Hematite Stability

Coagulation experiments were performed with the following fatty acids: propionic (3 carbon atoms, C3), caprylic (C8), capric (C10), and lauric (C12) acid. The supporting electrolyte concentration was maintained at 0.05 moles/liter with NaCl. Figure 4.17 shows the effect of the concentration of different fatty acids upon colloidal hematite stability. It can be seen that there is little or no effect on hematite stability when the fatty acid concentration is low. As the concentration of acids increases, the influence on hematite coagulation rate becomes noticeable. At first, the increase in acid concentration makes hematite less stable, and the minimum stability ratio is reached at the critical coagulation concentration. The stability ratio then increases if the fatty acid concentration is increased beyond the critical coagulation concentration. Although the plots of the coagulation rate versus acid concentration for C8, C10 and C12 resemble each other, the critical coagulation concentration values differ significantly. The successive critical coagulation concentrations differ by a factor of about 10. For the C3 data set the stability ratio flattens out when the C3 concentra-

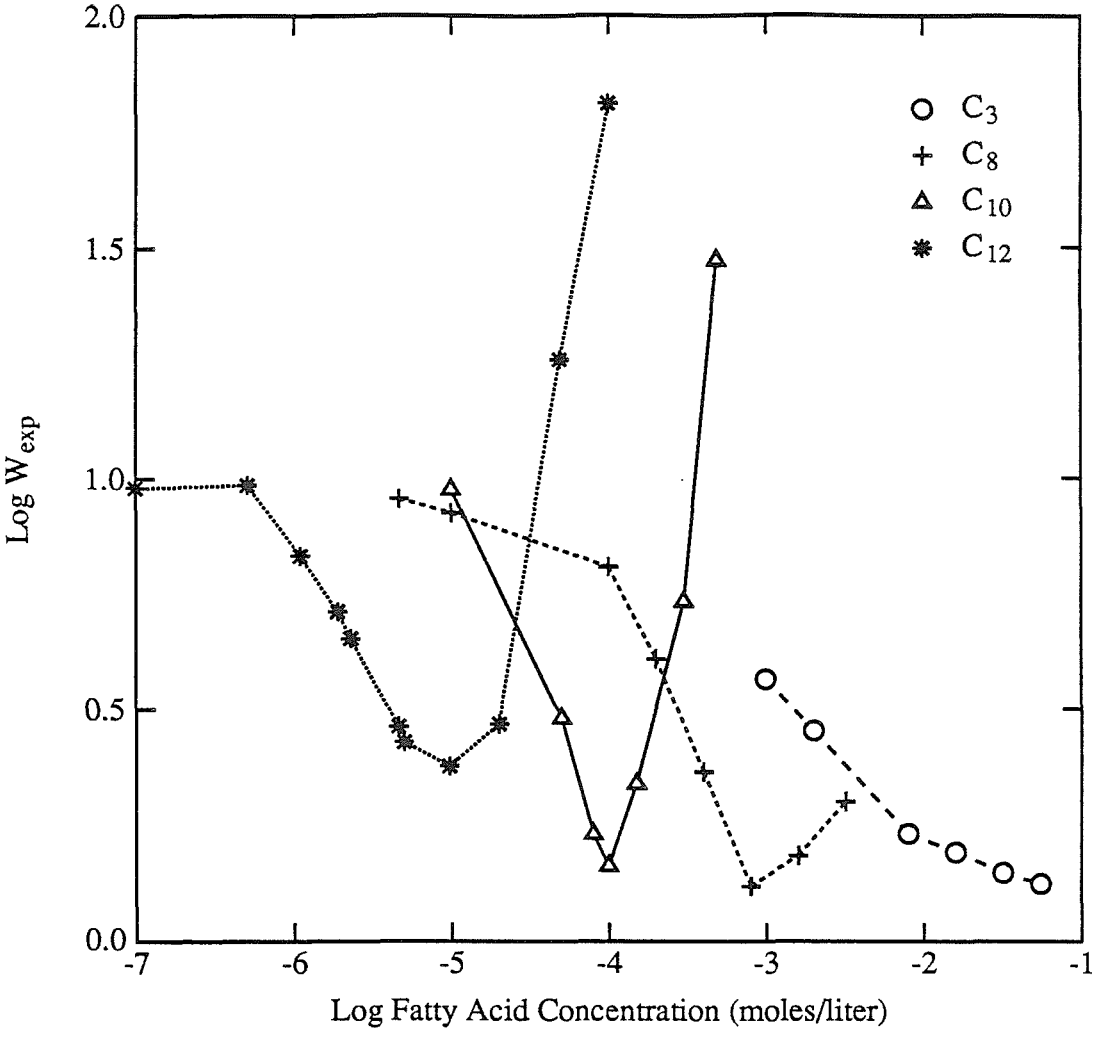

Figure 4.17: Experimentally derived stability ratio, W_{exp}, of a hematite suspension, plotted as a function of fatty acid concentration at pH 5.2. The ionic strength is 0.05M of NaCl.

tion is increased beyond the critical coagulation concentration. This behavior differs from that of fatty acids with a higher number of carbon atoms, which restabilize the suspension when their concentration is increased beyond the critical coagulation concentration.

4.2 Electrokinetic Properties of Colloidal Hematite

Electrokinetic techniques are widely used for obtaining information about the

charge and potential distribution at the solid/aqueous interface (Hunter, 1981). Depending on how the motion is induced there are four principal methods of obtaining electrokinetic information: (1) electrophoresis, (2) the streaming potential method, (3) electro-osmosis, and (4) the sedimentation potential method. In the this study micro-electrophoresis is used in which the movement of small particles, induced by an applied electric field, is viewed with the aid of a laser.

Oxide particles have a positive or negative charge due to proton adsorption. In natural water systems particles have been observed to be negatively charged (Tipping et al., 1981) due to the adsorption of both organic and inorganic dissolved anionic species. In the transition from river to estuary to open ocean, particles go through a concentration spectrum of electrolyte and the absolute value of their mobility is reduced as the result of diffuse layer compression by the high salt concentration (Hunter, 1981). Hence electrophoretic mobility data provide independent information on the sign of the surface charge, and the magnitude of this charge can be deduced by applying an appropriate model. Both non-specifically and specifically adsorbed ions in solution can reduce particle mobility. Specifically adsorbed ions are also capable of reducing the surface potential, and can reverse the surface potential if sufficient adsorbed species are present. In the electrophoretic mobility measurements described subsequently in this section the effects of pH and the type of specifically adsorbed ion are investigated. Both inorganic and organic specifically adsorbed species are considered. The importance of mobility measurements in relation to coagulation is discussed in Sec. 6.4.

4.2.1 pH and Mobility

For this and for all subsequent mobility measurements the temperature was maintained at 25° C. The effect of pH on the mobility of hematite particles at constant ionic strength is illustrated in Fig. 4.18. The two data sets differ by a factor of 10 in their ionic strength. It is observed that mobility of hematite in the presence of 0.05M

KCl is lower in magnitude than that in 0.005M KCl. It should also be noted that the two data sets intersect at about pH 8.5.

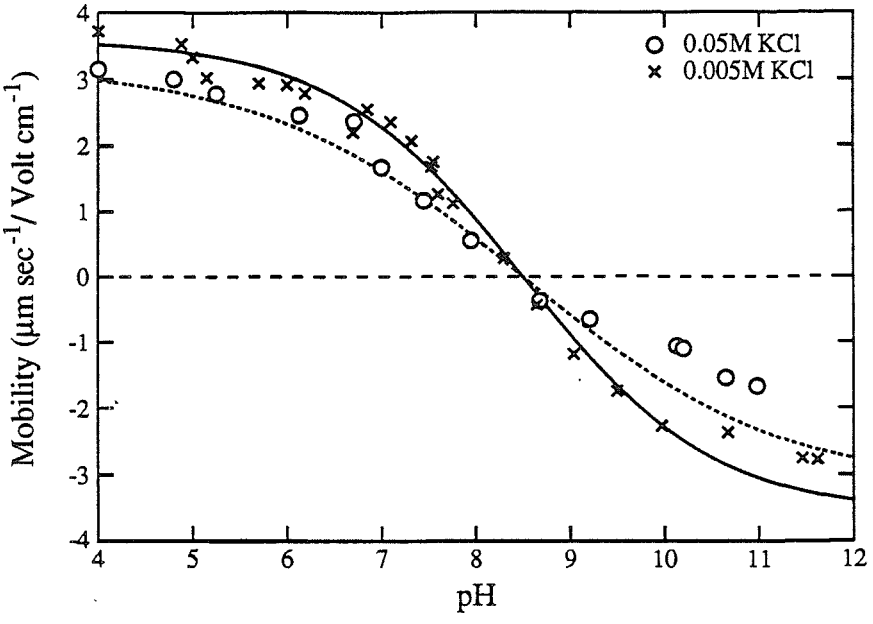

Figure 4.18: Electrophoretic mobility of a hematite suspension plotted as a function of pH. The ionic strength is adjusted by KCl, and is indicated in the figure.

4.2.2 Influence of Bivalent Ions: Sulfate and Magnesium

Hematite particle mobility was studied as a function of sulfate concentration at fixed pH. The ionic strength was 5 millimolar KCl, and the hematite particle concentration was 8.6 mg/l. Figure 4.19(a) shows that the mobility is reduced as sulfate concentration increases. At sulfate concentrations greater than 3 millimolar the sign of the mobility reverses. Figure 4.19(b) shows the influence of magnesium on hematite mobility. At pH 10.5 hematite particles are negatively charged in 5 millimolar KCl. As the magnesium concentration increases the particle mobility becomes less negative, and zero mobility is reached at a magnesium concentration of about 0.7 millimolar. In both cases, mobility is first reduced in magnitude as the concentration of bivalent ions increases, and subsequently the sign is reversed when the bivalent ion concentration is sufficiently high.

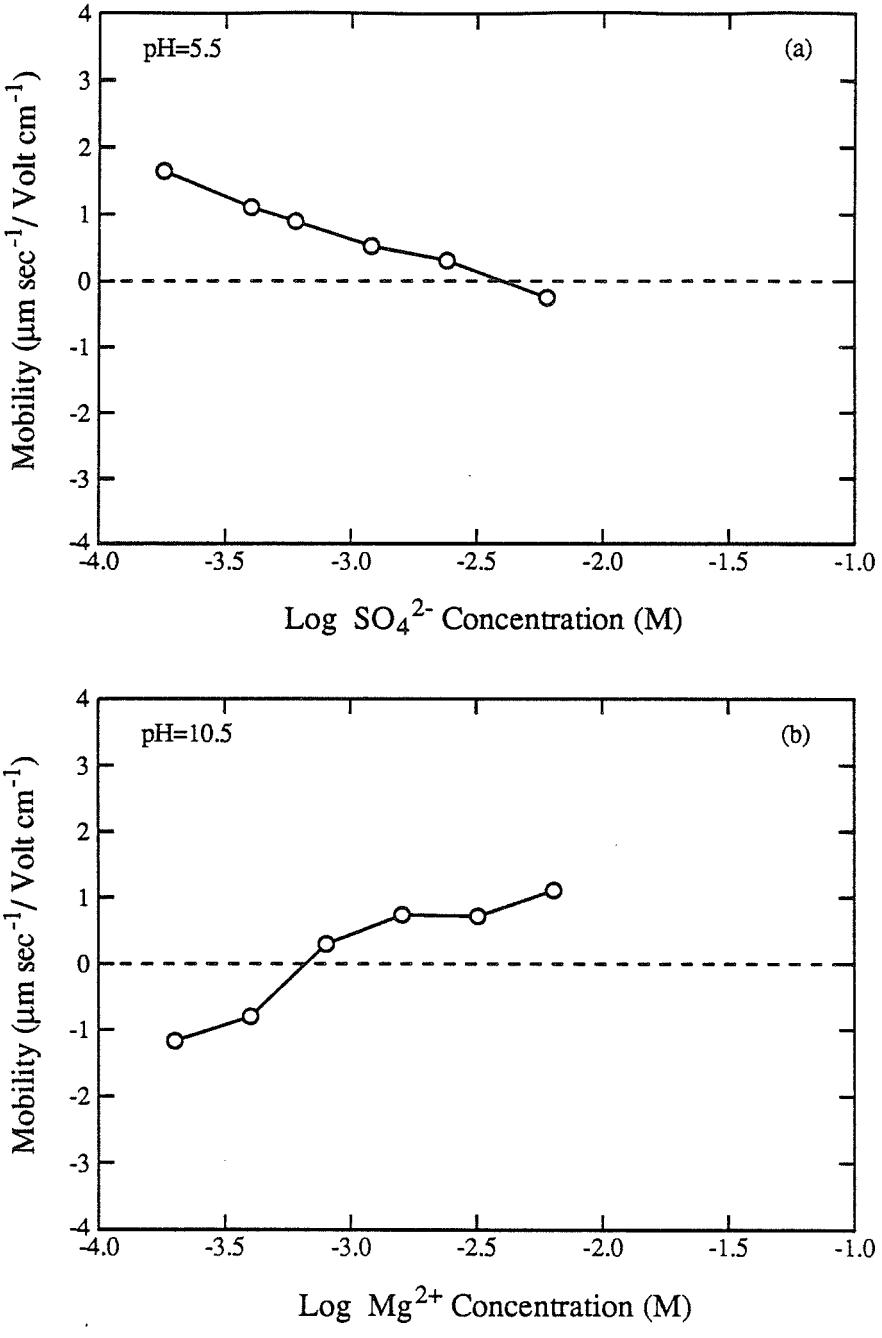

Figure 4.19: Electrophoretic mobility of a hematite suspension as a function of (a) sulfate concentration at pH 5.5, and (b) magnesium concentration at pH 10.5. The ionic strength is 0.005M of KCl, and the hematite concentration is 8.6 mg/l in both cases.

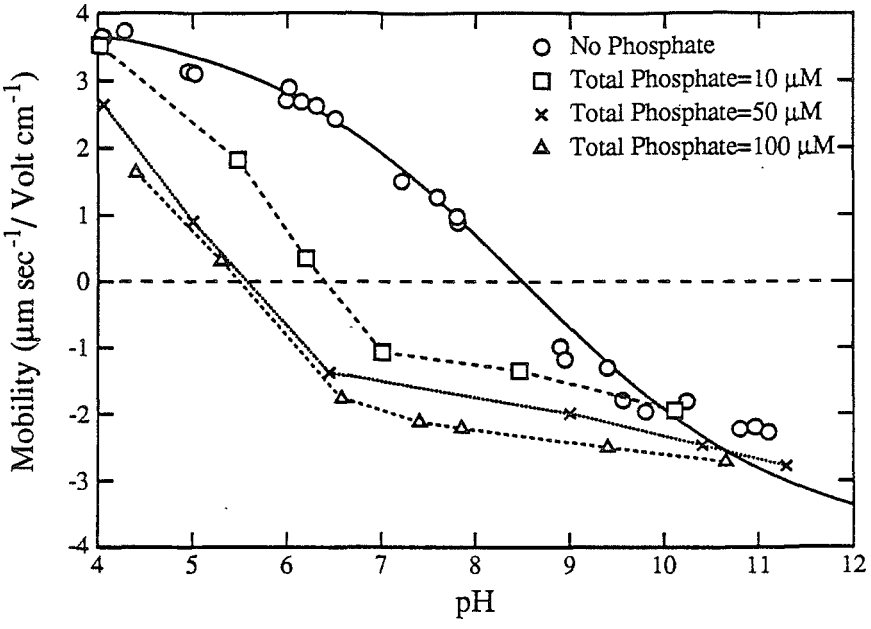

Figure 4.20: Electrophoretic mobility of a hematite suspension plotted as a function of pH in the presence of differing amounts of phosphate. The ionic strength is 0.01M of KCl, and the hematite concentration is 20.6 mg/l.

4.2.3 Influence of Phosphate on Hematite Mobility

The mobility of hematite particles was studied as a function of pH in the presence of phosphate. The results are shown in Fig. 4.20. The data set plotted on the far right-hand side has the same amount of KCl as the other data sets, but no phosphate was added. The phosphate concentration was varied from 10μM to 100μM and a significant shift in the pH of the isoelectric point, pH_{iep}, was observed, ranging from 2 units in 10μM phosphate to 3 units in 100μM phosphate.

4.2.4 Influence of Phthalate on Hematite Mobility

The electrophoretic mobility of hematite particles is influenced by the addition of phthalate ions, as illustrated in Fig. 4.21(a). At pH 6.2, hematite mobility is positive and of magnitude 2.4 $\mu m \cdot sec^{-1}/Volt \cdot cm^{-1}$ in 5 millimolar KCl. The presence of 0.2 millimolar phthalate ions in the suspension causes the mobility to be reduced to zero, and the mobility becomes negative when the phthalate ion concentration exceeds 0.2

millimolar.

Figure 4.21(b) shows the effect of varying pH in the presence of phthalate ions. The shift of pH_{iep} from 8.5 to 7.5 in the presence of 0.1 millimolar phthalate ions indicates there is a specific affinity of phthalate ions toward the surface iron-hydroxyl groups. The mobility range, however, is not as high as in the presence of phosphate ions (see Fig. 4.20), indicating that phthalate is not adsorbed as strongly as phosphate.

4.2.5 Influence of Fulvic Acid on Hematite Mobility

Fulvic acid was chosen as an example to study the effect of polymeric materials on hematite mobility. Figure 4.22 shows hematite mobility as a function of fulvic acid concentration for an ionic strength of 5 millimolar of KCl. At pH 6.6, in the absence of any specifically adsorbed species, the mobility is 2 $\mu m \cdot sec^{-1}/Volt \cdot cm^{-1}$. Fulvic acid is able to reduce the positive mobility to zero at a concentration of approximately 0.1 mg/l, and a further increase in acid concentration results in a sharp change in particle mobility to a large negative value.

The pH dependence of mobility in the presence of 0.1 mg/l fulvic acid is illustrated in Fig. 4.23. As a consequence of the addition of fulvic acid the value of pH_{iep} is shifted by approximately 2 units.

4.2.6 Influence of Fatty Acids of Varying Chain Length

The electrophoretic mobility of hematite in the presence of caprylic (C8), capric (C10) and lauric (C12) acid was studied and the results are summarized in Fig. 4.24. The supporting ionic strength is 5 millimolar KCl and the pH value is approximately 5.2. The mobility changes most rapidly when it is close to zero, while at larger absolute mobility values the slope is smaller, as was also seen in the case of fulvic acid (see Fig. 4.22). The three curves in Fig. 4.24 resemble each other in their general shape, but differ in the acid concentration at which zero mobility is attained. It can be seen that the fatty acid concentration required to achieve zero mobility is less for

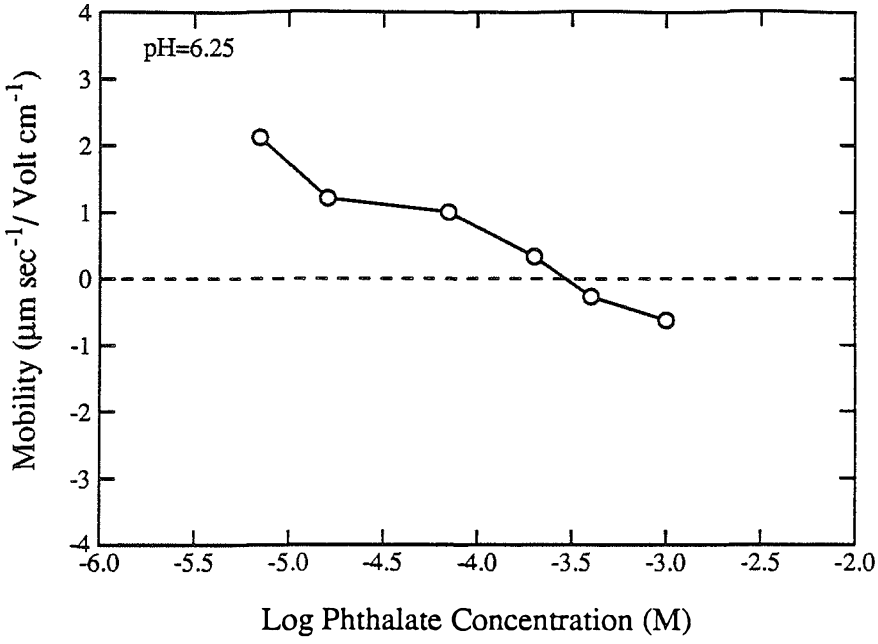

Figure 4.21(a): Electrophoretic mobility of a hematite suspension as a function of phthalate concentration at pH 6.25. The ionic strength is 0.005M of KCl, and the hematite concentration is 8.6 mg/l.

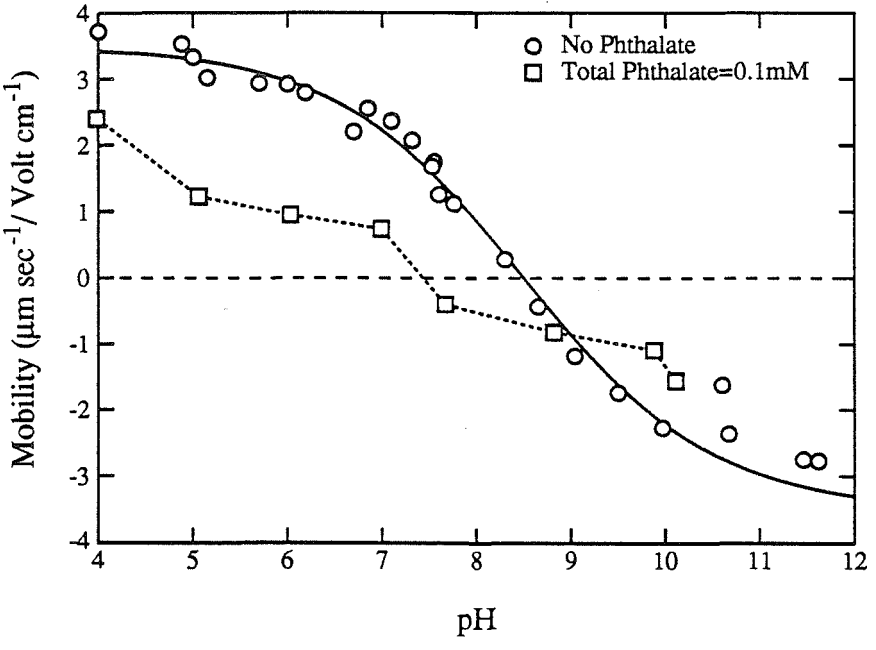

Figure 4.21(b): Electrophoretic mobility of a hematite suspension as a function of pH in the presence of 0.1mM of phthalate ions. The ionic strength is 0.005M of KCl, and the hematite concentration is 8.6 mg/l.

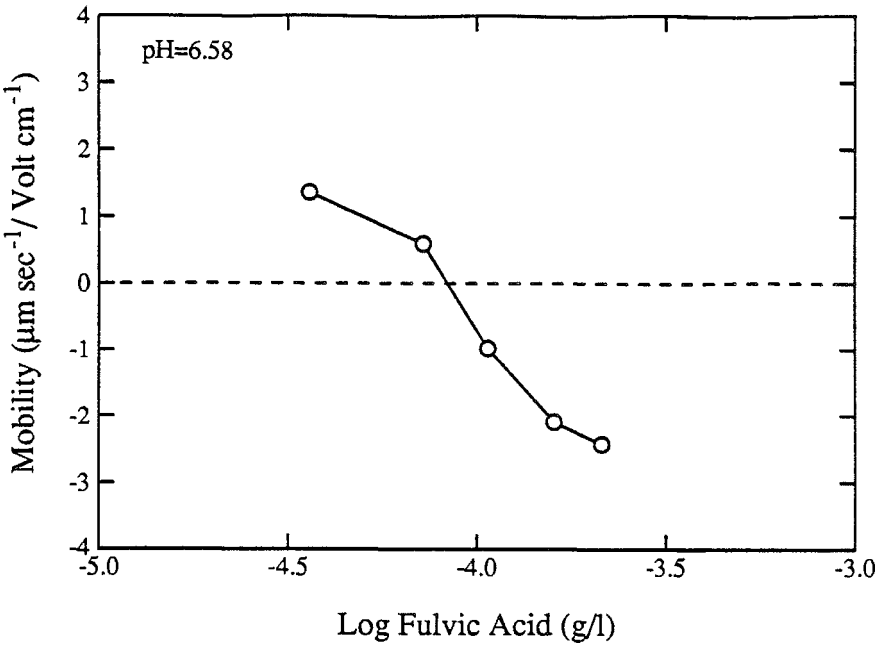

Figure 4.22: Electrophoretic mobility of a hematite suspension as a function of fulvic acid concentration at pH 6.58. The ionic strength is 0.005M of KCl, and the hematite concentration is 8.6 mg/l.

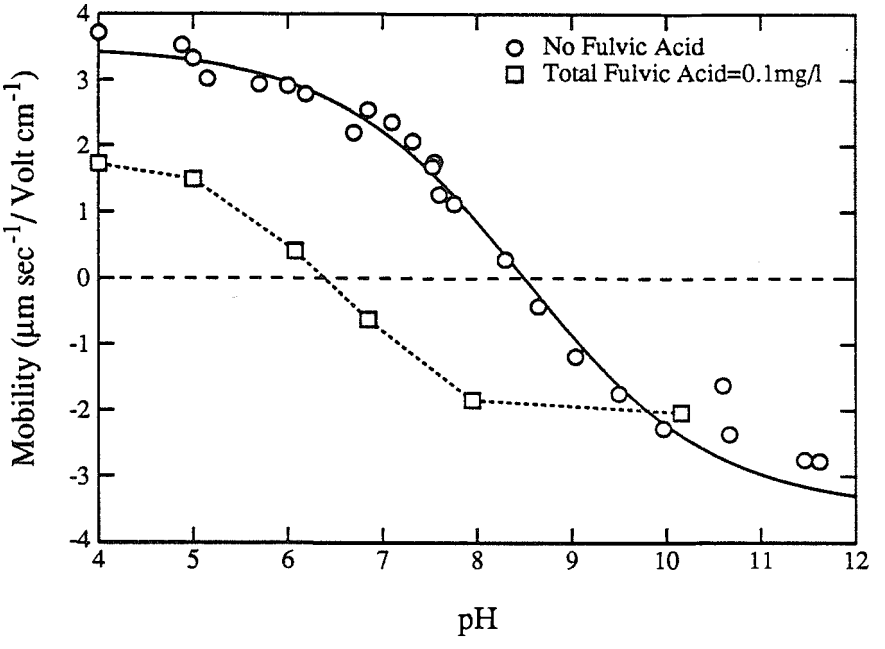

Figure 4.23: Electrophoretic mobility of a hematite suspension as a function of pH in the presence of 0.107 mg/l of fulvic acid. The ionic strength is 0.005M of KCl, and the hematite concentration is 8.6 mg/l.

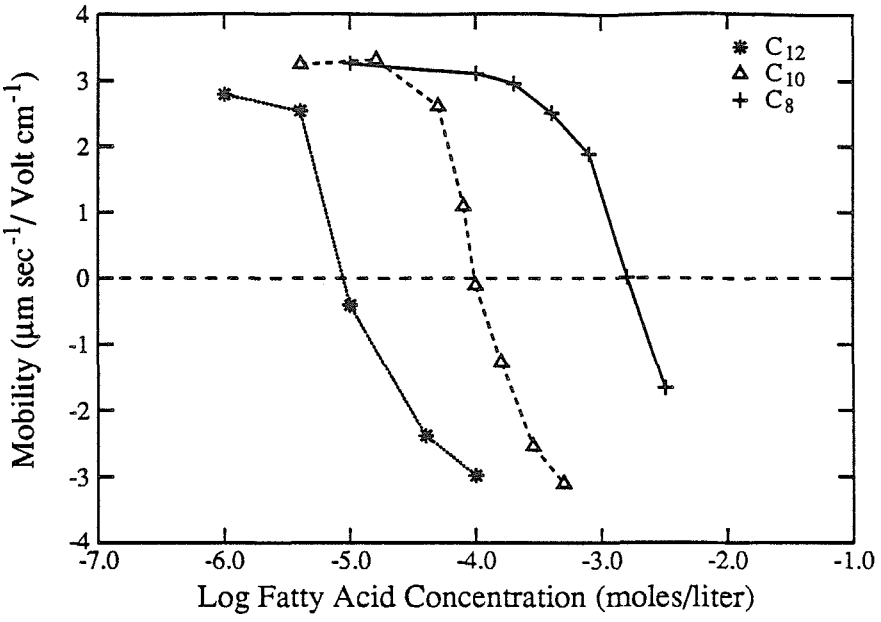

Figure 4.24: Electrophoretic mobility of a hematite suspension as a function of fatty acid concentration at pH 5.15. The ionic strength is 0.005M of KCl, and the hematite concentration is 8.6 mg/l. Lauric acid is denoted by C_{12}, capric acid by C_{10}, and caprylic acid by C_8.

molecules with a longer carbon chain length, and differs by a factor of 10 between C8 and C10, and between C10 and C12 for this set of experimental conditions.

4.3 Adsorption Results

A key to understanding particle stability and coagulation is the role of simple chemical changes in the aqueous phase which alter the electrostatic repulsive forces between particles. Mobility measurements are very useful in providing information on the sign and magnitude of particle surface charges due to chemical changes in the aqueous phase. Adsorption isotherms can yield quantitative chemical properties, such as the affinity of adsorbates for the particle surface. By applying an appropriate physical chemical model to absorption data equilibrium adsorption constants can be derived. With these constants the surface speciation and charge variation with pH can be calculated. By constructing a physical chemical model of the interface, surface

charges can be converted to potentials, which are used as input data for modeling particle mobility and stability (see Sec. 6.4). To understand the importance of the role played by adsorption in both coagulation and electrokinetic measurements adsorption isotherms were constructed.

4.3.1 Adsorption of Protons

Acid-base titration of a metal oxide in aqueous suspension is an effective means of obtaining the strength and extent of adsorption of protons and hydroxide ions on the surface of oxides. Titration of hematite particles was carried out in this research (see Sec. 3.2.3 for the procedure) and a detailed account of the modeling of the surface equilibrium constants is given in Sec. 2.4. For completeness, the results of the titration experiments are shown in Fig. 4.25, where surface charges derived from Eq. (2.34) are plotted against pH. The ionic strength was controlled by adding NaCl to yield final concentrations ranging from 0.0025M to 0.1M. The common intersection of the data sets indicates that the pH_{zpc} is at 8.5. It should be noted that at a given pH a higher surface charge corresponds to a more concentrated ionic medium. At first, this observation may appear to contradict the results of the electrokinetic mobility measurements (Fig. 4.18), where a lower mobility is associated with higher ionic strength. In fact, these results are consistent and can be explained by surface coordination chemistry and the diffuse layer model (see discussion in Sec. 5.1).

4.3.2 Adsorption of Phosphate

Phosphate forms strong complexes with Fe^{3+} in aqueous solution and the formation of such complexes on iron oxide surfaces has been studied by Sigg (1979) using goethite and Breeuwsma (1973) using hematite particles. Sigg applied the constant capacitance model to phosphate adsorption data and derived surface equilibrium constants. Since the equilibrium constants are model dependent, direct application of these constants to a diffuse layer model is not appropriate. In order to take advantage of existing data, the adsorption of phosphate as a function of pH was first estimated

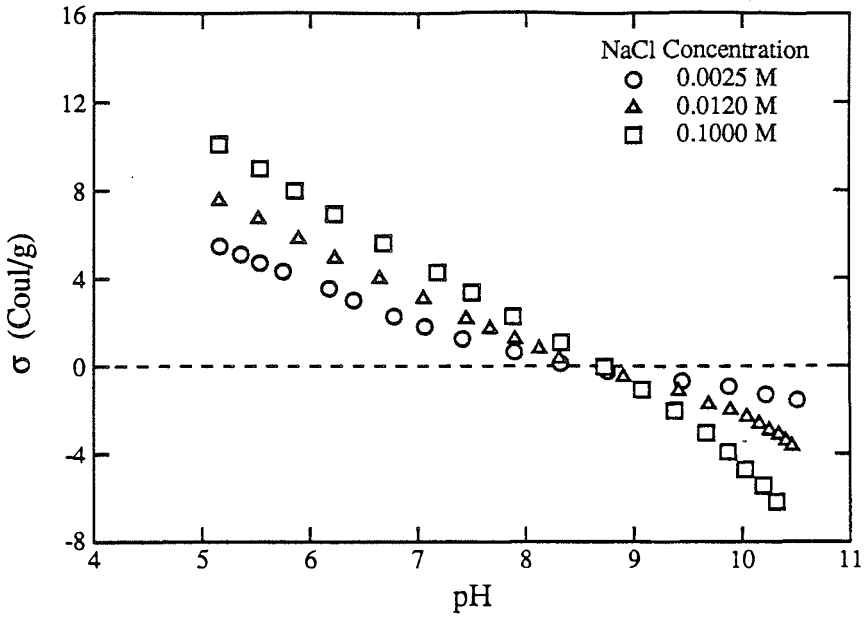

Figure 4.25: The surface charge, σ_0, on hematite particles plotted as a function of pH for differing ionic strengths.

according to Sigg's equilibrium constants based on the constant capacitance model, and adsorption experiments of phosphate as a function of pH were then conducted. Surface potential and charge are dependent on pH (see Fig. 4.25), so phosphate adsorption is expected to be enhanced by a positively charged surface at pH<pH_{zpc}, and inhibited at a negatively charged surface. Hence, knowledge of the experimental variation of the adsorption with pH is especially valuable since it permits modeling of the electrostatic influence on of phosphate on adsorption. Fig. 4.26 shows phosphate adsorption as a function of pH, where hematite particle concentration is 20.6 mg/l, the initial phosphate concentration is 50μM and the ionic strength is 5 millimolar. Within the range of pH studied, the adsorption decreases as the the pH increases. The adsorption data show a good agreement with those of Sigg's work and Breeuwsma's work. At pH>$pH_{zpc}$the adsorption is still significant; this indicates that phosphate has a strong affinity for the hematite surface. Surface equilibrium constants are derived using the SURFEQL computer model, and are presented in

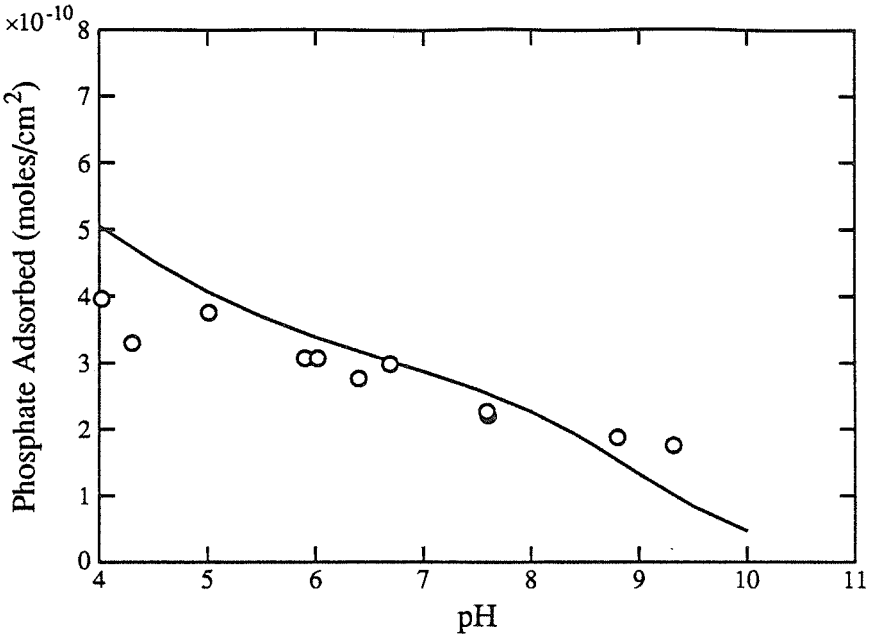

Figure 4.26: Phosphate adsorption as a function of pH for a hematite suspension. The initial phosphate concentration is 50μM, and the ionic strength is 5 millimolar. The solid line represents the results of the SURFEQL model (see Sec. 5.3).

Sec. 5.3.

4.3.3 Adsorption of Phthalate

In the coagulation and electrophoretic mobility measurements, phthalate ions have been shown to have specific chemical interaction with iron surfaces, although the surface complexes of phthalate are not as strong as those of phosphate. Balistrieri and Murray (1987) showed that the affinity of phthalic acid for the goethite surface lies between that of oxalic and salicylic acid. Adsorption of phthalic acid was investigated in this research. The procedure is described in Sec. 3.3.2 and the results are illustrated in Fig. 4.27. The y-axis is the concentration of adsorbed species expressed in moles of phthalate ions per square centimeter of surface area, and the x-axis shows the concentration remaining in solution in moles per liter. The solid mass concentration was 17.6 mg/l, the pH of the suspension was 6.2, and the supporting electrolyte concentration was 5 millimolar of $NaClO_4$. At constant pH, the adsorption of anions

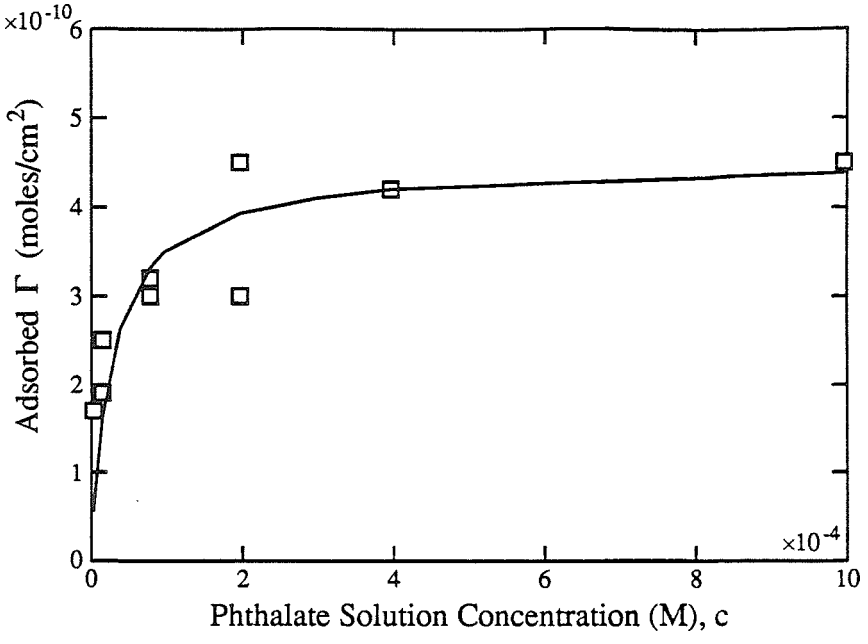

Figure 4.27: Adsorption density, Γ, of a hematite suspension as a function of phthalate concentration. Hematite concentration was 17.6 mg/l, pH=6.2 and ionic strength was 5 millimolar of $NaClO_4$. The solid line is modeled by the Langmuir isotherm, as discussed in the text.

is typically described by the Langmuir adsorption isotherm in the following form (Stumm and Morgan, 1981),

$$\Gamma = \frac{c \cdot K \cdot \Gamma_m}{1 + cK} \tag{4.5}$$

where Γ is the adsorption density which is expressed in moles/cm^2. Γ_m is the maximum adsorption density, expressed in the same units as Γ. c is the anion activity in M and K is the adsorption equilibrium constant which indicates the affinity of the anion for the surface. The unit of K is the reciprocal of the unit for anion activity, i.e., K is in M^{-1}.

Applying the Langmuir method to the data in Fig. 4.27, the maximum adsorption density, Γ_m, is found to be 4.5×10^{-10} moles/cm^2, which corresponds to 2.7 molecules/nm^2 or about one half of the surface hydroxide site density, Sd. This maximum coverage is equivalent to each molecule occupying 37Å^2. The equilibrium

constant K is derived as 3.5×10^4 M^{-1}. An electrostatic correction has not been applied to this equilibrium constant, and hence it is a conditional quantity. The general form of the equilibrium constants based on surface complex formation may account for the pH dependency; this is presented in Sec. 5.3.1.

4.3.4 Adsorption of Fatty Acids

Among the four fatty acids studied in the coagulation and electrophoretic mobility measurements, lauric acid (C12) had the largest effect on hematite stability; the concentration of fatty acid required to minimize the hematite stability is least for C12. Therefore, lauric acid was used in the adsorption studies to investigate the affinities of fatty acids for the hematite surface. For comparison the solid concentration was chosen to be similar to that used in the coagulation experiments (35.5 mg/l of Fe_2O_3). The ionic strength of the adsorption media was adjusted with NaCl to 0.05M and the pH was 5.2. Figure 4.28 shows amount of lauric acid (C12) adsorbed per unit surface area (in units of moles/cm^2) as a function of solution concentration in moles/liter. Unlike the adsorption data for phthalic acid (Fig. 4.27), the plot does not show the Langmuir adsorption behavior. Instead an exponential increase in adsorbed C12 is observed. The adsorption driving force has been postulated to be a combination of electrostatic interaction, specific chemical affinity, and hydrophobic interaction (Fuerstenau, 1981 and Ulrich et al., 1988).

There are two hypotheses regarding the configuration of the adsorbed species on the surface of particles. One group of researchers postulate that at low adsorbate concentration the surface coverage is not substantial. Fatty acid molecules may be adsorbed and lay flat on the solid surface. At high solution concentration, lateral interaction among fatty acids through the hydrophobic effect promotes adsorption and hemimicelle formation may result (see Fig. 5 of Gaudin and Fuerstenau, 1955). Another group of researchers (Gschwend, 1988) believe that carboxylate ions are attracted to the region next to a particle surface due to the Coulombic force, and micelle

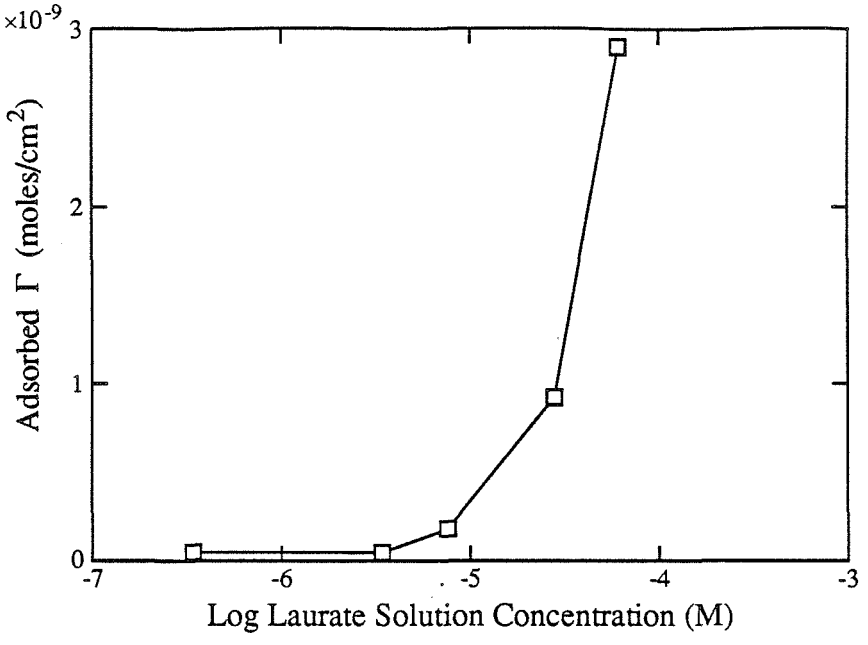

Figure 4.28: Adsorption density, Γ, of a hematite suspension as a function of laurate concentration. Hematite concentration was 35.5 mg/l, NaCl concentration was 0.05M and pH was 5.2.

formation may result if the anion concentration exceeds the critical micelle concentration. The data of this thesis seem to be consistent with the former hypothesis. The rapid increase in adsorbed C12 as a function of solution concentration shown in Fig. 4.28 can be explained by the lateral interaction of CH_2 groups in the hydrophobic tails. The monolayer coverage is determined by the size of the C12 molecule. For the carboxylate head group, the cross-sectional area is determined by the film pressure area isotherm method (Adamson, 1982) to be 20.5 Å^2. This corresponds to a monolayer coverage of 8×10^{-10} moles/cm^2, where the solution concentration is 3×10^{-5} M for the solid concentration used. At the adsorption pH condition (pH 5.2), the titration data in the absence of organic acid shows that the surface charge σ_0 is 0.11 coul/m^2, which corresponds to 8×10^{-11} moles/cm^2. The adsorption of fatty acid at monolayer coverage is sufficient to reverse the surface potential. The electrophoretic mobility data from Fig. 4.24 agree with this interpretation. A total C12 concentration of 8×10^{-6} M is able to bring the mobility to zero, and a negative

mobility is observed at a C12 concentration of 3×10^{-5}M.

The adsorption results in Fig. 4.28 can be quantified in terms of a surface complex formation reaction:

$$\equiv\text{FeOH} + \text{H}^+ + \text{L}^- \rightleftharpoons \equiv\text{FeL} + \text{H}_2\text{O} \tag{4.6}$$

where L represents the ligand, in this case laurate ions. The equilibrium constant is given by:

$$K_{HL} = \frac{(\equiv\text{FeL})}{(\equiv\text{FeOH})(\text{H}^+)(\text{L}^-)} \tag{4.7}$$

There are at least three contributions to the equilibrium constant: electrostatic interaction ΔG_{ele}, intrinsic chemical reaction ΔG_{chem}, and hydrophobic effects ΔG_{hyd}. In mathematical terms:

$$RT \ln K_{HL} = \Delta G_{ele} + \Delta G_{chem} + \Delta G_{hyd} \tag{4.8}$$

A detailed model calculation is presented in Sec. 5.3.3.

Both electrophoretic mobility data and stability data indicate that the affinities of fatty acids for hematite surfaces vary with the number of carbon atoms in their molecules. The relation of lauric acid adsorption to that of other fatty acids will be discussed in Sec. 5.3.3.

5. DISCUSSION OF RESULTS

5.0 Introduction

This chapter discusses the results presented in the previous chapter. Whenever possible discussions are based upon three data sets, namely, adsorption, electrokinetic mobility and stability of hematite particles. Adsorption of aqueous species on hematite accounts for the change in surface charge and potential as aqueous chemical conditions are varied, and mobility is a direct measure of the ζ-potential change as a result of this adsorption. Hematite stability can be interpreted on the basis of chemical reactions at the solid/aqueous interface.

5.1 The Effect of pH Variation

The suspension pH is a key chemical parameter in controlling adsorption, mobility, and particle stability. Figure 5.1 compares the surface charge density, electrophoretic mobility and stability ratio of hematite particles as a function of pH. (All these data and subsequent data shown in this chapter have been presented in chapter 4.) At pH_{zpc}, the surface charge density is zero, and the mobility is also zero. The stability ratio at this pH is a minimum. At extremes of pH, high surface charge densities are associated with high mobilities and stabilities for a given ionic strength. Comparing the data in panels (a) and (b) of Fig.5.1, at a constant pH, a higher surface charge corresponds to a more concentrated ionic medium, whereas a lower mobility is associated with high ionic strength. These observations seem to contradict each other,

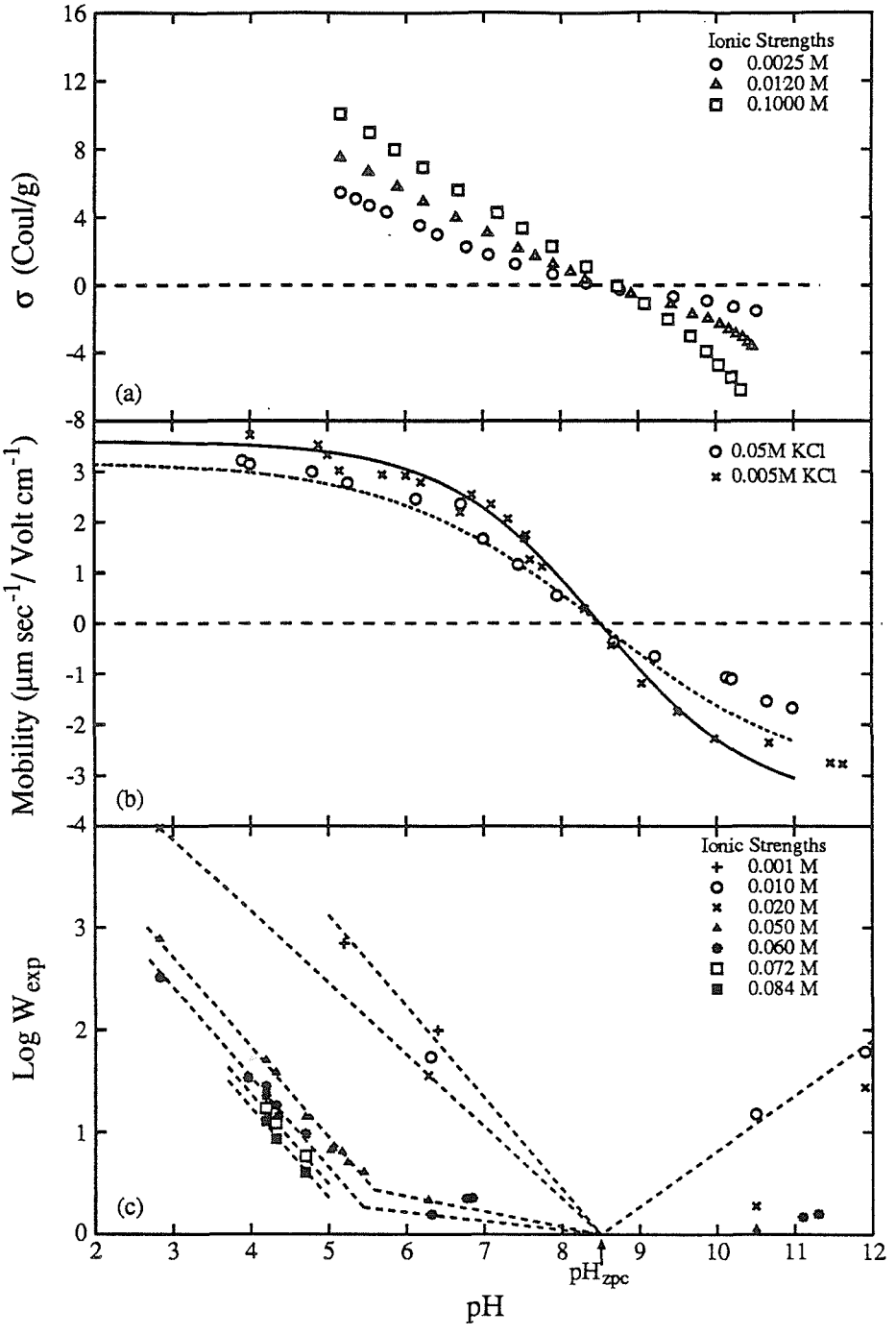

Figure 5.1: Comparison of hematite surface charge, σ, mobility, and stability ratio, W_{exp}, as a function of pH. Note that at pH_{zpc} the net surface charge and mobility are both zero, and the stability is a minimum.

hence it raises the following issues: (1) how to describe a solid/aqueous interface, (2) among available models which one is the most realistic and can be used to explain the interfacial charge and potential of hematite particles.

5.1.1 Description of the Physical Chemical Model

It has been recognized that protons are bonded to the surface of hematite particles through chemical reactions, and thus provide surface charge and potential at the metal oxide surface. Here protons are termed "potential determining ions" because of (1) the existence of chemical bonding between these ions and the surface groups, and (2) the alteration of surface potential as a result of the adsorption of these ions. According to this definition, potential determining ions are not limited to protons but include any ions which satisfy the conditions (1) and (2) above. For example, phosphate is considered a potential determining ion on hematite surfaces. This differs from the original definition of potential determining ions by Verwey and Overbeek (1948). Having a AgI colloid in mind, they defined Ag^+ and I^-, which also occur in the solid lattice, as the potential determining ions. They further showed that a changes in the concentration of ions in the solution phase results in a potential change on the surfaces given by the simple expression,

$$\Psi_0 = \frac{2.3RT}{F} \log \frac{c}{c_0} \tag{5.1}$$

where c_0 is the concentration of potential determining ions (here Ag^+ ions) at the zero point of charge.

In the case of hematite a simple application of Eq. (5.1) to yield the following is, in general, not valid,

$$\Psi_0 = \frac{2.3RT}{F}(pH_{zpc} - pH) \tag{5.2}$$

Equation (5.2) is based solely on electrochemical considerations. The surface speciation and charge as a function of solution pH have to be calculated through a chemical equilibrium within a coordination chemical framework.

The surface groups of a metal oxide are amphoteric and the surface chemical reactions have been written in Eq. (2.32) with the equilibrium constants expressed by Eq. (2.33). This model of oxide surface chemistry has been effectively applied to titration and adsorption data of metal oxides. Electrostatic effects have been accounted for differently, depending on the physical picture of the solid-aqueous interface assumed in each model. As a result, the intrinsic equilibrium constants for a metal oxide are usually model dependent.

The commonly used surface models are the Stern layer model, the diffuse layer model, the triple layer model and the constant capacitance model, all of which are described by Westall and Hohl (1980). In the description of interfacial structure the first three models are common in having a Gouy layer in the solution phase, but differ in the number of mean planes at which ions are placed. The constant capacitance model, however, has no diffuse layer in the solution phase. Instead, it is assumed that there is a mean plane in the solution phase where opposite charges are located.

The constant capacitance model can be viewed as a special case of the Stern model, where the diffuse layer vanishes. Consider a single flat surface whose interface is described by the Stern model, the total capacitance, C_t, is composed of C_1, the inner layer capacitance, and C_d the diffuse layer capacitance. The total capacitance is given by $1/C_t = 1/C_1 + 1/C_d$, where $C_d = d\sigma_d/d\Psi_d = A_1\sqrt{I}\cosh(zF\Psi_d/2RT)$ (Hunter, 1981). A schematic representation of C_t as a function of Ψ is illustrated in Fig. 5.2. This shows that the constant capacitance model is only valid at high ionic strength and/or low surface potential. Hence, to describe surface speciation over a span of ionic strength or potential, the constant capacitance model cannot be used.

5.1.2 The Charge-Potential Relationship of the Diffuse Layer Model

The diffuse layer model is applied to hematite surface speciation in this study for its simple physical representation of the interface, and because it has the least number of fitting parameters. In Fig. 5.3 the relationship between potential and distance from

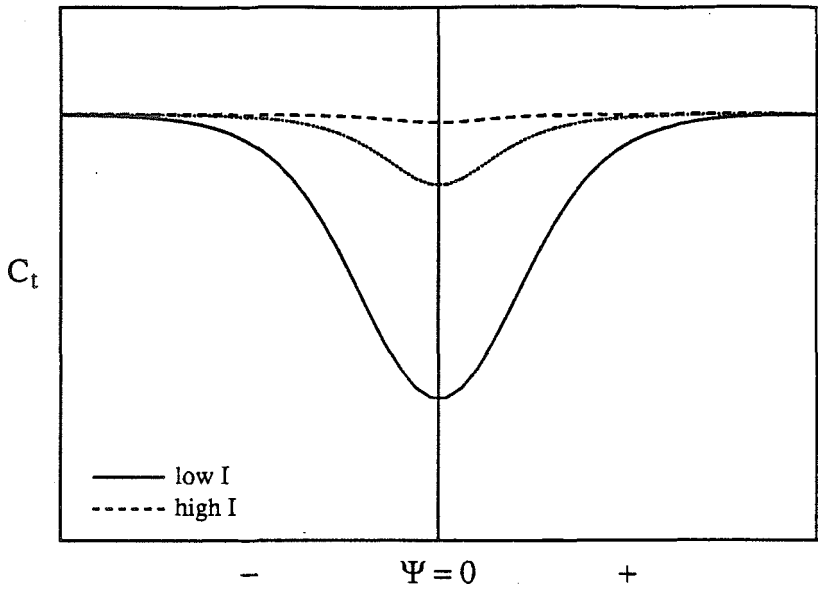

Figure 5.2: Schematic representation of the variation of the total capacitance, C_t, as a function of surface potential, as predicted by the Stern model. Curves for three different ionic strengths are shown.

the particle surface is illustrated. The potential determining ions are situated at the solid surface denoted as the σ_0 plane, and the counter ions are diffusely distributed in the solution phase according to the Boltzmann distribution. The relationship between Ψ_0 and σ_0 for a flat surface is given by (Verwey and Overbeek, 1948):

$$\sigma_0 = -\epsilon\epsilon_0 \left(\frac{d\Psi}{dx}\right)\Big|_{x=0} \tag{5.3}$$

or,

$$\sigma_0 = A\sqrt{I}\sinh\left(\frac{zF\Psi_0}{2RT}\right) \tag{5.4}$$

According to Eq. (5.4), the surface charge is proportional to the square root of the solution ionic strength, and therefore a lower surface charge is expected for low ionic strength. Fig. 5.3 illustrates the potential distribution at an aqueous/solid interface for two ionic strengths. At lower ionic strength the value of $(d\Psi/dx)|_{x=0}$ is smaller, and hence, by Eq. (5.3) yields a lower surface charge. Although the discussion is based on a plane surface, it can be applied to a spherical electric diffuse layer in the

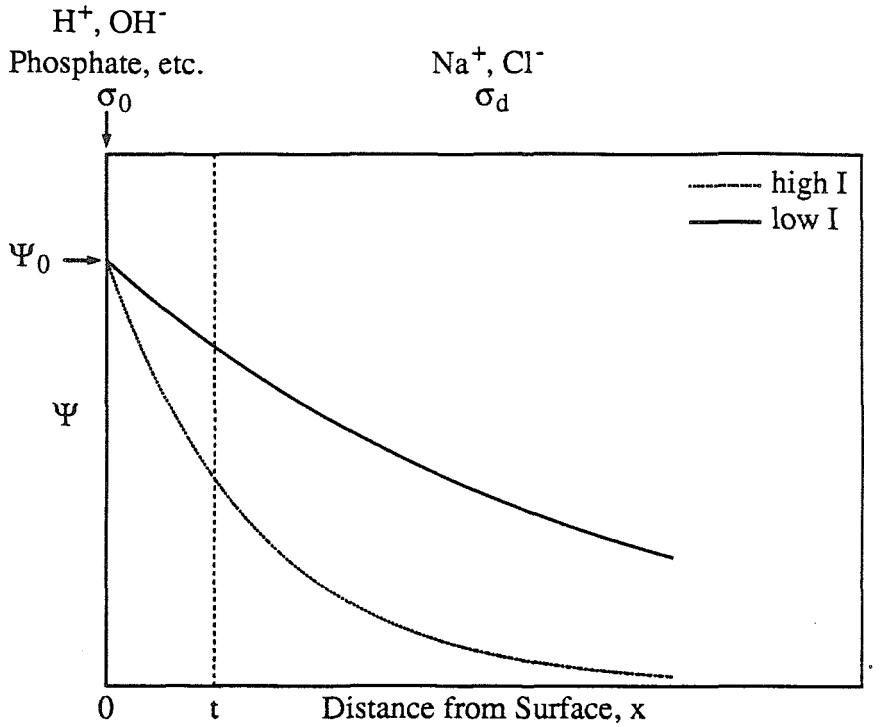

Figure 5.3: Schematic representation of the relationship between potential, Ψ, and distance from a flat surface, x, for high and low ionic strengths. Ions such as H^+, OH^- and phosphate are surface potential determining ions, located on the particle surface, whereas Na^+ and Cl^- are found in a diffuse layer around the particle.

limiting case, i.e., $\kappa a > 1$ (where no general analytical solution is available). Under such conditions σ_0 is still proportional to $\sqrt{I}$, as in the case of a plane surface. Thus the surface charge density is expected to be high at high ionic strength, as is observed in the titration data (Fig. 5.1(a)).

5.1.3 Particle Mobility, Surface Potential and the ζ-Potential

The electrokinetic mobility data can be transformed into potential values using the treatment presented by Wiersema et al. (1966) (see Appendix B). The potential calculated is proportional to the electrokinetic mobility, but usually differs from the surface potential because electrophoresis involves a tangential displacement of liquid along a particle surface. The mean plane at which the bulk liquid is separated from

the liquid dragged by a particle is called a slipping plane, and the potential on this plane is defined as the ζ-potential. The ζ-potential is usually less than the surface potential and is very sensitive to changes in the ionic strength (Dzombak and Morel, 1987).

The relationship between surface potential and ζ-potential depends on the physical model of the interface adopted. If it is assumed that the Gouy-Chapman diffuse layer model applies to hematite particles and that $\kappa a > 1$, the solution to a flat double-layer is applicable. This is derived as follows. The fundamental differential equation governing the potential and charge at the interface is (Eq. 2.18),

$$\nabla^2\Psi = \kappa^2 \frac{\sinh(zF\Psi/\mathrm{RT})}{(zF/\mathrm{RT})} \tag{5.5}$$

Substituting,

$$y = \frac{zF\Psi}{RT}, \quad y_0 = \frac{zF\Psi_0}{RT}, \quad \xi = \kappa x \tag{5.6}$$

and applying the boundary conditions $y \to 0$, $dy/d\xi \to 0$ as $\xi \to \infty$, the solution is (Verwey and Overbeek, 1948),

$$\mathrm{e}^{y/2} = \frac{\mathrm{e}^{y_0/2} + 1 + \left(\mathrm{e}^{y_0/2} - 1\right)\mathrm{e}^{-\xi}}{\mathrm{e}^{y_0/2} + 1 - \left(\mathrm{e}^{y_0/2} - 1\right)\mathrm{e}^{-\xi}} \tag{5.7}$$

Equation (5.7) is an implicit relationship between Ψ_0 and $\Psi(x)$, and can be used to evaluate $\Psi(x)$ if x and Ψ_0 are known. Conversely, if Ψ_0 and the ζ-potential are known from experiment, Eq. (5.7) yields the distance between the surface and the slipping plane (Morel and Dzombak, 1987). For small potentials the potential decays exponentially in the diffuse layer, and the surface potential is related to the ζ-potential by,

$$\zeta = \Psi_0 \exp(-\kappa t) \tag{5.8}$$

The dependence of the ζ-potential on ionic strength can be explained by inspection of Fig. 5.3. Assuming the slipping plane lies parallel to the surface at a distance

t it can be seen that the potential at t is higher for lower ionic strengths. The position of the slipping plane may not be the same for different ionic strengths, but the offset in t would not make a substantial difference to the potential at t, and the trend is for the potential to be higher for lower ionic strengths (Wiese and Healy, 1975). Therefore, the electrophoretic mobility is greater in magnitude for a solution of 0.005M KCl than for 0.05M KCl, as shown in Fig. 5.1(b).

5.1.4 The Dependence of Hematite Stability on pH

The interaction energy that particles experience during their encounter as a result of electrostatic and van der Waals interactions is calculated based on the assumption of constant potential or constant charge (Verwey and Overbeek, 1948). Recently, Chan (1985) has described the effects of varying charge and potential on the particle interaction energy, and has presented results of numerical models. The interaction energy calculated is higher under the assumption of constant charge than under the assumption of constant potential, with the interaction energy lying between these two values for the case of varying charge and potential. Consequently, an integration of the resulting total energy yields an upper limit on stability for the constant charge case, a lower limit for the constant potential case, and an intermediate value for the case of varying charge and potential. Model calculations are presented in Sec. 6.4, however the observed variation of stability with pH presented in Fig. 5.1(c) can be qualitatively explained by the corresponding mobility measurements. Assuming that the closest approach between particles is of the same order of magnitude as t shown in Fig. 5.3, the effective potential at t is inversely proportional to the ionic strength. At a given pH (e.g., pH=6 in Fig. 5.1) a high potential, Ψ_t, is associated with a low ionic strength. This high potential gives rise to a high interaction energy, and hence the stability ratio is large.

5.2 Hematite Particles in Inorganic Media

5.2.1 Particles in Non-Specifically Adsorbed Ionic Media

At a given pH, Fig. 5.1 shows the surface charge density, mobility and stability ratio of hematite as a function of ionic strength. Both panels (a) and (c) in Fig. 5.1 have NaCl as the media electrolyte, whereas in panel (b) KCl is the supporting electrolyte. The effect of Cl^- ions is non-specific because a specific chemical reaction would cause a shift in pH_{iep} at varying electrolyte concentrations. One may not rule out the possibility that Cl^- and Na^+ ions have similar interaction energies (which could also account for the lack of a shift in pH_{iep}). However, the equilibrium constant, K, for NaOH is extremely small ($\mathrm{Log}K$=–0.2) which indicates that the formation of ≡FeONa is unlikely. Hence, electrostatic interaction is the major force for coagulation in simple salt media. As stated earlier, in Figs. 5.1(a) and 5.1(b) Na^+ and K^+ are the cations, respectively, but both figures point to the same pH_{iep}(or pH_{zpc}). Thus, the behavior of K^+ is very similar to that of Na^+ in hematite suspensions. Preliminary kinetic coagulation experiments have shown that HCO_3^- has an effect on the aggregation of hematite similar to Cl^-. During titration experiments, CO_2 was carefully removed by using N_2 to purge the reaction vessel. In mobility measurements (Fig. 5.1(b)), purging was not applied to the electrophoretic cell. If the effect of CO_2 were substantial it would have caused a shift in pH_{iep}. The consistent value of pH_{iep} indicates that the effect of CO_2 is negligible.

5.2.2 The Effect of Temperature on Particle Stability

As temperature varies three processes must be considered. First, the adsorption of potential determining ions, and consequently the surface potential change due to the temperature variation; second, the re-arrangement of the counter ions in the diffuse layer; and third, the change in the liquid viscosity. The effect of varying temperature on the adsorption of protons and hydroxide ions on hematite surfaces has been reported by Fokkink (1987). He proposed that the influence of temperature

on proton adsorption is related to the enthalpy change at the oxide-solution interface. The direct consequence of this enthalpy change is a variation in the value of pH_{zpc} with temperature. Fokkink further postulated that the change in temperature shifts the position of pH_{zpc} but leaves the general features of the relationship between charge and pH the same. From his results (Fig. 5.4), it is noted that pH_{zpc} is shifted from 9.0 at T=10°C to 8.4 at T=35°C. When making stability measurements at constant pH (for example, in this research the pH is 5.56), the ΔpH ($\Delta pH = |pH_{mea} - pH_{zpc}|$) decreases as temperature is raised from 10°C to 35°C due to the reduction in pH_{zpc}. ΔpH is a measure of surface potential, and a net decrease of surface potential as temperature increases is expected. Hence, the stability of hematite particles is expected to fall with increasing temperature. The constant stability ratio shown in Fig. 4.7 as the temperature varies from 280K to 305K can be accounted for by the slow rate at which the adsorption of protons reaches equilibrium. Although a variation in temperature of 25°C results in a change in ΔpH of 0.6 units, the surface charge remains unaltered. Titration experiments of this study and others (Fokkink, for example) indicate that proton adsorption on hematite surfaces is slow (of the order of an hour). In coagulation experiments, the temperature was controlled using a water bath. Temperature equilibrium is achieved almost instantaneously because of the small volume of suspension in the cell, but surface chemical equilibrium may not be reached. The total experimental time, of the order of 5 minutes, may not be long enough for a new equilibrium on the surface to be reached. The surface speciation is likely to remain as in the bulk colloid which was kept at room temperature (21°C). Thus the variation of stability in our experiments over this temperature range is expected to be small.

Changes in the composition of the diffuse layer may occur during particle encounter. A higher diffusion coefficient is associated with higher temperature, which results in more rapid transfer of counter-ions in and/or out of the diffuse layer. As

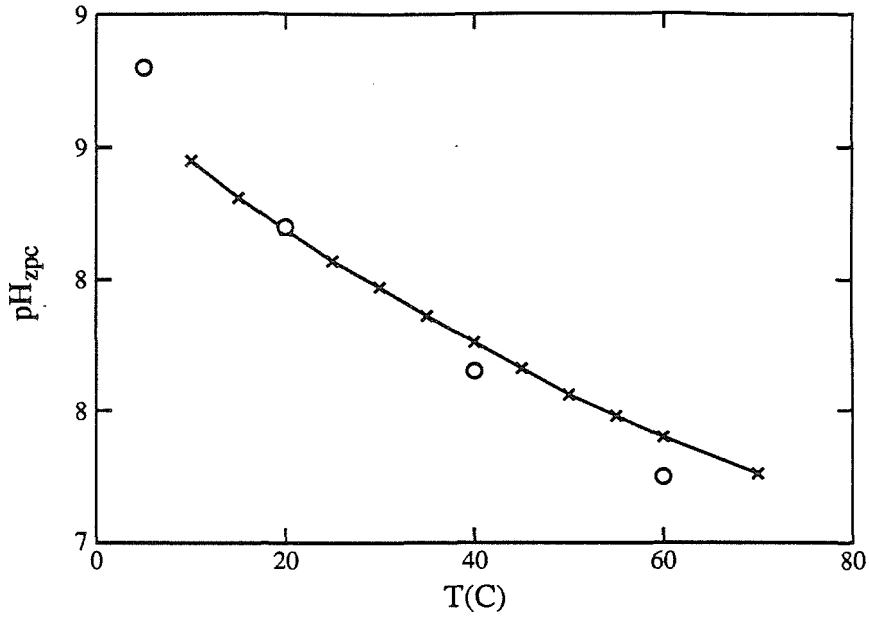

Figure 5.4: The variation of pH_{zpc} of hematite with temperature (from Fokkink, 1987). The open circles are data determined by acid-base titration, and the crosses from "ΔT" titrations.

pointed out by Lyklema (1980), referring to AgI colloidal systems, the diffuse part of the double layer adjusts itself rapidly when particles approach, and the time-limiting step is the surface charge equilibration. This is probably true for the hematite system, where the ion transfer in the diffuse layer may not result in any significant change in particle stability as temperature changes.

Temperature affects the diffusion controlled coagulation rate, as well as the actual coagulation rate, as is illustrated in Fig. 4.8. Since the rate expression indicates that $k_b = 4kT/3\mu$ for Brownian diffusion controlled coagulation, the total effect on the coagulation rate comes from the temperature itself, and the temperature-dependent viscosity, μ. The temperature, and consequently viscosity effects, apply to the coagulation rate of a colloidal suspension to the same extent as in the diffusion controlled case, in which chemical reactions are not the rate-limiting factor. Since the nature of the effects is physical, no extra chemical activation energy is involved, and

so the stability ratio is unaffected. It is thus concluded that unless a long equilibrium time is allowed (of the order of more than an hour), particle stability will not show substantial change with temperature in simple electrolyte media. The situation may change when a strongly adsorbed species is present, e.g., phosphate. The adsorption of an aqueous species may or may not be favored as the temperature changes, and the surface charge and potential could be affected. This in turn can have a direct influence on particle stability.

5.2.3 Hematite Particles in the Presence of Phosphate

In Sec. 4.3.2, data on the adsorption of phosphate on hematite surfaces are presented. In Fig. 4.26 results of the diffuse layer model calculation are plotted as a solid line, assuming that the surface species are $\equiv FeOH_2^+$, $\equiv FeOH$, $\equiv FeO^-$, $\equiv FePO_4H_2$, $\equiv FePO_4H^-$ and $\equiv FePO_4^{2-}$. Breeuwsma has proposed surface reactions leading to the same surface phosphate species as those given here (Breeuwsma, 1973). Sigg has proposed (Sigg, 1979) $\equiv Fe_2PO_4H$ and $\equiv Fe_2PO_4^-$ as two additional phosphate surface species, however Fig. 5.20 of her thesis shows that these species constitute less than 10 percent of the total adsorption over the pH range studied. By not including these species, the adsorption can still be reasonably well modeled, and the procedure is simplified. The equilibrium constants for $\equiv FeOH_2^+$ and $\equiv FeO^-$ are $K_{a1} = 10^{-7.25}$ and $K_{a2} = 10^{-9.75}$, respectively. The rest of the constants for phosphate species are modeled as follows: taking the equilibrium constants for the corresponding solution species, the surface species formation is calculated by the diffuse layer model, using the SURFEQL computer program. Then the modeled values are checked against the adsorption data, and adjustments are made to the formation constants for phosphate species. A good fit is achieved by using the reactions and equilibrium constants:

$$\equiv FeOH + 3H^+ + PO_4^{3-} \rightleftharpoons \equiv FePO_4H_2 + H_2O \qquad \log K_1 = 30.2$$

$$\equiv FeOH + 2H^+ + PO_4^{3-} \rightleftharpoons \equiv FePO_4H^- + H_2O \qquad \log K_2 = 25.2$$

$$\equiv FeOH + H^+ + PO_4^{3-} \rightleftharpoons \equiv FePO_4^{2-} + H_2O \qquad \log K_3 = 19.2$$

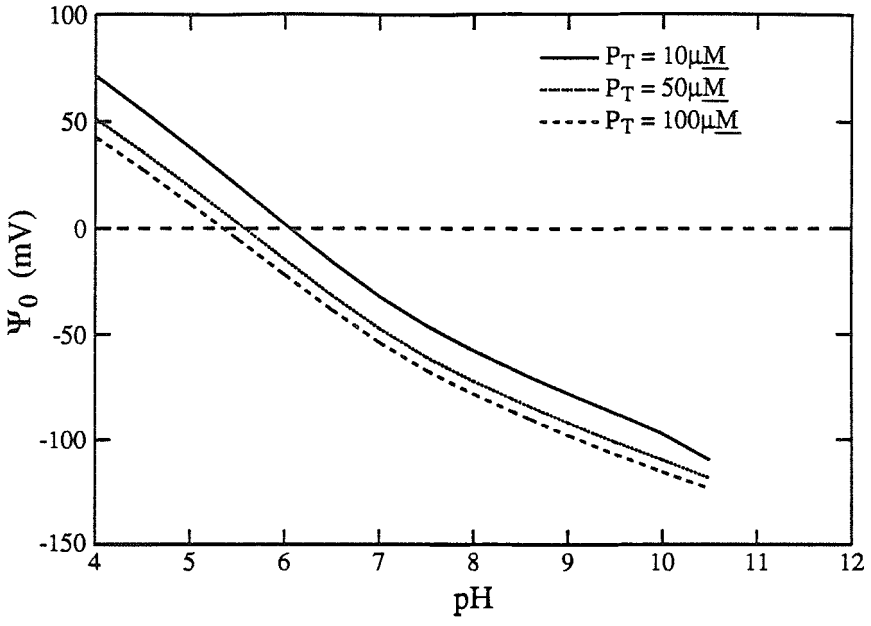

Figure 5.5: The variation of the surface potential, Ψ_0, as a function of pH for differing phosphate concentrations, showing the variation of pH_{iep}.

Using these constants, the surface potential in the presence of varying concentrations of phosphate is calculated using the diffuse layer model. The shift of the pH_{iep} due to the adsorption of phosphate ions is shown in Fig. 5.5. Electrophoretic mobility measurements show the direct consequence of phosphate adsorption. Although a large difference may exist between the absolute values of Ψ_0 and ζ potential, the zero potential condition has no ambiguity, and Ψ_0 and ζ coincide at the 0-plane and the t-plane. Overlaying the surface potential shown in Fig. 5.5 on the mobility measurements shown in Fig. 4.20 indicates identical shifts of pH_{iep} in the two plots. The good agreement between adsorption and electrophoretic mobility measurements provides confidence in the equilibrium constants derived from the model.

The kinetic coagulation data are consistent with the electrophoretic mobility measurements, and are also consistent with the phosphate adsorption data. Comparing the stability ratio as a function of phosphate concentration at pH 6.5 (Fig. 4.10) with the mobility data shown in Fig. 4.20 at the same pH, it may be seen that the mo-

bility is positive when the total phosphate concentration is less than 10μM, and the stability is due to the positive potential. When the phosphate concentration exceeds 10μM the adsorption of phosphate on the initially positively charged particles reverses the surface potential, and the stability is the result of the interactions of negatively charged particles. At a phosphate concentration of about 10μM pH_{iep} reaches zero, and the stability is a minimum.

The critical coagulation concentration of hematite at pH 6.5 for a monovalent ion, for example Cl^-, is of the order of 0.1M. The major phosphate species at this pH are $H_2PO_4^-$ and HPO_4^{2-}. A conservative estimate of the critical coagulation concentration of HPO_4^{2-} species due to the *electrostatic* effect through the Schulze-Hardy Rule is $0.1/2^6 = 1.6 \times 10^{-3}$M, whereas the experimentally determined phosphate concentration under corresponding conditions is 100 times smaller, 1×10^{-5}M. This small value of the phosphate concentration necessary to coagulate hematite is mainly due to the specific chemical reaction between phosphate and the surface groups. Hematite stability in the presence of phosphate demonstrates that the chemical effect is more important than the electrostatic effect, namely the compression of the diffuse layer. To model the stability of hematite in the presence of specifically adsorbed materials two steps are involved. First, the adsorption accounts for the speciation on the surface and the change in the surface potential and charge which takes place as the result of surface chemical reactions. Second, DLVO theory then predicts the stability based on the surface potential and charge relationship from the previous step and the solution condition at adsorption equilibrium. Detailed modeling work is addressed in Sec. 6.4.

5.2.4 Hematite and Sulfate, Calcium or Magnesium Ions

The coagulation kinetics data and the electrophoretic mobility measurements for magnesium and sulfate ions are presented in Sec. 4.1.4 and Sec. 4.2.2, respectively. The critical coagulation concentrations for various cations and anions are listed in

Table 5.1, which shows that the Schulze-Hardy rule applies to the bivalent ions. Since the Schulze-Hardy rule should not apply if specific adsorption occurs, the data show that the main interaction of magnesium and sulfate ions with the hematite surface is electrostatic, with the influence of specific chemical reactions being only minor. The average value of c.c.c for sulfate and magnesium at the same ΔpH is smaller than that for calcium, which indicates that specific chemical affinity of these ions for the surface may exist. The mobility data in Fig. 4.19 indeed show some specific effect, since the particle mobility reverses its sign when a sufficient concentration of sulfate or magnesium is present in the hematite suspension.

Ion	pH	c.c.c. (M)
Cl^-	6.5	8.0×10^{-2}
SO_4^{2-}	6.5	4.5×10^{-4}
HPO_4^{2-}	6.5	1.6×10^{-5}
Na^+	10.5	2.3×10^{-2}
Ca^{2+}	10.5	6.9×10^{-4}
Mg^{2+}	10.5	4.4×10^{-4}

Table 5.1: Critical coagulation concentration of inorganic ions.

From the critical coagulation concentrations at the same ΔpH, one can deduce that magnesium and sulfate have similar affinities for the surface. Although magnesium and sulfate are able to reverse the mobility, the affinity of these ions for the surface is by no means as strong as that of phosphate. The stability ratio fluctuates around unity as the concentrations of sulfate and magnesium increase beyond c.c.c, where in the phosphate system, particles are stabilized when the phosphate concentration is increased beyond c.c.c.

The mobility of hematite in the presence of magnesium and sulfate is small in absolute value, and corresponds to a ζ-potential of less than 15 mV according to the treatment of Wiersema et al. (1966) for converting mobility measurements to ζ-potentials. Depending on the type of ions, Dumont et al. (1976) found that the

concentration of various ions required to minimize the stability of iron oxide particles corresponds to a range of ζ-potential from 10 to 25 mV. Thus, particle stability at $\zeta <$ 15mV is expected to be low. In the presence of more than 1mM of $MgCl_2$, even though adsorption of Mg^{2+} at pH 10.5 reverses the negative surface potential (Fig. 4.19b), the resulting ζ potential is less than 15mV, and chloride ions can effectively destabilize the particles.

The coagulation kinetics data indicate the following decreasing order of effectiveness in causing particle coagulation:

$$\text{phosphate} > \text{sulfate} > \text{chloride at pH} < \text{pH}_{zpc}$$

and,

$$\text{magnesium} > \text{calcium} > \text{sodium} = \text{potassium at pH} > \text{pH}_{zpc}$$

Recalling the aqueous equilibrium constants of inorganic ions with Fe^{3+} (Table 2.1), phosphate forms the strongest complex among the anions considered. It is the surface chemical reaction that is able to change the surface charge and potential, thereby affecting the stability. Thus the chemical effect is more important than electrostatic interaction. A similar argument applies to the cations, where the formation of $\equiv FeOMg^+$ is more likely than $\equiv FeOCa^+$ since the equilibrium constant for $MgOH^+$ is $10^{2.56}$, whereas the equilibrium constant for $CaOH^+$ is 25 times smaller.

5.3 Hematite in the Presence of Organic Solutes

5.3.1 Hematite in the Presence of Small Organic Molecules

Specific chemical interaction plays an important role in coagulation kinetics not only in systems with inorganic ions but also in systems in which specifically-adsorbed organic molecules are present. Although phthalate ions do not adsorb as strongly as phosphate ions (Sec. 4.3.2), the agreement of adsorption, electrophoretic mobility, and stability measurements demonstrates elegantly the effect of chemical interaction on colloid stability. In Fig. 5.6 adsorption density, mobility, and the stability ratio are compared as a function of the total phthalate ion concentration. At low acid

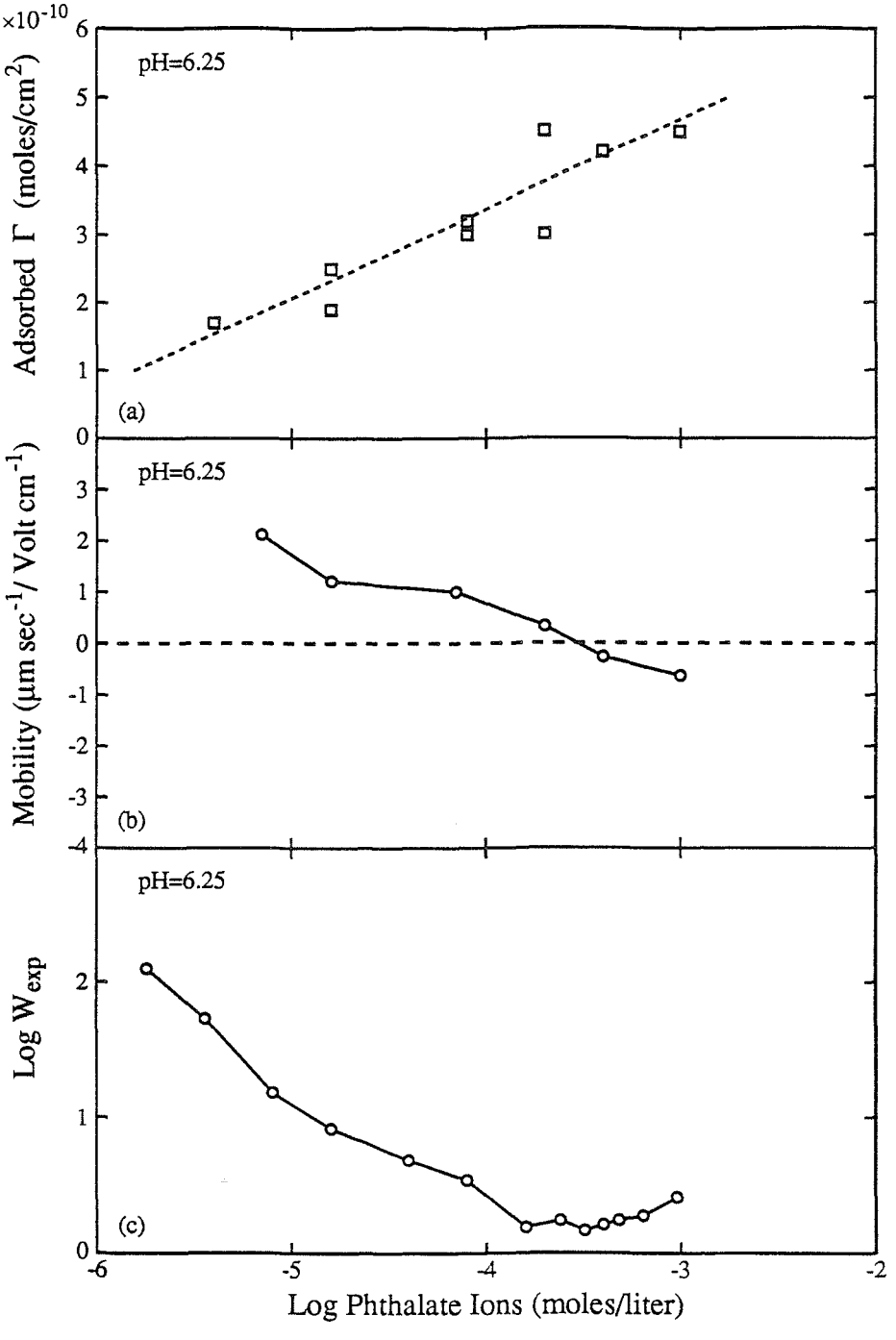

Figure 5.6: Comparison of hematite adsorption density, Γ, mobility, and stability ratio, W_{exp}, as a function of phthalate concentration at pH 6.25. Note that at the concentration at which the stability is a minimum the mobility equals zero. Also at the same concentration the maximum adsorption density is reached at which the hematite surface is completely covered.

concentration (say, total phthalate concentration of 1μM), the adsorption density is of the order of 1×10^{-10} moles/cm^2. This corresponds to 1/8 of the total sites. The majority of surface sites are occupied by surface hydroxyl groups in protonated or neutral species, which suggests that the surface behaves more or less the same way electrostatically as when no organics are present in the oxide suspension. The mobility data show that at 1μM phthalate concentration the mobility is unaffected by the presence of phthalate ions. Consequently, particles have a high stability ratio of the order of 100. At higher organic concentration, the adsorption of negative phthalate ions is able to reduce the surface potential, and at a total phthalate concentration of 2×10^{-4}M the potential is near zero, as is shown in the mobility measurements in Fig. 5.6. At this phthalate concentration the stability ratio is a minimum, which indicates that the coagulation is diffusion controlled.

When the phthalate concentration is further increased beyond 2×10^{-4}M, the mobility data show that the surface potential reverses in sign. If phthalate ions did not specifically adsorb on the hematite surface, we would expect that the mobility would level off, remaining at zero when the phthalate concentration is increased beyond 2×10^{-4}M. The increase in adsorption density indicates that the chemical bonding between phthalate and surface hydroxyl groups is strong, since the negatively charged phthalate ions must overcome a negative surface potential to be adsorbed. The adsorption results in an increased negative surface potential which is responsible for the rise of the stability ratio. However, we do not expect that the stability ratio will increase substantially when phthalic acid concentration is greater than 10^{-3}M for two reasons. Using Langmuir's treatment, we find that the maximum adsorption density corresponds to $\sim 40\text{Å}^2$ per molecule adsorbed on the surface. This specific area is of the same order of magnitude as the cross-sectional area calculated for phthalate ions. Hence, further adsorption of phthalate is restricted due to the lack of available surface to accommodate more molecules. Consequently, the surface potential will be

approximately constant when the acid concentration exceeds 1×10^{-3}M. In addition, an increase in phthalate ion concentration is unavoidably accompanied by an increase in the concentration of counterions, such as Na^+. In the presence of a high concentration of positive ions, the stability is expected to be reduced through electrostatic interactions.

A quantitative treatment of surface speciation can be made through equilibrium modeling. Consider the reactions,

$$\equiv FeOH + 2H^+ + L^{2-} \rightleftharpoons \equiv FeHL + H_2O \qquad K_{HL} \tag{5.9}$$

$$\equiv FeOH + H^+ + L^{2-} \rightleftharpoons \equiv FeL^- + H_2O \qquad K_L \tag{5.10}$$

Where L^{2-} represents phthalate ions, which are treated as potential determining ions. The equilibrium constants, K_{HL} and K_L, are determined by fitting the plot of adsorption as a function of solution concentration. The solid line in Fig. 5.7 shows the model calculation, where $\log K_{HL}$=16.45, $\log K_L$=11.28, in addition to the constants for surface hydroxyl species. The model yields a good estimation at higher adsorption densities although it overestimates the adsorbed organic acid at lower solution concentration. The equilibrium constants are used to verify the variation of surface potential with total phthalate concentration as illustrated in Fig. 5.8. The solid line corresponds to the model calculation, whereas the data points are the ζ-potential evaluated from the mobility measurements using Wiersema's treatment. Two physical pictures of the relation of surface potential and ζ-potential are proposed, and are sketched in Fig. 5.9. (1) At high surface coverage, it is assumed that the surface potential is essentially the same as the ζ-potential. It is reasonable to assume that phthalate ions occupy the space adjacent to the surface and all other ions are pushed out of this space and distributed in the solution at a distance t from the surface. Hence, if the mobility is measured at the t-plane, the corresponding potential should be similar to the surface potential, and the exponential decay in Ψ starts at t,

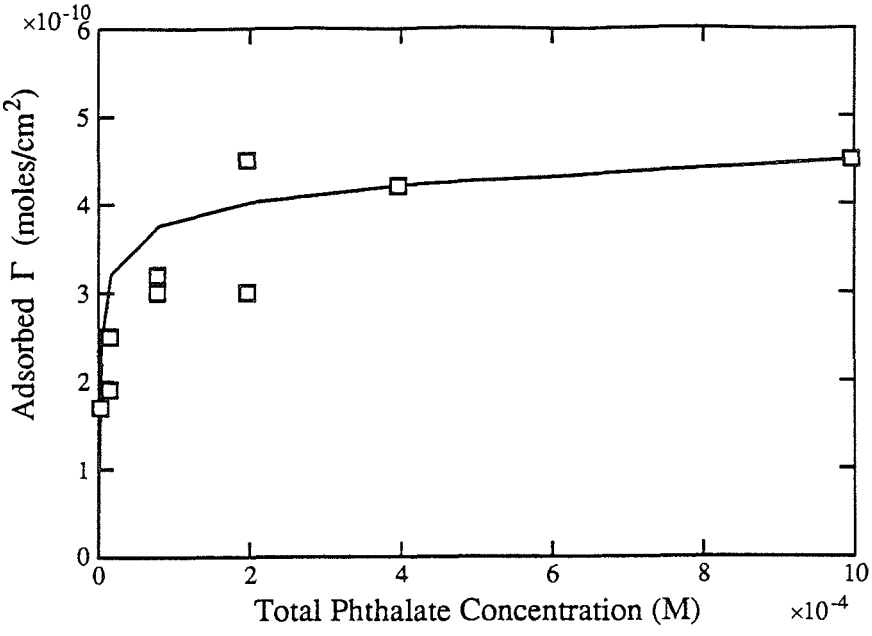

Figure 5.7: Adsorption density, Γ, of a hematite suspension as a function of total phthalate concentration.

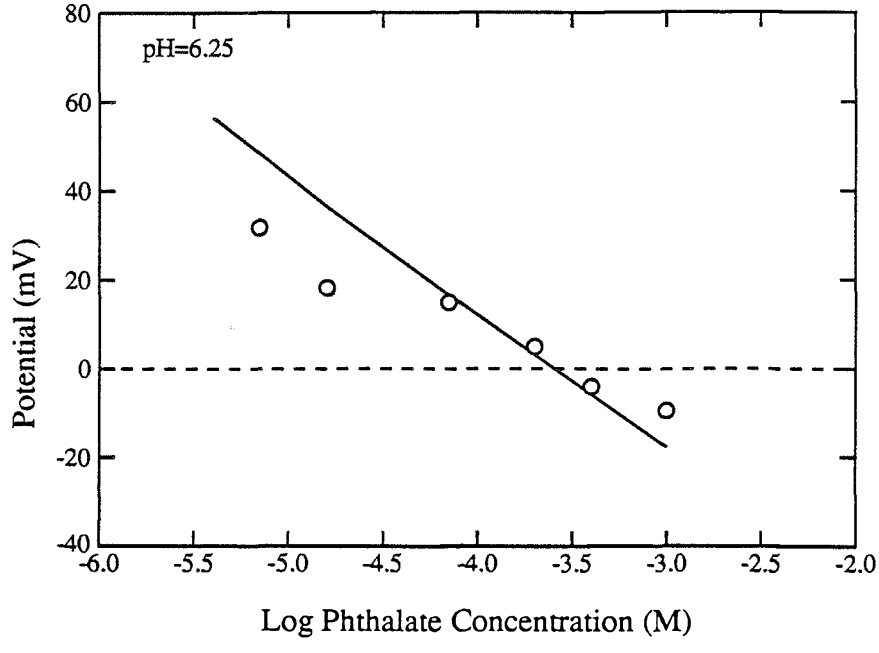

Figure 5.8: Surface potential in millivolts as a function of phthalate concentration at pH 6.25. The solid line corresponds to a model calculation, and the data points are the ζ-potential evaluated from the mobility data using Wiersema's treatment.

following the Gouy-Chapman theory. (2) At low adsorption density, the ζ-potential corresponds to the potential at a distance t from the surface, where the potential follows the exponential decay modeled by Gouy-Chapman theory. At low adsorption coverage, small counter ions coexist within the t layer with the organic molecules. Therefore, the potential decay starts at the 0-plane.

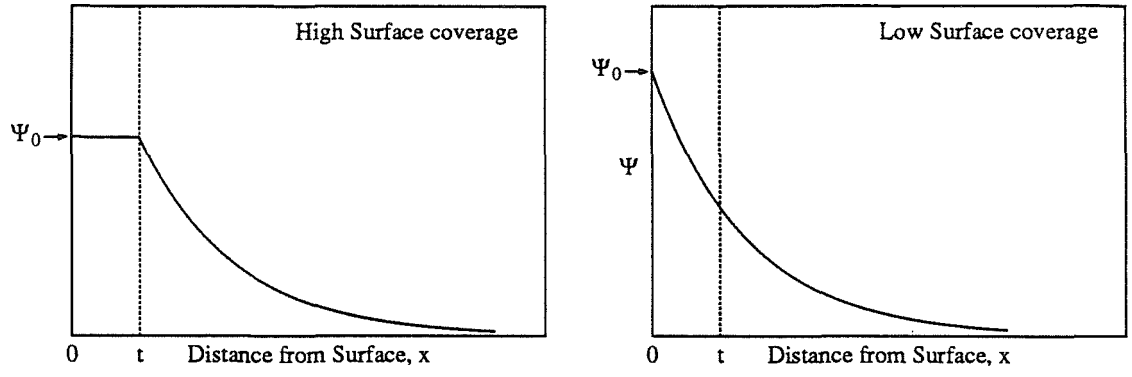

Figure 5.9: Schematic representation of the variation of potential with distance from the particle's surface for particles with a high surface coverage (left) and a low surface coverage (right) of adsorbed species.

The data in Fig. 5.8 can be interpreted by employing the two pictures presented above. At high coverage, the ζ-potential from mobility measurements coincides quite well with the surface potential calculation. At low adsorption density, the ζ-potential is somewhat smaller than the modeled surface potential, which is expected as the ζ-potential corresponds to the reduced potential at t.

It would give more confidence in the accuracy of K_{HL} and K_L if we could verify the equilibrium constants using adsorption data as a function of pH. Although we do not have such adsorption data available, electrophoretic mobility data can also be used for this purpose. The variation of mobility with pH can be modeled by the surface equilibrium model. In panel (a) of Fig. 5.10, the surface potential is plotted as a solid line. The dashed line represents the reduced potential at t=4.0 nm. In panel

(b), the species distribution is modeled by an equilibrium calculation. Comparing (a) and (b), the adsorption ceases to be substantial at pH>8.0. If it is assumed that the surface is fully covered at pH<8.0, the ζ-potential should be similar to the surface potential. At pH>8.0, the ζ-potential should follow the reduced potential calculated at t=4.0 nm. In panel (c) the stability ratio is plotted, and shows agreement with the mobility data. At pH around 6.5 the mobility is approximately zero as a result of adsorption of phthalate, and the corresponding stability is also a minimum. At pH 4, although the adsorption is substantial the particles still carry a net positive charge, which in turn results in relative stability. The adsorption is not substantial at pH 10. The surface charge and potential are determined by surface hydroxyl groups. Corresponding to the high mobility at pH 10, a high stability ratio is predicted.

Oxalate is expected to have a similar effect to that of phthalate on hematite coagulation. Comparing the acidity constants for the two acids, oxalic acid dissociates more strongly, which indicates a weaker complex with H^+ or other Lewis acids, such as Fe^{3+}. Consequently, we expect phthalate ions to form stronger surface complexes than oxalate ions. The coagulation data in Fig. 4.12 support this hypothesis. At a total concentration equal to 10^{-5}M, a considerably smaller stability ratio in the presence of phthalate is observed compared with that for oxalate. This is due to the stronger adsorption of phthalate, which results in a reduced surface potential. The adsorption of oxalate ions is less extensive, hence particles have relatively high potential and stability. Oxalate acts more like a non-specifically adsorbed ion, since there is no clear indication of an increased stability ratio when the oxalate exceeds the critical coagulation concentration. Compared with the sulfate coagulation data, oxalate seems to complex with hematite surfaces more strongly than does sulfate .

5.3.2 Effect of Polymeric Organic Matter

It has been shown in studies by Hunter and Liss (1982) and Tipping (1981) that adsorption of dissolved natural organic matter accounts for the surface properties of

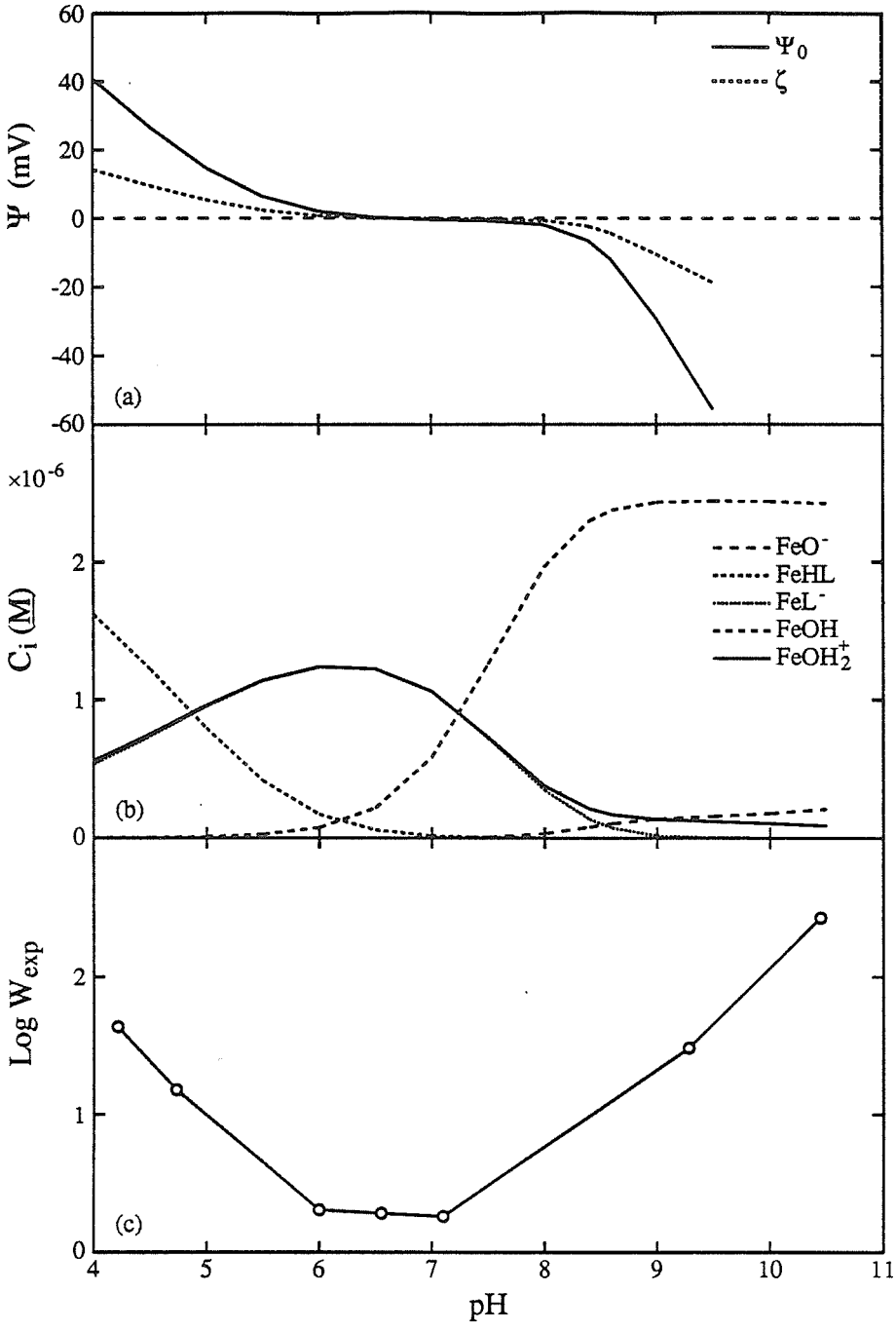

Figure 5.10: Comparison of hematite surface potential, Ψ, surface species distribution, C_i, and stability ratio, W_{exp}, as a function of pH in the presence of 0.2 millimolar phthalate ions.

various types of naturally occurring particles. The presence of natural organic matter changes the surface potential and charge, and consequently the electrostatic interaction between particles is altered. Hence, the chemical interaction between natural organic matter and particle surfaces plays a key role in determining the observed coagulation rate. The results in electrophoretic mobility and coagulation kinetic studies presented in this research show the influence of adsorption on coagulation.

Carboxylic groups have been shown to have a strong affinity for hematite surfaces (Sec. 5.3.1). A polymer molecule with a large number of carboxylic groups, such as polyaspartic acid, is expected to exert a stronger effect than simple organic molecules on hematite stability, as is explained by Lyklema (1985). Lyklema pointed out that polymer adsorption is driven by the free energy of bonding polymer segments to the adsorbent. As a result, adsorption of polymers is widely observed since only modest segment adsorption free energy is needed. Regarding the conformation of polyelectrolytes, Lyklema pointed out that they lay flat on surfaces. This feature was modeled as patch formation by Kasper (1971). During particle encounter, the particles orient themselves in an energetically favorable position in which the reduced local potential shielded by the patches favors the aggregation. The effect of polyaspartic acid (PAA) on the coagulation rate of hematite is shown in Fig. 4.14. The plot resembles Fig. 4.12(b) in which the stability ratio is plotted as a function of phthalate concentration. However, the concentration corresponding to the minimum stability is much lower for PAA ($\sim 2\times10^{-5}$g/l, or 6×10^{-7} M of –COOH) than for phthalate ($\sim 5\times10^{-2}$g/l, or 6×10^{-4} of –COOH). At the pH of the study, the side chain carboxylic groups in PAA are fully dissociated (pK=3.9), and the polymer structure is shown overleaf.

As the PAA concentration increases from zero to 2×10^{-5}g/l, the binding of carboxylic groups to the hematite surface effectively reduces the positive surface potential, hence a decreased stability ratio is observed. As the PAA concentration is

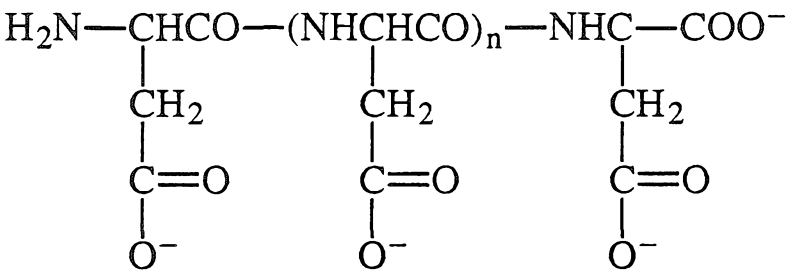

increased beyond 2×10^{-5}g/l the large number of negative carboxylic groups is able to reverse the surface potential, resulting in an increase in the stability ratio.

The coagulation of hematite in the presence of fulvic (FA) and humic acid (HA) follows the same trend as in the presence of polyaspartic acid. Since carboxylic groups are dominant in natural organics (Thurman and Malcolm, 1983) the organic substances are essentially negatively charged polyelectrolytes. Table 5.2 lists the properties of Suwannee River fulvic acid (after Thurman and Malcolm, 1983). Fulvic acid contains 6 millimoles/g of the functional group –COOH. The critical coagulation concentration of fulvic acid is 10^{-4} g/l (see Fig. 4.14). This corresponds to 6×10^{-7}M of –COOH. Thus the critical coagulation concentration of fulvic acid and PAA is the same in terms of –COOH. The molecular weight of Suwannee River humic acid is 3000–5000, and is larger than that of fulvic acid (1000–1700). However, both contain approximately the same number and type of functional groups. Humic acid and fulvic acid therefore have a similar effect on hematite stability, as may be seen in Fig. 4.14.

Preliminary adsorption experiments have revealed that the adsorption of FA on hematite surfaces is of the high affinity type. This agrees with the observations of other researchers (Lyklema, 1985). The electrophoretic mobility data (Fig. 4.22) show that the adsorption of fulvic acid on hematite is due not only to the electrostatic interaction of polyanions and positive surface species. If electrostatic interaction were the sole driving force for adsorption, the mobility would be expected to be reduced to zero as the FA concentration increases, and would remain at zero as

Table 5.2: Properties of Suwannee River fulvic acid (Thurman and Malcolm, 1983).

1. Elemental analysis			
C = 51.3	N = 0.56		ash = <0.05
H = 4.32	S = <0.2		
O = 42.9	P = <0.1		
2. Functional groups (mmol/g)			
$-CO_2H$ (titration)	= 6.0	phenolic –OH	= 2.1
$-CO_2H$ (NMR-solid)	= 6.2		= 1.7
$-CO_2H$ (NMR-liquid)	= 6.0		= 3.6
hydroxyl (NMR solid)	= 8.6	carbonyl (NMR) solid	= 1.7
hydroxyl (NMR) liquid	= 5.4		
3. Carbon distribution (%)			
aromatic	20.8		
aliphatic	36.7		
C-OH	20.1		
CO_2H	14.6		
phenolic	3.9		
carbonyl	4.0		
4. Amino acids = 36 nmol/mg			
% N (AA) = 10%			
5. % carbohydrate = 4%			
6. Molecular weight = 1200 ± 200			
7. ^{14}C age = less than 30 yr			

the concentration of FA is further increased. The substantial reversal in mobility arises from the specific chemical interaction in addition to the electrostatic force. Consequently, the mobility data account for the observed stability ratio (Fig. 4.14), where at (FA)$< 1 \times 10^{-4}$g/l the stability is obtained through net repulsions of positive surfaces, and at (FA)$> 1 \times 10^{-4}$g/l the stability arises from the repulsion due to the negative potentials.

5.3.3 The Effect of Fatty Acids

The equilibrium constants for surface species formation can be obtained by fitting the adsorption data with a surface equilibrium model. The surface equilibrium model can in turn reveal the driving force for the adsorption. In the case of the adsorption of lauric acid on hematite surfaces, the surface complex formation is expressed by Eq. (4.6). Laurate ion is denoted by L, and the acid solution concentration, L_T, is the sum of (HL) and (L^-). If the pH is much larger than the deprotonation constant of the acid, pK, the equilibrium fatty acid concentration is dominated by (L^-). According

to Eq. (4.6), a plot of logΓ as a function of logL_T is expected to have a slope of 1, so long as the alteration of surface potential as a result of adsorption is small. This feature is preserved whether the adsorbate is of the high affinity type (large value of K_{HL}) or of the low affinity type. The increase in K_{HL} usually results in an increase in the absolute value of the adsorption density. However, when the adsorption of anions results in a significant reduction in surface potential, the adsorption density is reduced due to the less favorable electrostatic interaction, and often levels off when the surface potential is reversed as the result of adsorption (or when the number of available surface sites is limited). This may best be described by the Langmuir isotherm (see phthalate adsorption, Fig. 4.27).

The observed rapid rise in the adsorption of lauric acid as the solution fatty acid concentration increases (Fig. 4.28) cannot be explained by either specific or electrostatic interaction, nor a combination of both. An explanation of the adsorption isotherm requires a combination of electrostatic, specific and lateral interactions of fatty acids. Specific and electrostatic interactions are both operative during the adsorption process, but the lateral interaction energy depends on the extent of adsorption. At low fatty acid concentration a large surface area is able to accommodate organic molecules in the tangential orientation. The entropy change as a result of fatty acids partially escaping from the aqueous solution contributes to the total adsorption energy. At high laurate ion concentration the surface is crowded. A radial orientation of the adsorbate is more likely since it allows a larger number of anions to be accommodated on the surface. The interaction between the hydrophobic tails yields an additional energy for adsorption. To summarize, the adsorption equilibrium constant is represented by:

$$K_{HL} = f(\theta) \tag{5.11}$$

where $\theta = \Gamma/\Gamma_m$ is the extent of adsorption. Using SURFEQL, the adsorption data in Fig. 4.28 can be modeled by the diffuse layer model. The equilibrium constants

are fitted by a polynomial as follows:

$$\log K_{HL} = 9.868 + 9.0 \times 10^{-3}\theta - 6.551 \times 10^{-5}\theta^2 + 1.766 \times 10^{-6}\theta^3 \qquad (5.12)$$

Since the electrostatic interaction is modeled through an equilibrium calculation the equilibrium constant given by Eq. (5.12) is the result of specific interaction and hydrophobic energy.

The mobility data and stability ratios from coagulation experiments both show systematic change with variations in concentration and in the carbon number of the molecules. In general, the adsorption of fatty acid is represented by Eq. (4.7), where K_{HL} is proportional to the adsorption density and inversely proportional to the aqueous anion concentration. If we write $K_{HL} = A \cdot \Gamma / L_T$ (A is a constant), and assume that each individual group of $-CH_2$ contributes an energy ϕ to the total hydrophobic interaction energy, then $\Delta G_{hyd} = n\phi$, where n is the number of carbon atoms in the fatty acid molecule. Using Fuerstenau's approach (1971), Eq. (4.8) can be modified to:

$$\frac{A\Gamma_{ads}}{L_T} = \exp[-(\Delta G_{elec} + \Delta G_{chem} + n\phi)/RT] \qquad (5.13)$$

When the mobility reaches zero, the contribution due to electrokinetic energy vanishes; this corresponds to the minimum stability, and hence L_T equals the critical coagulation concentration. The slope of a plot of log(c.c.c.) versus n yields the energy ϕ for each $-CH_2$ group. Using the mobility data in Fig. 4.28, ϕ is determined to be (1.2±0.1)RT Joules/mole (Fig. 5.11).

Since C12, C10 and C8 differ only in the number of carbon atoms in their hydrophobic tails, the specific chemical contribution through the carboxylic group remains the same for all these molecules. At the same mobility, the electrostatic contribution is also similar, hence the difference in equilibrium constants is due only to hydrophobic interaction. With the experimentally determined values of ϕ, K_{HL} for C10

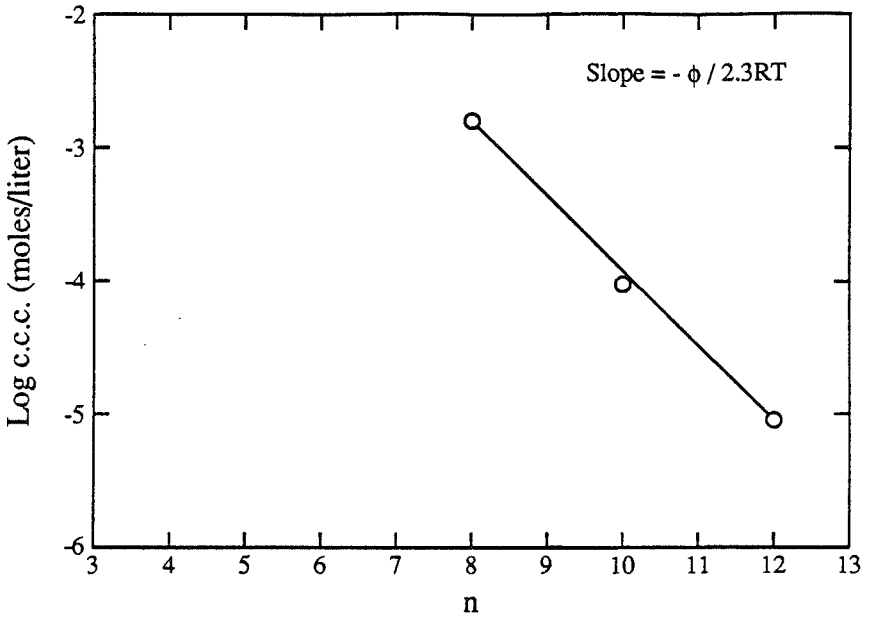

Figure 5.11: Critical coagulation concentration of fatty acids as a function of the number, n, of carbon atoms in the molecule.

and C8 is easily modeled. For example, at point a in Fig. 5.12, $\log K_{HL}$ is determined for C12 by fitting the corresponding adsorption data to be 10.39. The constant for C10 at point b differs from K_{C12} by $\exp(2\phi/RT)$ or a numerical value of $\log K_{C10} = 9.27$. Similarly, K_{C8} at point c is given by $K_{C8} = K_{C12}/\exp(4\phi/RT) = K_{C12}/\exp(5.16)$ and $\log K_{C8} = 8.15$.

Hematite stability and mobility data in the presence of a series of fatty acids (Fig. 4.17 and Fig. 5.12) have demonstrated the importance of hydrophobic interaction. Each 10-fold decrease in c.c.c when the number of carbon atoms in the chain increases by 2 is attributed to the extra hydrophobic contribution of two ($-CH_2$) groups.

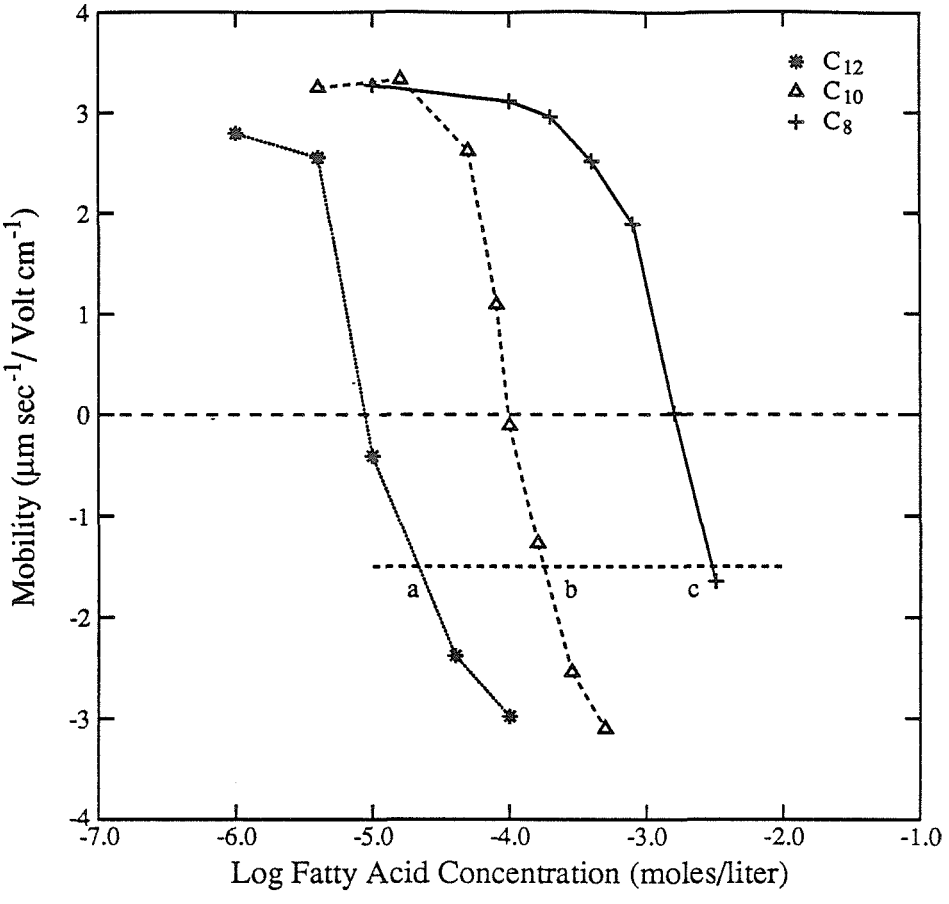

Figure 5.12: Mobility of a hematite suspension as a function of fatty acid concentration. Molecules containing differing numbers of carbon atoms are compared.

6. SUMMARY AND CONCLUSIONS

6.0 Introduction

The coagulation kinetics of hematite particles have been examined in the presence of various electrolytes using a light scattering technique. The stability ratios derived, combined with the results from electrokinetic and adsorption measurements, reveal the special importance of specific adsorption on coagulation and particle electrokinetic mobility. Adsorption measurements provide information about different adsorption mechanisms: electrostatic interaction of counter ions with surface groups, the chemical formation of the surface species, and lateral interactions of hydrophobic chains in organic molecules as a result of van der Waals attraction between $-CH_2$ groups. The processes involved in adsorption have direct consequences on particle mobility. If only electrostatic interaction is involved in adsorption, the mobility approaches zero asymptotically as electrolyte concentration increases. When surface chemical formation is involved, the mobility is first reduced to zero, and subsequently reverses in sign as the concentration of the specifically adsorbed ion increases. In the absence of specifically adsorbed ions the isoelectric point, pH_{iep}, is not affected as electrolyte concentration changes in the plot of mobility against pH (see Fig. 4.18). Conversely, the adsorption of aqueous ions results in a shift in pH_{iep} (see Fig. 4.20). The key to understanding the dependency of coagulation kinetics on aqueous chemistry is: the adsorption of aqueous ions at hematite surfaces alters the surface charge and poten-

tial, which in turn changes the total interaction energy during particle encounters.

6.1 Surface Chemical Properties

6.1.1 Adsorption of Protons

In an aqueous suspension, hematite particles develop charges on their surfaces by acid–base chemical reactions between surface hydroxyl groups and protons. This process can be described within a coordination chemical framework, and the surface chemical reactions are expressed as:

$$\begin{aligned} \equiv FeOH_2^+ &\rightleftharpoons \equiv FeOH + H^+ \quad K_{a1}^{int} \\ \equiv FeOH &\rightleftharpoons \equiv FeO^- + H^+ \quad K_{a2}^{int} \end{aligned} \tag{6.1}$$

Equilibrium constants are obtained by applying the diffuse layer model to titration data, and the modeled surface charges agree well with the experimental results, as may be seen from Figs. 2.4 and 2.5. The titration data in Fig. 2.4 indicate that the pH_{zpc} of the hematite surface is 8.5±0.1. This value is verified by electrokinetic measurements (see Fig. 4.18). Table 6.1 compares the properties of the hematite particles used in this study with those from other studies. James and Parks (1982) have summarized several investigations of hematite pH_{zpc} and conclude that in simple electrolytes pH_{zpc} lies between 8 and 9, averaging about 8.5. It should be noted that the equilibrium constants for surface protonation/deprotonation depend on the model applied. The equilibrium constants derived in this work are based on the diffuse layer model and are corrected for electrostatic interactions for ionic strengths ranging over three orders of magnitude.

6.1.2 Adsorption of Phosphate

Phosphate strongly interacts with hematite surface groups, and inner-sphere complexes are believed to form at the surface. The adsorption data are modeled by applying the diffuse layer model to equilibrium chemical reactions. The phosphate surface complexes ($\equiv FeH_2PO_4$, $\equiv FeHPO_4^-$ and $\equiv FePO_4^{2-}$) and the corresponding equilibrium constants are given in Table 6.2.

Reference	Sample Preparation	pH_{zpc}	Electrolyte	Specific Surface Area	Surface Equilibrium Constants
Parks and deBruyn (1962)	Hydrolysis of $Fe(NO_3)_3$ at boiling point	8.50	KNO_3	BET: $15m^2/g$ Postulated: $60m^2/g$	N.A.
Breeuwsma (1973)	Hydrolysis of $Fe(NO_3)_3$ at neutral pH (by adding KOH) at boiling point	8.50	KCl	BET: Batch A: $31m^2/g$ Batch B: $18m^2/g$ Batch C: $21m^2/g$	Triple Layer Model* $pK_1=6.7\pm0.3$ $pK_2=10.3\pm0.3$ $pK_{Cl}=7.5\pm0.3$ $pK_K=9.5\pm0.3$ $C_1=90\mu F/cm^2$ $C_2=20\mu F/cm^2$ Site density$=10nm^{-2}$
Penners (1985)	Hydrolysis of $FeCl_3$ at 100°C, seeded growth	9.50	KCl	BET: $26.5m^2/g$ Estimated from average diameter: $14.3m^2/g$	N.A.
Dumont et al. (1971)	Hydrolysis of $Fe(NO_3)_3$ at 100°C, pH 1.6	9.27 8.20	KCl $KClO_4$	$44.6m^2/g$ $24.5\ m^2/g$	N.A.
This work	Hydrolysis of $Fe(ClO_4)_3$ at 100°C	8.50	NaCl	BET: Batch 1: $40.0m^2/g$ Estimated from averaged diameter: Batch 1: $38.3m^2/g$ Batch 2: $16.3m^2/g$	Diffuse Layer Model $pK_{a1}^{int}=7.25$ $pK_{a2}^{int}=9.75$ Site density$=4.8nm^{-2}$

* Estimated by James and Parks (1982) by applying Triple Layer Model to batch B hematite.

Table 6.1: Comparison of hematite properties.

6.1.3 Adsorption of Magnesium and Sulfate

The electrophoretic mobility measurements in the presence of varying concentrations of magnesium at pH 10.5 and varying sulfate concentrations at pH 5.5 demonstrate that these ions are able to reverse the surface potential (see Sec. 4.2.2). This indicates that magnesium and sulfate are both specifically adsorbed on the surface of hematite particles. However, the complexes formed are not as strong as those of phosphate.

6.1.4 Adsorption of Phthalate

Phthalate ions are found to have a strong affinity for the hematite surface. The adsorption of phthalate ions is found to shift pH_{iep} to lower values, as shown in Sec.

(a) Surface equlibrium expressions.

	Log K
$\equiv FeOH + H_3PO_4 \rightleftharpoons \equiv FePO_4H_2 + H_2O$	8.55
$\equiv FeOH + H_2PO_4^- \rightleftharpoons \equiv FePO_4H^- + H_2O$	5.65
$\equiv FeOH + HPO_4^{2-} \rightleftharpoons \equiv FePO_4^{2-} + H_2O$	6.85
$\equiv FeOH + H_2(Phth) \rightleftharpoons \equiv FeH(Phth) + H_2O$	8.09
$\equiv FeOH + H(Phth)^- \rightleftharpoons \equiv Fe(Phth)^- + H_2O$	5.87
$\equiv FeOH + HL \rightleftharpoons \equiv FeL + H_2O$	4.97*

(b) Aqueous equilibrium expressions.

	Log K
$Fe(OH)^{2+} + H_3PO_4 \rightleftharpoons FeH_2PO_4^{2+} + H_2O$	3.69
$Fe(OH)^{2+} + H_2PO_4^- \rightleftharpoons FeHPO_4^+ + H_2O$	5.14
$Fe(OH)^{2+} + H_2(Sal) \rightleftharpoons FeH(Sal)^{2+} + H_2O$	4.28
$Fe(OH)^{2+} + H_2(Ox) \rightleftharpoons FeH(Ox)^{2+} + H_2O$	5.29
$Fe(OH)^{2+} + H(Sal)^- \rightleftharpoons Fe(Sal)^+ + H_2O$	6.02
$Fe(OH)^{2+} + H(Ox)^- \rightleftharpoons Fe(Ox)^+ + H_2O$	5.66
$Fe(OH)^{2+} + H(Pro) \rightleftharpoons Fe(Pro)^{2+} + H_2O$	1.61

* L represents laurate, "Phth" phthalate, "Sal" salicylate, "Ox" oxalate, "Pro" propionate.

Table 6.2: Comparison of surface and aqueous equilibrium constants.

4.2.4. Assuming monodentate surface species, $\equiv FeHL$ and $\equiv FeL^-$, the adsorption data are fitted in Sec. 5.3.1 using the diffuse layer model. The equilibrium constants for phthalate are also listed in Table 6.2.

6.1.5 Adsorption of Fatty Acids

The adsorption of lauric acid on hematite particles shows that hydrophobic interaction between $-CH_2$ groups contributes substantially to the total adsorption energy, in addition to contributions from specific chemical bonding and electrostatic interaction (see Sec. 4.3.4). The hydrophobic energy is proportional to the number of $-CH_2$ groups in the fatty acid molecule, and is also a function of the extent of adsorption. Assuming that laurate ions form a surface complex $\equiv FeL$, the adsorption data are fitted in Sec. 5.3.3 by the diffuse layer model, and the equilibrium constant is expressed as a function of adsorption extent in Eq. (4.7). It was found that each $-CH_2$ group in a fatty acid chain contributes (1.2±0.1)RT Joules/mole to the total

adsorption energy.

6.1.6 Adsorption of Polyelectrolytes

Polyaspartic acid and naturally occurring humic acid and fulvic acid show high affinities for the hematite surface. Strong adsorption is due to the carboxyl segments in the molecules which strongly bond to the surface by both specific chemical bonding and electrostatic interactions.

6.1.7 Surface vs. Aqueous Complex Formation Constants

The correlation observed by Sigg and Stumm (1981) and Kummert and Stumm (1980) between aqueous solution phase formation constants and those for the corresponding surface complex can be examined for the adsorption of inorganic and organic ligands on the surface of hematite particles. The equilibrium constants for aqueous complex formation are compared with those for surface complexes in Fig. 6.1. Data obtained by Sigg (1979) on goethite and by Kummert (1979) on aluminum oxide are also plotted in the same figure, together with the results of this work. The acidity constant for H(Phth) is similar to that of H(Ox), so the aqueous equilibrium constant for $Fe(Phth)^+$ is assumed to equal that of $Fe(Ox)^+$. Similarly, the acidity constant for $H_2(Phth)$ is close to that of $H_2(Sal)$, so the aqueous equilibrium constant for $FeH(Phth)^{2+}$ is assumed to equal that of $FeH(Sal)^{2+}$. The aqueous equilibrium constant for lauric acid is assumed to equal that of propionic acid. Data in Fig. 6.1 are quite scattered as a result of the various errors involved in the experiments and the models. For example, neglecting the electrostatic correction associated with a 50 mV charged surface can produce an order of magnitude error in the surface equilibrium constants. Despite the error associated with each data point, there is an apparent correlation between the equilibrium constants for surface complexes and those for the corresponding solution complexes. However, because of the large scatter in this correlation a quantitatively accurate surface equilibrium speciation cannot be deduced by direct application of the constants for the solution complexes. It is still necessary

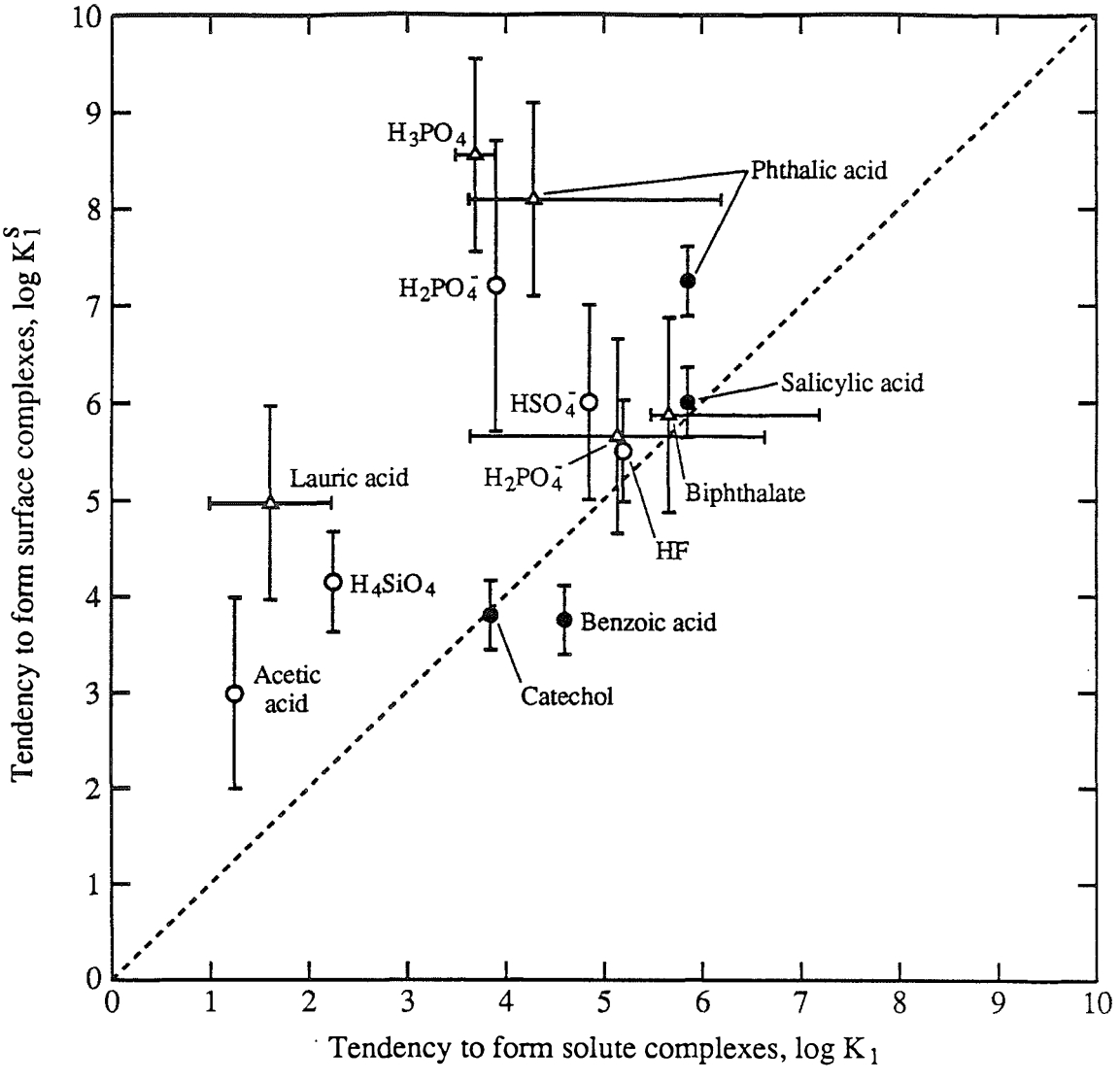

Figure 6.1: Relationship between coordination in solution and at oxide surfaces (after Kummert and Stumm , 1980). Open circles are for α-FeOOH, filled circles for γ-Al_2O_3, and open triangles for α-Fe_2O_3 (this work).

to obtain an adsorption isotherm in order to derive the surface equilibrium constants. The equilibrium constants of aqueous complexes, nevertheless, can be used to qualitatively estimate the extent of adsorption.

6.2 Hematite Coagulation Kinetics

6.2.1 Hematite Particles in Inorganic Media

The pH is a very important parameter in controlling the coagulation kinetics of hematite particles. Hematite particles have the least stability at pH 8.5, where the net surface charge is near zero. In non-specially adsorbed electrolyte media hematite particles become more stable as pH deviates more from pH_{zpc}.

Sodium, potassium, calcium and chloride ions are found to be non-specific for hematite surfaces. In the presence of these ions, the coagulation of a hematite colloidal suspension is due to the compression of the diffuse layer.

Unpublished work by Anderson (University of Wisconsin) and Bales (University of Arizona) appears to indicate that HCO_3^- and CO_3^{2-} may interact specifically with metal oxide surfaces in water; however, there are no definitive data at the present time. On the basis of the observations made in this study it seems that there are only weak interactions of HCO_3^- and CO_3^{2-} at the hematite surface. The general question of HCO_3^- and CO_3^{2-} interaction with metal oxide remains open for future research.

Magnesium and sulfate are found to interact weakly with the hematite surface, since they are able to reverse the mobility of the particles. The concentrations required to coagulate a hematite particle suspension at the same ΔpH (with respect to pH_{zpc}) are found to be less than that for non-specifically adsorbed ions. Among all the inorganic ions studied, phosphate was the most strongly adsorbed on the hematite surface. The adsorption of phosphate results in a reduced surface charge. The critical coagulation concentration for phosphate is dependent on pH, and is much less than predicted by DLVO theory. Among inorganic ions, the order of the effectiveness in causing hematite particles to coagulate is:

$$\text{phosphate} > \text{sulfate} > \text{chloride}, \quad \text{at } pH < pH_{zpc}$$

and

$$\text{magnesium} > \text{calcium} > \text{sodium} \sim \text{potassium}, \quad \text{at } pH > pH_{zpc}$$

6.2.2 Hematite in the Presence of Organic Solutes

Small organic molecules, such as phthalate and oxalate ions, show specific interaction with hematite surface hydroxyl groups. Phthalate ions form stronger complexes on the hematite surface than sulfate ions, and are more effective in causing a hematite particle suspension to coagulate. Oxalate ions lie between phthalate and sulfate in terms of their effect on hematite particle stability.

In the presence of fatty acids, hydrophobic interactions are operative in addition to the specific chemical and electrostatic interactions. As a result molecules with longer carbon chains have a greater effect on the stability of a hematite suspension than molecules with shorter carbon chains and the same functional groups. Comparing the stability of a hematite suspension in the presence of phthalate ions (Fig. 4.12(b)) with that in the presence of caprylate ions (Fig. 4.17), phthalate ions appear to be more effective in causing hematite coagulation, although both ions have eight carbon atoms in their molecules. Phthalate ions possess two carboxyl groups, and bidentate complex formation between phthalate and hematite may account for the stronger effect of phthalate ions on hematite stability compared with caprylate ions.

The influence of organic molecules on hematite stability can be explained qualitatively by recognizing the influences of hydrophobic contributions and steric effects on the binding of organic molecules to the hematite surface. At pH 6, the order of effectiveness of organic anions in causing hematite coagulation is,

laurate>caprate>caprylate> propionate

Polyelectrolytes, such as polyaspartic acid, humic and fulvic acid, are observed to have the strongest effect on the stability of hematite among all the ions studied. At pH<pH_{zpc}, the critical coagulation concentrations for organic species in terms of *carbon* are summarized in Table 6.3. At pH about 6.5, the concentrations (in terms of carbon) required to achieve the minimum stability are at least 100 times less for PAA, FA and HA than those of simple organic species, such as oxalic and phthalic

acids. The strong effect of polyelectrolytes on hematite stability can be accounted for by the adsorption characteristics of polyelectrolytes. Polyelectrolytes are adsorbed on surfaces due to the bonding of each segment to the surface sites. Since many segments are linked together (linearly or branched) in a polyelectrolyte, the overall interaction energy can be very high, even if the adsorption energy of an individual segment is small. The carboxyl groups in FA and HA are the important segments in accounting for the adsorption of these organic molecules on the hematite surface. The critical coagulation concentrations in terms of –COOH at pH 6.5 are the same for both PAA and FA (6×10^{-7}M). The combined effect of the electrostatic energy, the specific chemical energy, and the hydrophobic energy of each segment favors adsorption, and consequently the naturally occurring fulvic and humic acids are the most effective materials in influencing hematite particle stability.

pH	Organics	c.c.c. (M)
6.2	Oxalic	4.0×10^{-4}
6.2	Phthalic	1.6×10^{-3}
6.8	PAA	6.0×10^{-7}
6.5	FA	4.3×10^{-6}
6.8	HA	3.6×10^{-6}
5.2	C_{12}	1.2×10^{-5}
5.2	C_{10}	1.0×10^{-3}
5.2	C_8	8.0×10^{-3}
5.2	C_3	3.0×10^{-1}

Table 6.3: Critical coagulation concentration of organics in terms of moles of carbon.

6.3 Effect of Temperature on Hematite Stability

Moderate changes in suspension temperature (e.g. 8–35°C) appear to have little effect on the stability of hematite particles in the presence of non-specific electrolytes. In the presence of specifically adsorbed species the situation can be different. For example, if adsorption of an anion on a positive surface is highly exothermic a decrease in temperature favors adsorption. Consequently, the concentration needed to re-

duce the surface potential would be less at lower temperature. At low temperature, species with exothermic adsorption characteristics have a stronger effect on coagulation. Conversely, at high temperature, species which are endothermically adsorbed have a stronger effect than at low temperature.

6.4 Modeling of Hematite Stability Ratios

Hematite stability ratios as a function of pH are modeled by applying the DLVO theory of colloid stability (Sec. 2.3). The stability ratio, W, given by Eq. (2.31), has been calculated numerically. For convenience the relevant equations from Chapter 2 are given below. The stability ratio is calculated from,

$$W = \int_0^\infty \frac{\beta(u')}{(2+u')^2} \exp\left(V_T/\mathrm{kT}\right) du' \Big/ \int_0^\infty \frac{\beta(u')}{(2+u')^2} \exp\left(V_A/\mathrm{kT}\right) du' \tag{6.2}$$

where, $u' = H'/(\delta + a)$, and $H' = H - 2\delta$. The function β is given by,

$$\beta(u) = \frac{6u^2 + 13u + 2}{6u^2 + 4u} \tag{6.3}$$

The total interaction energy, V_T, is evaluated as the sum of the van der Waals attraction energy, V_A, and the repulsive electrostatic energy, V_R. If $s = R/a$ and A is the Hamaker constant of the particle,

$$V_A = -\frac{A}{6}\left[\frac{2}{s^2-4} + \frac{2}{s^2} + \ln\left(\frac{s^2-4}{s^2}\right)\right] \tag{6.4}$$

and,

$$V_R = 4\pi\epsilon\epsilon_0 a' \left(\frac{\mathrm{RT}}{F}\right)^2 \left(\frac{R-a'}{R}\right) Y^2 \ln\left[1 + \frac{a'}{R-a'}\exp\left(-\kappa(R-2a')\right)\right] \tag{6.5}$$

where $a' = a + \delta$, and $Y = 4\tanh(zF\Psi_\delta/4RT)$.

The Hamaker constant, A, for hematite in water is reported to lie in the range 2 to 6×10^{-20} Joules (see Table 6.4). In our model calculations, a value of 6×10^{-20} Joules is used for hematite in water.

The potential Ψ_δ is taken as equal to the ζ-potential, which is derived from mobility data by applying Wiersema's approach (Appendix B). This substitution is

Reference	Hamaker Constant (J)	Medium
Visser (1972)	$10.6\text{-}15.5\times10^{-20}$	Vacuum
Fowkes (1965)	4.5×10^{-20}	Water
Fowkes (1967)	3.4×10^{-20}	Water
Dumont and	15.2×10^{-20}	Vacuum
Watillon (1971)	6.3×10^{-20}	Water
Matijevic (1981)	6.2×10^{-20}	Vacuum
	4.4×10^{-20}	Water
Penners (1985)	4.0×10^{-20}	Water
Breeuwsma (1973)	$2\text{-}4\times10^{-20}$	Water

Table 6.4: Hamaker constants for hematite.

justified if the δ-plane coincides, or nearly coincides, with the slipping plane. The distance, δ, is defined as the Stern layer thickness. It is often taken as the radius of the adsorbed species. Since chloride is the counter ion in our acidic media ($pH<pH_{zpc}$) for stability ratio determinations, δ is assumed to equal the chloride ion radius, i.e. 1.81Å. The distance from the surface to the slipping-plane must lie at least a distance equivalent to the size of the adsorbed ions away from the surface, because mobility is measured at a physical surface. Hence, the distance from the surface to the slipping-plane is not the same as that to the Stern plane. To distinguish these distances, we use t to denote the distance from the surface to the slipping plane. Mpandou and Siffert (1984) studied the adsorption of propionate on TiO_2 and measured the mobility in the presence of propionate. They found that the slipping plane is 4Å (the length of the tail group: $-CH_2CH_3$) away from the Stern plane. The value of 4Å is probably reasonable for the molecule they considered, but is too large for our case. Lyklema and de Wit (1978) used t=5.4Å for K^+ to model their iron oxide potential at the critical coagulation concentration. As an approximation, we assume that the slipping plane is 3.6Å away from the surface.

Thus, Ψ_t was used in place of Ψ_δ, and a value of $t = 3.6$Å replaced δ in calculating V_R. It was assumed that $\Psi_t = \zeta$, where ζ was evaluated from mobility data (Appendix

B). The result of the model is compared with the experimental values in Fig. 6.2, where the modeled stability ratio as a function of pH is drawn as a solid line and the experimental results are plotted as triangles. There is a good agreement between the experiment and model calculation. Since the surface potential is dependent on proton concentration, $\log W$ as a function of pH can be viewed as reflecting the variation in the stability ratio as a function of surface potential.

At a constant pH of 10.5, hematite surfaces maintain approximately a constant potential, and we can model the stability ratio as a function of Na^+ concentration. Substituting $\Psi_t = -32$ mV, and $t = 4.0$Å, the stability ratios are calculated and experimental and model results are shown in Fig. 6.3. It can be seen that a good agreement is obtained between the results of the experiments and the model. The reduction in the stability ratio illustrated in Fig. 6.3 is due to the compression of the diffuse layer as the sodium concentration increases.

On the basis of model calculations we can characterize the relationship between stability ratio and aqueous species concentration as follows.

(1) Specifically adsorbed species affect surface potential. Hence the variation of stability with concentration reflects the dependence of the stability ratio on surface potential.

(2) Non-specifically adsorbed species do not affect surface potential, but influence the stability ratio by compressing the diffuse layer.

(3) When the concentration of specifically absorbed species exceeds the background ionic strength the stability ratio is influenced by both changes in the surface potential and compression of the diffuse layer.

In the presence of the specifically adsorbed species, such as phosphate, the stability ratio as a function of ion concentration exhibits type (1) characteristics, if the background ionic strength is constant. If the potential determining ion concentration is raised above the background electrolyte concentration, then the stability ratio

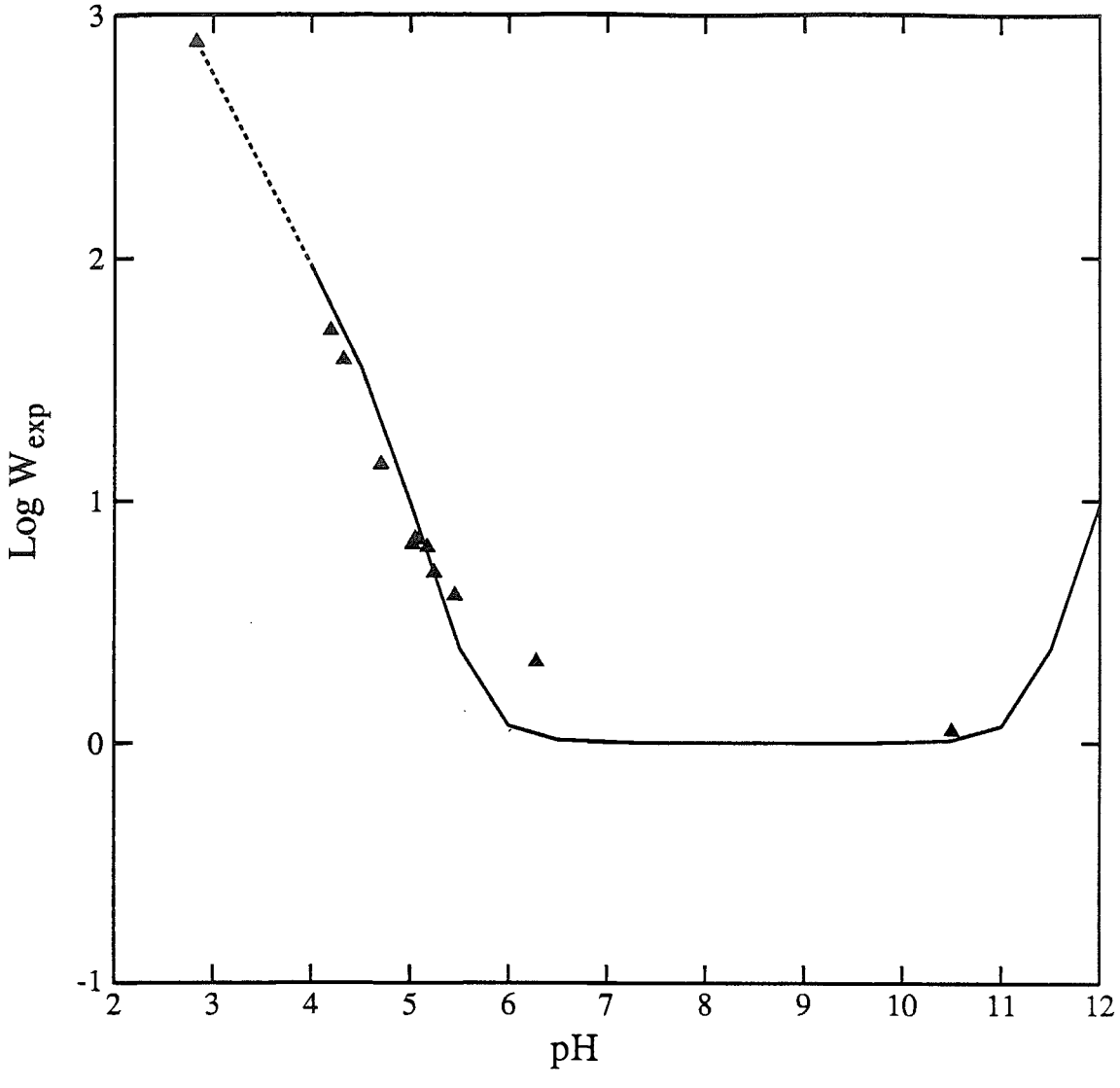

Figure 6.2: Stability ratio of a hematite suspension as a function of pH. Filled triangles are experimental values, and the solid line represents a DLVO model calculation. Ψ_t equals the ζ-potential given in Appendix B. Ionic strength=0.05M, t = 3.6Å, Hamaker constant, $A = 6 \times 10^{-20}$ Joules.

will exhibit type (3) behavior. For example, the dependency of the stability ratio on phosphate concentration at pH 6.55 (see Fig. 4.10) reflects a strong dependence of the stability ratio on surface potential. The change in surface potential caused by the adsorption of phosphate was calculated by applying the diffuse layer model (Fig. 5.5) and the relation of surface potential to ζ-potential (or Ψ_t) was discussed in

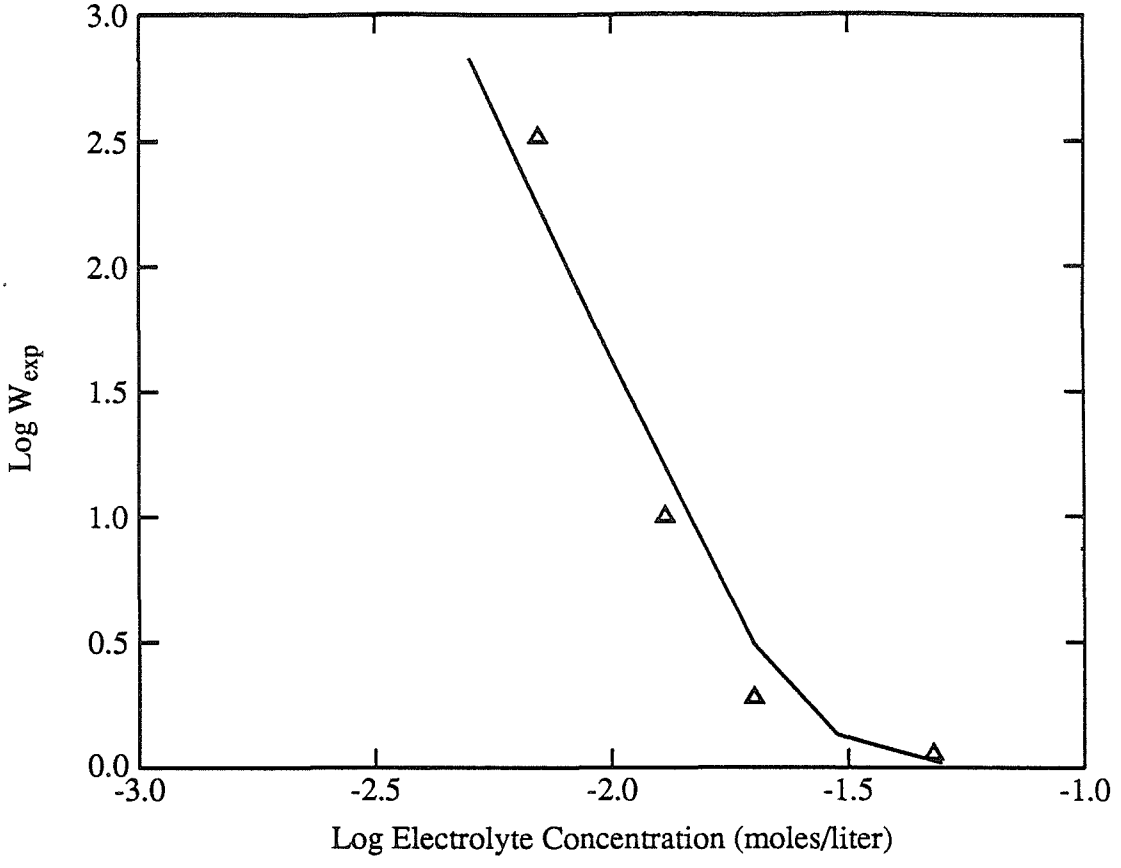

Figure 6.3: Stability ratio of a hematite suspension as a function of sodium concentration at pH 10.5. Open triangles are experimental values, and the solid line represents a DLVO model calculation. $\Psi_t = -32\text{mV}$, $t = 4.0\text{Å}$, Hamaker constant, $A = 6\times10^{-20}$ Joules.

Sec. 5.1.3. The value of the stability ratio is dependent on the potential, Ψ_t, which can be estimated from the mobility data in the presence of the corresponding amount of phosphate.

It is assumed in the calculation of V_R that the ions within the diffuse layer adjust themselves fast during particle encounters, so that the potential Ψ_t is unaltered. Although the input parameters of the model are not precisely known, reasonable stability ratios are predicted when the potential Ψ_t is derived from mobility measurements, and t is estimated from the size of the adsorbed ions.

The mobility and stability ratio of hematite particles are dependent on adsorption.

When strongly adsorbed species are present in the hematite suspension, the surface chemical properties are influenced by adsorption; consequently a shift of pH_{iep} is observed in the mobility. The adsorption of a strongly adsorbed ion is able to reverse the surface potential (e.g., at pH 6.5, phosphate adsorption can change positive surface potential to negative). The stability ratio as a function of ion concentration shows a characteristic "V" shape, where the stability is due to a positive potential on one side of the "V" and a negative potential on the other side. Adsorption plays a key role in determining the observed coagulation rates and mobility of hematite particles.

7. IMPLICATIONS AND FUTURE WORK

7.0 Introduction

The rapid removal of river-borne particles is a common phenomenon in estuaries, where the salinity changes as river water and sea water mix. Using the membrane filtration technique, Sholkovitz (1976) studied the non-conservative behavior of river-borne organics and inorganics. He attributed the removal process to flocculation, which he used as a general term to denote the transition from the "dissolved" to the solid phase, i.e., coagulation, flocculation and precipitation. He concluded that the flocculation of river-introduced colloidal humic substances and their associated inorganic trace elements is the main factor in controlling the non-conservative behavior of river-borne particles in estuaries. In connection with the technique he used, the term "filtrable" is more appropriate than "dissolved". Hence, filtrable iron can be mostly colloidal iron oxides. It has been recognized (Mayer, 1982; Fox and Wofsy, 1983; and Hunter, 1983) that "dissolved" iron in river waters is mainly in the form of colloidal Fe(III) oxides stabilized by river humic acids, and is flocculated as the seawater electrolyte concentration increases.

On the basis of the observations in this work, iron removal in estuarine waters is interpreted as the consequence of coagulation of colloidal iron oxides with adsorbed humic acids. Since the coagulation kinetics presented in this work were investigated by a light scattering technique and field studies on iron removal were based on mem-

brane filtration, a bridge is needed to connect the results obtained from these two techniques. In the next section hematite stability determination by the membrane filtration techniques is first described. It is found that the light scattering technique yields the same stability ratio for hematite as the filtration method. Field studies of iron removal in natural water systems using filtration techniques can therefore be interpreted using the results in this thesis. The chapter concludes with a discussion of possible future work.

7.1 Filtration Methods vs. Light Scattering Techniques

In the membrane filtration method, a filter of a certain cutoff size is used. For practical purposes, one filter size of 0.45μm is commonly used, although a range of 0.01 to 100μm filters is reported in filtration measurements in the literature. The procedure for iron determination in the estuarine zone by the filtration method is summarized as follows. A river water sample is first filtered, and the amount of iron in the filtrate is measured (by colorimetric or spectrophotometric methods). The iron determined is defined as "dissolved iron". The filtered river water is then mixed with seawater (simulating the estuarine mixing zone), allowed to settle and subsequently filtered. The iron remaining in the filtrate is measured and the amount of iron removed is determined.

In the filtration method, the collected mass on a filter corresponds to the mass of aggregated particles as a result of changing ionic strength and time. The basis of the light scattering technique, however, is the change in the number concentration and the size of the particles. The rate of change in the mass concentration of the filtrable particles can be related to the change in number concentration by assuming a certain shape and the size distribution for the filtrable particles.

7.1.1 Experimental Procedure

An experiment based on the filtration procedure was designed and carried out in

this research as a case study. A nuclepore filter of pore size 0.1μm was used since singlet particles go through the filter, but aggregates of two or more particles in general do not. Preliminary experiments showed that monodispersed particles completely pass the filter with a recovery of at least 95%. The filtrate iron mass concentration can be determined by dissolving the oxide in acid, and then measuring the total iron by atomic absorption spectrophotometry. For a quick and simple measurement, a calibration curve was made using a spectrophotometer at $\lambda = 364$nm for different hematite mass concentrations. Figure 7.1 shows a linear relationship between the total extinction of light and hematite mass concentration. Preliminary experments showed that in the presence of 0.01M NaCl, the stability ratio of hematite at pH 11 is about 20 (see Fig. 4.5). If the initial particle number concentration is 3×10^9 cm^{-3} the coagulation characteristic time is 15 minutes.

Based on these estimates, the filtration experiment was carried out as follows. Approximately 3 mg/l of hematite particles were dispersed in a beaker at pH 11. NaCl was introduced into the suspension to make the final ionic strength 0.013M. At 5 minute intervals 10ml of suspension was withdrawn, filtered, and the concentration of hematite in the filtrate was determined.

7.1.2 Results and Interpretation

The results of the filtration experiment are presented in Fig. 7.2, where the amount of material remaining in the filtrate (normalized with respect to the initial concentration) is plotted against time. The figure shows that in the first 5 minutes of the experiment about 40% of the colloidal hematite particles are removed. The iron removal is entirely due to the coagulation of colloidal particles. The removal process slows down as the experiment progresses. The behavior of colloidal hematite removal resembles the filtration results presented by Mayer (1982), who showed the filtrable iron fraction as a function of time when river water and seawater were mixed.

The results of the filtration study presented in Fig. 7.2 are in terms of mass

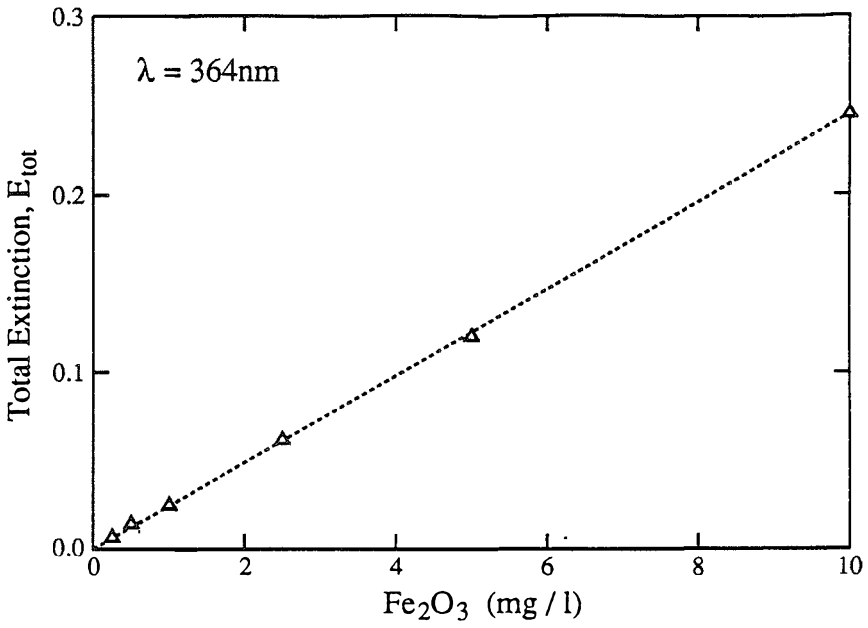

Figure 7.1: Calibration curve used to determine hematite mass concentration from total light extinction at wavelength $\lambda = 364$nm.

concentration. The conversion of a mass concentration to a number concentration is readily made since hematite particles are approximately spherical in shape and monodispersed. The evolution of the particle size distribution as a result of coagulation of initially monodispersed particles is given by Smoluchowski's simplified equations (Sec. 2.1). The mass of a particle of diameter d, with density ρ, can be calculated from $\pi d^3 \rho/6$ and the number concentration can be converted to a mass concentration. Fig. 7.3 shows the hematite mass fraction as a function of time of a hematite suspension undergoing coagulation. This plot is related to the variation of number concentration with time shown in Fig. 2.1. Although the total number concentration is reduced by coagulation, the total mass concentration is conserved. The hematite mass remaining in the filtrate (i.e., what passes through the 100nm filter) at the time of filtration corresponds to the mass of singlets. The experimentally determined number of singlets remaining as a function of time is compared with that predicted by theory in Fig. 7.3, in which the data points are derived from the filtration

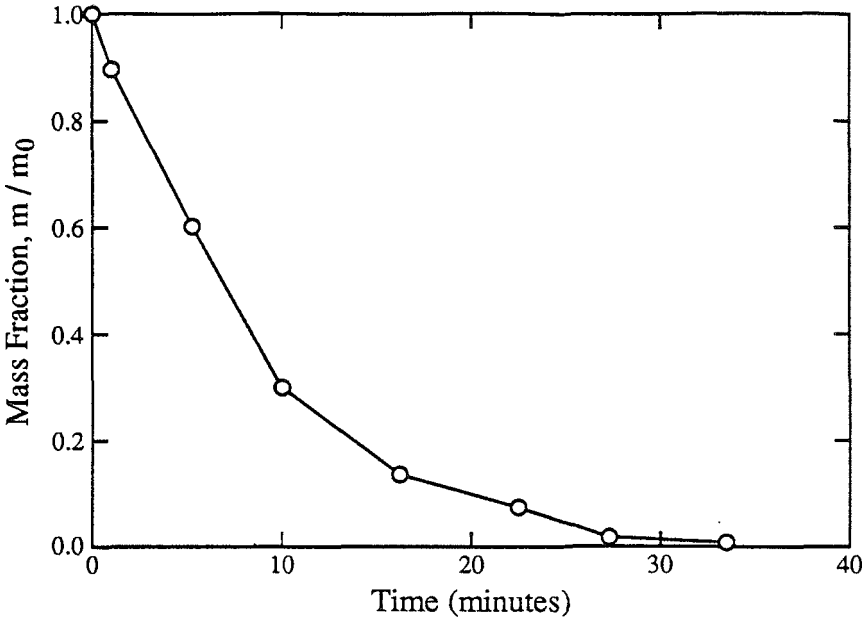

Figure 7.2: Mass fraction remaining in filtrate plotted as a function of time for a hematite suspension of 3.62 mg/l. The ionic strength is 1.3×10^{-2}M, and the pH is 11.0.

results of Fig. 7.2. In Fig. 7.3 time is normalized by dividing by the characteristic coagulation time, τ, of 15 minutes. The data points at the initial stage of coagulation ($t/\tau < 1$) follow the predicted mass concentration of singlets fairly well. At times exceeding the coagulation characteristic time, the experimental results deviate from the theoretical prediction. The underlying assumption in interpretating the filtration results is that the total mass is conserved, but in reality, the total mass may not be conserved due to the mass loss to the wall of the container. This loss may be cumulative over time which may provide an explanation for the observed deviation in the hematite mass fraction from the theory at longer experimental time.

Nevertheless, the results of the initial stage filtration experiment are sufficient for comparison with the results obtained by the light scattering method, since the coagulation rate constants were derived from the initial light scattering data (Sec. 4.1). For the experimental conditions pertaining (3.62mg/l, pH=11, (NaCl)=0.013M), the

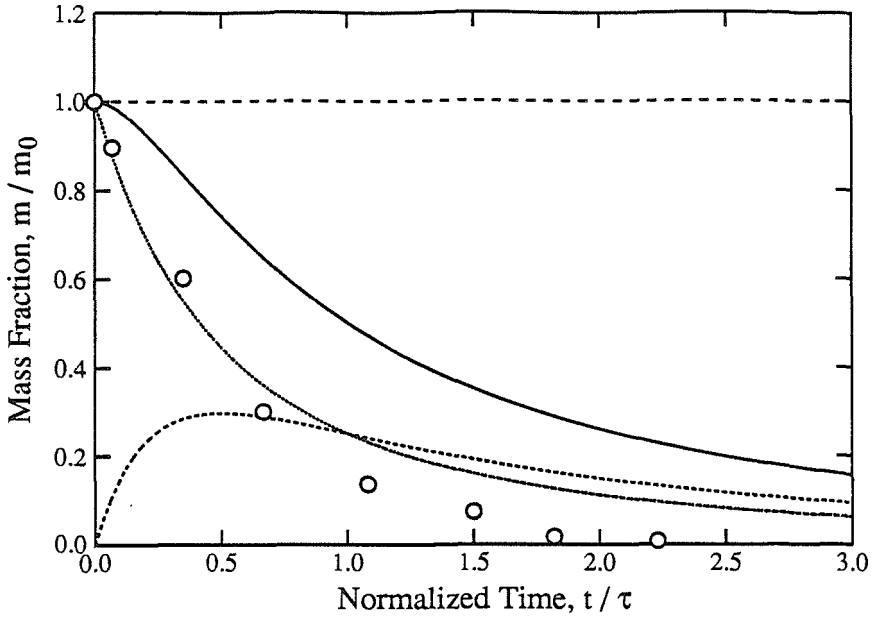

Figure 7.3: Mass fraction as a function of normalized time. The dotted line and the short dashed line represent the mass fraction of singlets and doublets, respectively. The solid line is the sum of these two fractions. The total mass, shown by a long dashed line, is conserved during coagulation. The open circles are data from Fig. 7.2.

fast diffusion controlled time scale is of the order of 40 seconds. The longer actual coagulation time of 15 minutes is due to the repulsion between particles during their encounter. Comparison of these time scales yields a stability ratio of 20. This is the same value as that derived from coagulation data by the light scattering technique. Using a simple monodispersed hematite suspension, the stability ratio obtained from the light scattering method agrees well with the result from the filtration method. Hence, it is concluded that the initial filtration results of field studies can be interpreted on the basis of coagulation kinetics determined by light scattering techniques.

7.2 Implications for Natural Water Systems

Riverine filtrable iron is reported to exist mostly in the form of mixed iron oxide-organic matter colloids, of diameter less than 0.45μm. (Boyle et al., 1977). In the estuarine zone, iron is observed to be not conserved, and this behavior is attributed to

aggregation, which is induced by the increased concentration of seawater electrolytes (Boyle et al., 1977; Hunter, 1983; and Mayer, 1982). The behavior of riverine iron oxide in estuaries may be interpreted on the basis of the findings of this research.

7.2.1 The Origin of the Surface Charge

In the range of pH 6.5 to 8.2 (which are the typical values of river water to seawater), the mobilities of hematite particles are negative in the presence of 0.1 mg/l fulvic acid (Fig. 4.23), even though the hematite particles themselves are positively charged in simple salt solutions over the same pH range. Sholkovitz (1976) found that in all his river samples, although humic acids account for only 4-20% of the total organic matter, the humic acid concentration exceeds 0.3 mg/l, which is sufficient to cause iron oxide particles to reverse their surface charge. The adsorption of humic acid on the surface of iron oxide is a possible explanation for the general observation of negatively charged particles in lakes, rivers and estuaries.

7.2.2 Stability of Particles in Lake Waters

From the present research we conclude that hematite particles (and iron oxide particles of similar surface properties) are relatively stable in most lake environments, where pH is near 7, ionic strength is low, and humic acid concentration exceeds 0.1 mg/l. The stability ratio of hematite particles in the presence of 0.3 mg/l of humic acids (Fig. 4.16) is in the range of 10 to 1000 in the presence of 0.5 to 1 millimoles/liter of Ca^{2+}. Field studies by Tipping and Ohnstad (1984) showed that the coagulation rate is of the order of 10^{-13} cm^3/sec in a lake water environment ($Ca^{2+} + Mg^{2+} \sim 3 \times 10^{-4}M$, pH $\sim 6.6 - 6.9$). Comparing this rate constant with the diffusion-controlled constant ($3.2 \times 10^{-12} cm^3/sec$), particles occurring in lakes have a stability ratio of about 30. Laxen and Chandler (1983) reported a detailed study of the size distribution of iron and manganese species in freshwater lakes. Using the membrane filtration method, they obtained a particle size distribution in a range of 0.01 to 100μm. They observed a close correspondence between the size distribution of

particles in lake waters and the theoretical predictions made by O'Melia on the basis of particle coagulation and sedimentation. The rate of aggregation of their lake particles were reported to be relatively slow. If it is assumed that the iron they collected in the lake water is in the form of Fe_2O_3 and that the average size is 0.5μm, the time scale for diffusion-controlled coagulation is estimated to be 15 hours. The lifetime of average particles was found to be 7–77 days; this indicates that the stability ratio of particles used by Laxen and Chandler is in the range 10 to 120. These two examples demonstrate that the adsorption of humic substance in typical lake environments (low ionic strength, near neutral pH) greatly increases the stability of iron oxide particles.

Coagulation in a naturally occurring particle suspension (e.g., lake waters) may be affected by the heterogeneous distribution of the particles (0.01-100μm). Small particles swept up by large particles as a consequence of differential sedimentation can contribute to the overall coagulation rate. Large particles ($>$ 1μm in diameter) are also expected to be subjected to fluid shear and turbulence during particle collision. The presence of different kinds of particles in natural waters, e.g., SiO_2, Al_2O_3, etc., is expected to influence particle coagulation rates. At pH 6.5, for example, coagulation between SiO_2 particles and iron oxides particles may readily take place because of the favorable electrostatic interactions. Hence it is expected that the coagulation rate in a natural water system will be faster than in a controlled laboratory experiment where only monodispersed particles are used.

7.2.3 Coagulation of Particles in Estuaries

In the estuarine zone, salinity varies from near 0 to 3.5%, which corresponds to an ionic strength ranging from that of incoming river water to that of seawater, which is about 0.7M. Over this span of ionic strength, the stability of iron oxide particles can vary greatly and the coagulation rate of the particles is determined by the chemical composition of the river water and the river flow rate (through the mixing ratio and, consequently, the particle number concentration and ionic strength). On the

basis of the findings of this research, the mixing of river waters and seawater can affect the stability of iron oxide particles by changing the pH from near 7 (typical of river waters) to near 8 (typical of seawater). Thus the pH becomes closer to the pH_{zpc} of 8.5, thereby promoting coagulation. The sulfate concentration in seawater ($\sim$0.028M) is higher than in fresh water, and the increase in sulfate concentration in estuaries can influence oxide particle stability through specific chemical reactions, in addition to the effects of electrostatic interactions. If humic substances or phosphate concentrations are high in the river water, iron oxide particles will be negatively charged and the stability of these particles will be high if salinity is <0.5% (< 0.1M). At higher salinity (> 0.5%), coagulation appears to be mainly a diffusion controlled process, independent of river water chemical composition.

The results of estuarine studies by Sholkovitz (1976) using the filtration method show that at salinity > 1.5%, "dissolved" iron is removed from solutions of mixed river waters and seawater by a 0.45μm filter in half an hour (removal was 75–100%). A similar experiment by Hunter (1983) confirmed that at 1.0–1.5% salinity "dissolved" iron (mainly as hydrous Fe(III) oxides) was aggregated into particles larger than 1.2μm, and was completely removed from solution by a 1.2μm filter. In the examples described above, the particle stability ratio is essentially 1, resulting from the compression of the electrical diffuse layer, even though river-borne particles may have high negative surface potential due to the adsorption of humic substances.

Although particle transport has been shown to be rate limiting in coagulation at high salinity, the role of chemistry cannot be neglected in understanding the behavior observed in natural systems. The chemical composition of river water is a key to understanding the surface properties of river-borne particles. The functional groups on the surface of particles are also important in understanding the scavenging of trace elements in the process of coagulation.

7.2.4 Temperature and Coagulation

Mayer (1982) studied aggregation of river filtrable iron (colloidal iron) as a function of temperature (seasonality) during estuarine mixing. He found that the coagulation rate is dependent on temperature, and a slower rate is observed at lower temperature. Since the experiment was made by filtration and the pore size of the filter was between 0.2–0.4μm, it can be deduced that collisions are the result of the thermal energy of the small particles, and the collision rate is thus affected by changes in temperature. On the basis of our work, it can be deduced that at the ionic strength of his study (0.16M or 0.83% salinity), the stability of the particles is of the order of 1, and the overall coagulation rate is given by $k_a = 4kT/3\mu$. This rate expression shows that the temperature effect on coagulation rate is from temperature itself and the temperature dependent viscosity. According to this rate expression, a slower coagulation rate is expected during winter for these submicron colloidal suspensions. Temperature changes are expected to have an effect on other transport mechanisms, which might be involved in estuaries and lakes. The influence of temperature on fluid shear and turbulence induced coagulation may occur through changes in fluid properties, such as the viscosity and density.

7.3 Recommendations for Future Work

7.3.1 The Structure of Iron Oxide

Hematite particles were used in all experiments throughout this research. We have demonstrated the importance of the chemical reactions between certain aqueous ions (those specifically adsorbed) and surface hydroxyl groups of hematite in controlling the particle coagulation rate. It is of interest to know whether these findings can be generalized to other iron oxide suspensions. Goethite, for example, has similar surface groups, and extensive adsorption data exist for several aqueous species, e.g., phosphate, on the surface of goethite. Each oxide has a different crystal structure, and hence has different site densities and surface energies of adsorption (e.g., differ-

ences in pH_{zpc}, and ΔpK_a for proton adsorption). It is expected that oxides with different crystal structures will have quantitatively different stability behavior. The general shape of stability ratio vs. pH with respect to pH_{zpc}may be similar, but the magnitude of stability ratio at the same ΔpH (pH$-pH_{zpc}$) for different iron oxides will be different. The effect of the same adsorbed species on stability of different oxides may differ because the adsorption energies of the aqueous species are not expected to be the same at the surface of different oxides. An understanding of the effect of the oxide crystal structure on adsorption is essential in predicting the stability of these oxide particles.

At the present time, there is little information on the effect of temperature on surface chemistry of various oxides. Furthermore, adsorption of interesting ions (such as phosphate) on the surface of iron oxides as a function of temperature is also lacking. Hence a knowledge of site density, pH_{zpc}, ΔpK_a, pH_{iep} (in the presence of strongly adsorbed ions, such as phosphate, and humic acids) at a constant temperature is helpful in understanding the relation between oxide crystal structure and particle stability.

Hematite is representative of iron oxides, even though we know individual oxides, e.g., α-FeOOH, β-FeOOH, γ-Fe_2O_3, etc., will differ in detail. Amorphous iron oxides, which are commonly found in natural waters, lack a definite crystal structure and a quantitative application of the findings from hematite particles to amorphous particles is difficult. However, the energy relationships presented by Kummert and Stumm (1980) on anion adsorption on metal oxides and aqueous metal-ion complex formation shows the importance of the type of metal ion in the oxide surface in determining the adsorptive behavior (although there are large uncertainties involved in the experimental results, as may be seen in Fig. 6.1). Hence, at least a qualitative understanding to the chemical behavior of naturally occurring iron oxides can be gained.

7.3.2 Effects of Other Particles

Small particles ($< 1\mu$m) serve us well in understanding electrostatic or diffuse-layer effects in general, and specific effects of chemistry (e.g., adsorption of H^+, phosphate, humic substances, etc.) on coagulation since the collision process is simply regulated by thermal energy. It is important to know whether the results deduced using small particles can be extended to a system composed of larger particles the same kind (e.g., Fe_2O_3 from 0.01 to, say, 10μm), where fluid shear, turbulence and differential settling also cause particle collisions. If chemical and electrostatic effects are insensitive to changes in particle size, it can be expected that the stability ratio derived from kinetic studies of small particles is applicable to large particles. In addition, the stability ratio derived from the initial coagulation rate can be expected to be the same throughout the coagulation process, although the dominant transport mechanism may change from Brownian collision for the submicron sized particles to fluid shear or differential sedimentation controlled processes when particles have aggregated to form large (above 1μm) clusters.

The presence of other kinds of particles is expected to affect the stability ratio. For example, at pH 6.5, positively charged hematite particles will coagulate with negatively charged SiO_2 particles as a result of the favorable electrostatic energy. In natural water environments, heterogeneous particle size distributions are commonly observed (Ali, et al., 1984; Laxen et al., 1983), and particles are usually made of different kinds of metal oxides (and biological particles). Heterogeneous coagulation kinetics may be better understood by combining a knowledge of the chemical aspects of coagulation and fluid transport models.

REFERENCES

Adamson, A.W., (1982), *Physical Chemistry of Surfaces*, 4th ed., John Wiley & Son, New York

Ali, W., O'Melia, C.R. and Edzwald, J.K., (1984), "Colloidal Stability of Particles in Lakes: Measurement and Significance," *Water Sci. Technol.*, **17**, 701

Balistrieri, L.S. and Murray, J.P., (1987), "The Influence of the Major Ions of Seawater on the Adsorption of Simple Organic Acids by Goethite," *Geochim. Cosmochim. Acta*, **51**, 1151

Bell, G.B., Levine, S. and McCartney, L.N., (1970), "Approximate Methods of Determining the Double-layer Free Energy of Interaction between Two Charged Colloid Spheres," *J. Colloid Interface Sci.*, **33**, No.3, 335

Boyle, E.A., Edmond, J.M. and Sholkovitz, E.R., (1977), "The Mechanism of Iron Removal in Estuaries," *Geochim. Cosmochim. Acta*, **41**, 1313

Breeuwsma, A., (1973), Adsorption of Ions on Hematite (α-Fe_2O_3), *Ph.D. Thesis*, Agricultural University, Wageningen, The Netherlands

Breeuwsma, A. and Lyklema, J., (1973), "Physical and Chemical Adsorption of Ions in the Electrical Double Layer on Hematite (α-Fe_2O_3)," *J. Colloid Interface Sci.*, **43**, No.2, 437

Brunauer, S., Emmett, P.H. and Teller, E., (1938), *J. Amer. Chem. Soc.*, **60**, 309

Chan, D.Y.C., (1985), Free Energies of Electrical Double Layers at the Oxide-Solution Interface, *ACS Symposium Series 323*, Davis, J.A., ed.

Chan, D.Y.C., (1983), "The Free Energies of an Electrical Double Layer," *J. of Colloid Interface Sci.*, **95**, 193

Davies, S.H.R., (1985), Mn(II) Oxidation in the Presence of Metal Oxides, *Ph.D. Thesis*, California Institute of Technology, Pasadena, CA

Davis, J.A., (1982), "Adsorption of Natural Dissolved Organic Matter at the Oxide/Water Interface," *Geochim. Cosmochim. Acta*, **46**, 2381

Debye, P., (1909), *Ann. Physic*, **30**, 59

Dumont, F. and Watillon, A., (1971), "Stability of Ferric Oxide Hydrosols," *Discuss. Faraday Soc.*, **52**, 352

Dumont, F., Dang, V.T. and Watillon, A., (1976), "Study of of Ferric Oxide Hydrosols from Electrophoresis, Coagulation, and Peptization Measurements," *J. Colloid Interface Sci.*, **55**, No.3, 678

Dzombak, D.A. and Morel, F.M.M., (1987), "Adsorption of Inorganic Pollutants in Aquatic Systems," *J. Hydraulic Engineering*, **113**, No.4 430

Faughnan, J., (1981), *SURFEQL/MINEQL Manual*, Caltech, Pasadena, Unpubl.

Faust, B.C., (1985), Photo-induced Reductive Dissolution of Hematite (α-Fe_2O_3) by S(IV) Oxyanions, *Ph.D. Thesis*, California Institute of Technology, Pasadena, CA

Fokkink, L.G.J., (1987), Ion Adsorption on Oxides, Surface Charge Formation and Cadmium Binding on Rutile and Hematite, *Ph.D. Thesis*, Agricultural University, Wageningen, The Netherlands

Fowkes, F.M., (1965), Attractive Forces at Interfaces, *Chemistry and Physics of Interfaces*, Ross, S., ed., ACS Publication, Washington, D.C.

Fowkes, F.M., (1967), *Surfaces and Interfaces*, Vol. 1, Burke, J.J., ed., Syracuse Univ. Press, New York

Fox, L. and Wofsy, S.C., (1983), "Kinetics of Removal of Iron Colloids from Estuaries," *Geochem. Cosmochim. Acta*, **47**, 211

Fuchs, N., (1934), "Über Die Stabilität und Aufladung Der Aerosole," *Z. Physik*, **89**, 736

Fuerstenau, T.W., (1971), The Adsorption of Surfactants at Solid–Water Interfaces, *The Chemistry of Biosurfaces, Vol.1*, Hair, M.L., ed., Marcel Dekker, New York

Fuerstenau, T.W., (1981), The Adsorption of Oleate from Aqueous Solution onto Hematite, *Adsorption from Aqueous Solutions*, Tewari, P.H. ed., Plenum Publ.

Gaudin, A.M. and Fuerstenau, D.W., (1955), "Quartz Flotation with Cationic Collectors," *Transactions AIME*, **202**, 958

Gibbs, R.J., (1983), "Effect of Natural Organic Coatings on the Coagulation of Particles," *Environ. Sci. Technol.*, **17**, 237

Gregory, J., (1977), Effects of Polymers on Colloid Stability, *The Scientific Basis of Flocculation*, Sijthoff and Noordhoff, The Netherlands

Gregory, J. and Wishart, A.J., (1980), "Deposition of Latex Particles on Alumina Fibers," *Colloids and Surfaces*, **1**, 313

Gschwend, P.M. and Reynolds, M.D., (1987), "Monodisperse Ferrous Phosphate Colloids in an Anoxic Ground Plume," *J. Contam. Hydrol.*, **1**, 309

Hahn, H.H and Stumm, W., (1968), "Kinetics of Coagulation with Hydrolyzed Al(III), the Rate-Determination Step," *J. Colloid Interface Sci.*, **28**, No.1, 134

Hamaker, H.C., (1937), "The London-Van der Waals Attraction between Spherical Particles," *Physica*, **4**, 1058

Honig, E.P., Roeberson, G.J. and Wiersema, P.H., (1971), "Effect of Hydrodynamic Interaction on the Coagulation Rate of Hydrophobic Colloids," *J. Colloid Interface Sci.*, **36**, No.1, 97

Hsu, W.P. and Matijević, E., (1985), "Optical Properties of Monodispersed Hematite Hydrosols," *Applied Optics*, **24**, No.11, 1623

Hull, M. and Kitchener, J.A., (1969), "Interaction of Spherical Particles with Planar Surfaces," *Trans. Faraday Soc.*, **65**, 3093

Hunt, J., (1980), Coagulation in Continuous Particle Size Distribution; Theory and Experimental Verification, *Ph.D. Thesis*, California Institute of Technology, Pasadena, CA

Hunter, K.A. and Liss, P.S., (1982), "Organic Matter and the Surface Charge of Suspended Particles in Estuaries Waters," *Limnol. Oceanogr.*, **27**, No.2, 322

Hunter, K.A., (1983), "On the Estuarine Mixing of Dissolved Substances in Relation to Colloid Stability and Surface Properties," *Geochimica Cosmochim. Acta*, **47**, 467

Hunter, K.A., (1980), "Microelectrophoretic Properties of Natural Surface-active Organic Matter in Coastal Seawater," *Limnol. Oceanogr.*, **25**, No.5, 807

Hunter, R.J., (1981), *Zeta Potential in Colloid Science*, Academic Press, London

James, R.O. and Parks, G.A., (1982), Characterization of Aqueous Colloids by Their Electrical Double-Layer and Intrinsic Surface Chemical Properties, *Surface and Colloid Science*, Vol.12, Matijivić ed., Plenum, New York

Jurinak, J.J., (1966), "Surface Chemistry of Hematite: Anion Penetration Effect on Water Adsorption," *Soil Sci. So. Amer. Proc.*, **30**, 559

Kasper, D.R., (1971), Theoretical and Experimental Investigations of the Flocculation of Charged Particles in Aqueous Solutions by Polyelectrolytes of Opposite Charge, *Ph.D. Thesis*, California Institute of Technology, Pasadena, CA

Kerker, M., (1969), *The Scattering of Light and Other Electromagnetic Radiation*, Academic Press, New York

Kerker, M., Scheiner, P., Cooke, D.D. and Kratohvil, J.P., (1979), "Absorption Index and Color of Colloidal Hematite," *J. Colloid Interface Sci.*, **71**, No.1, 176

Kummert, R. and Stumm, W., (1980), "The Surface Complexation of Organic Acids on Hydrous γ-Al_2O_3," *J. Colloid Interface Sci.*, **75**, 373

Kummert, R., (1979), Die Oberflächenkomplexbildung von organischen Säuren mit Gamma-Aluminiumoxid und ihre Bedeutung für natüliche Gewässer *Ph.D. Thesis*, Eidgenössischen Technischen Hochschule Zürich, Zürich

Laxen, D.P.H., and Chandler, I.M., (1983), "Size Distribution of Iron and Manganese Species in Freshwaters," *Geochim. Cosmochim. Acta*, **47**, 731

Lykema, J. and de Wit, J.N., (1978), "Colloid Stability of Silver Iodide in Water-Ethylene Glycol Mixtures," *Colloid Polymer Sci.*, **256**, 1110

Lyklema, J., (1978), Surface Chemistry of Colloids in Connection with Stability, *The Scientific Basis of Flocculation*, Sijthoff and Noordhoff, The Netherlands

Lyklema, J., (1985), How Polymers Adsorb and Affect Colloid Stability, *Proceedings of the Engineering Foundation Conference*, Sea Island, Geogia

Lyklema, J., (1980), "Colloid Stability as a Dynamic Phenomena," *Pure Applied Chem.*, **52**, 1221

Matijivić, E. and Scheiner, P., (1978), "Ferric Hydrous Oxide Sols," *J. Colloid Interface Sci.*, **63**, No.3, 509

Matijević, E., Kuo, R.J. and Kolny, H., (1981), "Stability and Deposition Phenomema of Monodispersed Hematite Sol," *J. Colloid Interface Sci.*, **80**, No.1, 94

Mayer, L.M., (1982), "Aggregation of Colloidal Iron during Estuarine Mixing: Kinetics, Mechanism and Seasonality," *Geochim. Cosmochim. Acta*, **46**, 2527

McCartney, L.N. and Levine, S., (1969), "An Improvement on Derjaguin's Expression at Small Potentials for the Double Layer Interaction Energy of Two Spherical Colloidal Particles," *J. Colloid Interface Sci.*, **30**, No.3 345

Micale, F.J., Kiernan, D. and Zettlemoyer, A.C., (1985), "Characterization of the Surface Properties of Iron Oxides," *J. Colloid Interface Sci.*, **105**, No. 2, 570

Mie, G., (1908), *Ann. Physik*, **25**, 377

Morel, F.M.M., (1983), *Principles of Aquatic Chemistry*, John Wiley & Sons, New York

Mpandou, A. and Siffert, B., (1984), "Sodium Carboxylate Adsorption onto TiO_2: Shortest Chain Length Allowing Hemimicelle Formation and Shear Plane Position in the Electric Double Layer," *J. Colloid Interface Sci.*, **102**, No.1, 138

Napper, D.H. and Hunter, R.J., (1972), Hydrosols, *Chap.8, Surface Chemistry and Colloids*, MTP International Review of Sci.,Vol.7, M. Kerker, ed., Butterworths, London

O'Melia, C.R., (1987), Particel-particle Interactions, *Chap.14, Aquatic Surface Chemistry*, Stumm, W. ed., John Wiley & Sons, New York

Ottewill, R.H. and Sirs, J.A., (1957), "Automatic Spectrophotometric Recording of the Coagulation of Hydrophobic Sols," *Photoelectric Spectrometry Group, Bulletin*, **10**, 262

Ottewill, R.H. and Shaw, J.N., (1966), "Stability of Monodisperse Polystyrene Latex Dispersions of Various Sizes," *Discus. Faraday Soc.*, **42**, 154

Parfitt, R.L., (1978), "Anion Adsorption by Soils and Soil Materials," *Advan. Agronomy*, **30**, 1

Parks, G.A. and DeBruyn, P.L., (1962), "The Zero Point of Charge of Oxides," *J. Phys. Chem.*, **66**, 967

Peck, A.S., Raby, L.H. and Wadsworth, M.E., (1966), "An Infrared Study of the Flotation of Hematite with Oleic Acid and Sodium Oleate," *Trans. AIME*, **235**, 301

Penners, N.H.G., (1985), THe Preparation and Stability of Homodisperse Colloidal Hematite (α-Fe_2O_3), *Ph.D. Thesis*, Agricultural University, Wageningen, The Netherlands

Penners, N.H.G. and Koopal, L.K., (1986), "Preparation and Optical Properties of Homodisperse Hematite Hydrosols," *J. Colloid Interface Sci.*, **19**, 337

Penners, N.H.G. and Koopal, L.K., (1987), "The Effects of Particle Size on the Stability of Hematite (α-Fe_2O_3) Hydrosols," *Colloids and Surfaces*, **28**, 67

Perrin, D.D., (1979), Organic Ligands, *Stability Constants of Metal-Ion Complexes*, Pergermon, Oxford

Schindler, P.W., Furst, B., Dick, R. and Wolf, P.U., (1976), "Ligand Properties of Surface Silanol Groups," *J. Colloid Interface Sci.*, **55**, 469

Schindler, P., (1981), Surface Complexes at Oxide-Water Interfaces, *Adsorption of Inorganics at the Solid/Liquid Interface*, Anderson, N. and Rubin, A., eds., Ann Arbor Sci., Michigan

Schwertmann, U. and Taylor, R.M., (1977), Iron Oxides, *Chap.5, Minerals in Soils Environments*, Soil Science Soc. of America, Madison, Wisconsin

Sholkovitz, E.R., (1976), "Flocculation of Dissolved Organic and Inorganic Matter during the Mixing of River Water and Seawater," *Geochim. Cosmochim. Acta*, **40**, 831

Sigg, L., (1985), Metal Transfer Mechanism in Lakes, *Chemical Processes in Lakes*, Stumm, W., ed., Wiley, New York

Sigg, L., (1987), Surface Chemical Aspects of the Distribution and Fate of Metal Ions in Lakes, *Chap.12, Aquatic Surface Chemistry*, Stumm, W. ed., Wiley-Interscience, New York

Sigg, L. and Stumm, W., (1981), "The Interaction of Anions and Weak Acids with the Hydrous Goethite (α-FeOOH) Surface," *Colloid and Surfaces*, **2**, 101

Sigg, L., (1979), Die Wechselwirkung von Anionen und Schwachen Säuren mit α-FeOOH (Goethit) in Wässriger Lösung, *Ph.D. Thesis*, Eidgenössischen Technischen Hochschule Zürich, Zürich

Sillèn, L.G. and Martell, A.E., (1964), *Stability Constants of Metal-Ion Complexes*, The Chemical Soc., London

Sillèn, L.G. and Martell, A.E., (1971), *Stability Constants of Metal-Ion Complexes*, Supplement No.1, 2nd ed., The Chemical Soc., London

Smith, R.M. and Martel, A.E., (1976), *Critical Stability Constants*, Vol.4, Plenum, New York

Smoluchowski, M.V., (1917), "Versuch Einer Mathematischen Theorie der Koagulationskinetik Kolloider LöSungen," *Z. Phys. Chem*, **92**, 129.

Somasundaran, P., Healy, T.W and Fuerstenau, T.W., (1964), "Surfactant Adsorption at the Solid–Liquid Interface–Dependence of Mechanism on Chain Length," *J. Phys. Chem.*, **68**, 3562

Spielman, L.A., (1970), "Viscous Interactions in Brownian Coagulation," *J. Colloid Interface Sci.*, **33**, No.4, 562

Sposito, G., (1983), "On the Surface Complexation Model of the Oxide Aqueous Solution Interface," *J. Colloid Interface Sci.*, **91**, No.2, 329

Stumm, W. and Morgan, J.J., (1981), *Aquatic Chemistry*, 2nd ed., John-Wiley & Sons, New York

Stumm, W. and Morgan, J.J., (1962), "Chemical Aspects of Coagulation," *J. Amer. Water Works Assoc.*, **54**, 971

Thurman, E.M. and Malcolm, R.L., (1983), Structural Study of Humic Substances: New Approaches and Methods, *Terrestrial Humic Materials*, Christman, R.F. and Gjessing, E.T., ed., Ann Arbor Sci., Michigan

Tipping, E. and Higgins, D.C., (1982), "The Effect of Adsorbed Humic Substances on the Colloid Stability of Haematite Particles," *Colloid and Surfaces*, **5**, 85

Tipping, E., (1981), "The Adsorption of Aquatic Humic Substances by Iron Oxides," *Georchim. Cosmochim. Acta*, **45**, 191

Tipping, E. and Ohnstad, M., (1984), "Colloid Stability of Iron Oxide Particles from a Freshwater Lake," *Nature*, **308**, 266

Ulrich, H., Stumm, W. and Ćosović B., (1988), "Adsorption of Alophatic Fatty Acids on Aquatic Interfaces. Comparison between Two Model Surfaces: The Mercury Electrode and δ-Al_2O_3 Colloids," *Environ. Sci. Technol.*, **22**, No.1, 37

Van der Hulst, H.C., (1981), *Light Scattering by Small Particles*, 2nd, ed., Dover Publications, New York

Verwey, E.J.W. and Overbeek, J.Th.G., (1948), *Theory of the Stability of Lyophobic Colloids*, Elsevier, Amsterdam

Visser, J., (1972), "On Hamaker Constants: A Comparison between Hamaker Constants and Lifshitz-van der Waals Constants," *Advan. Colloid Interface Sci.*, **3**, 331

Watillon, A. and Joseph-Petit, (1966), "Interactions between Spherical Particles of Monodisperse Polystyrene Latices," *discuss. Faraday Soc.*, **42**, 143

Wehrli, B. and Stumm, W., (1987), "Oxygenation of Vanadyl(IV); Effect of Coordinated Surface-Hydroxyl Groups and OH^-" *In press*,

Westall, J.C., Zachary, J.L., and Morel, F.M.M., (1976), MINEQL, a Computer Program for the Calculation of Chemical Equilibrium Composition from Aqueous Systems, *Technical Note, No.18*, Parsons Labs, MIT, Cambridge

Westall, J.C. and Hohl, H., (1980), "A Comparison of Electrostatic Models for the Oxide/Solution Interface," *Advan. Colloid Interface Sci.*, **12**, 265

Westall, J.C., (1982), FITEQL, a Computer Program for Determination of Chemical Equilibrium Constant from Experimental Data, *Report 82-01*, Oregon State University, Corvallis, OR

Wickramasinghe, N.C., (1973), *Light Scattering Functions for Small Particles*, John Wiley & Son, New York

Wiersema, P.H., Loeb, A.L. and Overbeek, J.Th.G., (1966), "Calculation of the Electrophoretic Mobility of a Spherical Colloid Particle," *J. Colloid Interface Sci.*, **22**, 78

Wiese, G.R. and Healy, T.W., (1975), "Coagulation and Electrokinetic Behavior of TiO_2 and Al_2O_3 Colloidal Dispersion," *J. Colloid Interface Sci.*, **51**, No.3, 427

Appendix A

A.0 Results of Coagulation Kinetics Experiments

Each experiment to measure the variation of total light extinction with time, such as that shown in Fig. 4.1, involves the measurement of many data points. In the tables in this appendix we do not give all these data values, but instead tabulate for each experiment the initial slope, $(dE_{tot}/dt)_0$, and the corresponding stability ratio, W_{exp}, derived using Eq. (4.2). The complete set of experimental points is stored on floppy diskettes, which are available upon request. The file number referred to in the tables identifies which diskette the complete data set is stored on. The mass concentration of hematite is given in mg/l in the column labeled "Conc.".

File #	Conc. (mg/l)	NaCl (M)	pH	$(dE_{tot}/dt)_0$	W_{exp}
231	84.60	0.018	2.83	1.090×10^{-5}	9626.0
232	84.60	0.051	2.83	1.360×10^{-4}	771.5
233	84.30	0.060	2.83	3.219×10^{-4}	323.6
234	82.90	0.060	3.96	2.968×10^{-3}	34.0
235	33.30	0.059	4.35	1.141×10^{-3}	14.3
237	33.70	0.060	11.32	1.049×10^{-2}	1.6
238	20.20	0.060	11.10	4.053×10^{-3}	1.5
239	6.80	0.020	10.46	3.582×10^{-4}	1.9
242	7.40	0.017	11.95	2.931×10^{-5}	27.4
243	7.40	0.015	11.95	1.311×10^{-5}	61.2
244	33.70	0.057	4.19	5.979×10^{-4}	27.9
245	33.50	0.060	4.19	7.242×10^{-4}	22.7
246	33.60	0.048	4.19	3.290×10^{-4}	50.3
247	33.30	0.084	4.19	1.274×10^{-3}	12.8
248	33.40	0.072	4.19	9.505×10^{-4}	17.2
281	24.11	0.060	6.77	3.775×10^{-3}	2.3
282	23.43	0.060	6.84	3.541×10^{-3}	2.3
2101	83.07	0.060	4.32	5.537×10^{-3}	18.3
2102	82.74	0.072	4.32	8.198×10^{-3}	12.2
2103	82.42	0.084	4.32	1.162×10^{-2}	8.6
2104	83.39	0.048	4.32	2.679×10^{-3}	38.0
2105	33.35	0.048	4.70	1.160×10^{-3}	14.1
2106	33.23	0.060	4.70	1.687×10^{-3}	9.6
2107	33.10	0.072	4.70	2.763×10^{-3}	5.8
2108	32.97	0.084	4.70	3.955×10^{-3}	4.0
2121	33.70	0.050	5.24	3.293×10^{-3}	5.1
331	36.00	0.050	5.05	2.729×10^{-3}	7.0
510	20.17	0.059	6.32	3.792×10^{-3}	1.6
640	16.99	0.002	6.40	4.227×10^{-5}	100.1
642	16.94	0.010	6.31	7.771×10^{-5}	54.1
643	16.86	0.024	6.28	1.166×10^{-4}	35.7
644	16.73	0.048	6.28	1.900×10^{-3}	2.2
657	6.57	0.140	4.70	5.121×10^{-4}	1.2
671	33.80	0.050	5.05	2.396×10^{-3}	7.0
683	33.90	0.042	4.70	8.711×10^{-4}	19.3
691	36.00	0.050	5.17	2.958×10^{-3}	6.4
6114	34.40	0.001	5.20	2.489×10^{-5}	697.0
6121	33.80	0.050	5.45	4.113×10^{-3}	4.1
732	6.85	0.013	10.47	4.586×10^{-5}	15.0
734	6.77	0.048	10.46	5.963×10^{-4}	1.1
778	11.47	0.050	5.02	2.308×10^{-4}	8.4

Table A.1: Stability of a hematite suspension as a function of pH.

File #	Conc.	NaCl (M)	$(dE_{tot}/dt)_0$	$k_a(1)$ cm^3/sec	$k_a(2)$ cm^3/sec	W_{exp}
683	33.90	0.042	8.711×10^{-4}	1.449×10^{-13}	4.017×10^{-15}	19.34
2105	33.35	0.048	1.160×10^{-3}	1.994×10^{-13}	5.528×10^{-15}	14.06
2106	33.23	0.060	1.687×10^{-3}	2.921×10^{-13}	8.097×10^{-15}	9.60
2107	33.10	0.072	2.763×10^{-3}	4.822×10^{-13}	1.337×10^{-14}	5.81
2108	32.97	0.084	3.955×10^{-3}	6.957×10^{-13}	1.928×10^{-14}	4.03
657	6.57	0.140	5.121×10^{-4}	2.268×10^{-12}	6.288×10^{-14}	1.24

Table A.2: Stability of a hematite suspension as a function of NaCl concentration. $k_a(1)$ and $k_a(2)$ are estimated coagulation rate constants derived from Eqs. (4.3) and (4.4). the pH is 4.7.

File #	Conc. (mg/l)	T (K)	$(dE_{tot}/dt)_0$	k_b cm^3/sec
385	9.84	308	6.984×10^{-4}	7.878×10^{-12}
386	9.27	298	4.909×10^{-4}	6.158×10^{-12}
387	9.51	288	3.767×10^{-4}	4.653×10^{-12}
391	9.24	308	5.507×10^{-4}	7.878×10^{-12}
392	9.24	298	4.928×10^{-4}	6.158×10^{-12}
393	9.24	293	4.565×10^{-4}	5.380×10^{-12}
394	9.24	288	3.913×10^{-4}	4.653×10^{-12}
397	9.24	281	3.043×10^{-4}	3.730×10^{-12}

File #	$(dE/dt)_0$	$k_a(1)$ cm^3/sec	1/T(K)	W
385	7.213×10^{-6}	1.379×10^{-12}	0.00325	5.71
386	5.713×10^{-6}	1.092×10^{-12}	0.00336	5.64
387	4.165×10^{-6}	7.964×10^{-13}	0.00347	5.84
391	6.450×10^{-6}	1.233×10^{-12}	0.00325	6.39
392	5.772×10^{-6}	1.104×10^{-12}	0.00336	5.58
393	5.347×10^{-6}	1.022×10^{-12}	0.00341	5.26
394	4.583×10^{-6}	8.763×10^{-13}	0.00347	5.31
397	3.564×10^{-6}	6.815×10^{-13}	0.00356	5.47

Table A.3: Stability of a hematite suspension as a function of temperature. The pH is 5.56$\pm$0.01, and the background ionic strength is 0.05M of NaCl.

File #	Conc. (mg/l)	Sulfate (M)	$(dE_{tot}/dt)_0$	W_{exp}
4126	20.19	2.400×10^{-4}	6.599×10^{-4}	9.1
4127	20.27	1.200×10^{-4}	4.685×10^{-5}	128.6
4128	20.11	3.600×10^{-4}	2.379×10^{-3}	2.5
4129	20.03	4.700×10^{-4}	3.812×10^{-3}	1.5
4130	19.95	5.900×10^{-4}	3.924×10^{-3}	1.5
4131	20.31	6.000×10^{-4}	3.973×10^{-3}	1.5
4132	20.27	1.200×10^{-3}	4.329×10^{-3}	1.4
4133	19.95	5.900×10^{-3}	4.191×10^{-3}	1.4
503	20.31	3.600×10^{-4}	2.544×10^{-3}	2.4
505	20.15	5.900×10^{-4}	3.450×10^{-3}	1.7
506	20.15	5.900×10^{-3}	3.783×10^{-3}	1.6
507	19.76	1.150×10^{-2}	3.439×10^{-3}	1.7
508	20.39	2.400×10^{-3}	3.653×10^{-3}	1.7
509	20.47	1.200×10^{-3}	3.396×10^{-3}	1.8
580	17.13	1.200×10^{-4}	3.880×10^{-5}	110.9
582	17.03	3.000×10^{-4}	6.871×10^{-4}	6.2

File #	Conc. (mg/l)	Calcium (M)	$(dE_{tot}/dt)_0$	W_{exp}
602	6.81	1.000×10^{-4}	3.200×10^{-6}	212.5
605	6.69	2.700×10^{-3}	6.128×10^{-4}	1.1
606	6.61	4.000×10^{-3}	6.448×10^{-4}	1.0
711	6.75	2.000×10^{-3}	6.013×10^{-4}	1.1
712	6.87	2.000×10^{-4}	9.027×10^{-6}	76.7
713	6.85	3.900×10^{-4}	1.390×10^{-4}	4.9
714	6.87	2.000×10^{-4}	1.097×10^{-5}	63.1
715	6.82	7.900×10^{-4}	5.761×10^{-4}	1.2
716	6.85	3.900×10^{-4}	1.186×10^{-4}	5.8
718	6.87	2.000×10^{-4}	8.650×10^{-6}	80.0
719	6.85	3.900×10^{-4}	1.158×10^{-4}	5.9
720	6.83	7.900×10^{-4}	4.819×10^{-4}	1.4
721	6.74	1.900×10^{-3}	5.777×10^{-4}	1.2

File #	Conc. (mg/l)	Magnesium (M)	$(dE_{tot}/dt)_0$	W_{exp}
722	6.85	2.000×10^{-4}	6.505×10^{-5}	10.6
725	6.85	3.900×10^{-4}	4.283×10^{-4}	1.6
726	6.82	7.800×10^{-4}	6.286×10^{-4}	1.1
727	6.87	2.000×10^{-4}	6.350×10^{-5}	10.9
728	6.85	3.900×10^{-4}	4.897×10^{-4}	1.4
729	6.82	7.800×10^{-4}	6.360×10^{-4}	1.1

Table A.4: Stability of a hematite suspension in the presence of bivalent ions (sulfate, calcium, and magnesium). In all three cases the background ionic strength is 1mM of NaCl. The pH values are as follows. Sulfate pH=6.57±0.03; calcium pH=10.50±0.04; magnesium pH=10.61±0.08.

File #	Conc. (mg/l)	Phosphate (M)	$(dE_{tot}/dt)_0$	W_{exp}
439	20.00	3.100×10^{-4}	9.135×10^{-6}	641.9
441	20.24	1.960×10^{-3}	2.238×10^{-3}	2.7
442	20.40	1.200×10^{-3}	2.302×10^{-4}	26.5
443	20.31	1.600×10^{-3}	8.529×10^{-4}	7.1
444	20.15	2.300×10^{-3}	3.474×10^{-3}	1.7
445	20.00	2.700×10^{-3}	4.054×10^{-3}	1.4

File #	Conc. (mg/l)	Phosphate (M)	$(dE_{tot}/dt)_0$	W_{exp}
476	20.55	4.000×10^{-5}	1.891×10^{-4}	32.7
477	20.47	8.000×10^{-5}	8.518×10^{-4}	7.2
478	20.39	1.200×10^{-4}	1.758×10^{-3}	3.5
479	20.31	1.600×10^{-4}	2.162×10^{-3}	2.8
480	20.23	2.000×10^{-4}	2.754×10^{-3}	2.2
484	20.55	4.000×10^{-4}	3.109×10^{-3}	2.0
485	20.47	7.900×10^{-4}	4.154×10^{-3}	1.5
487	20.20	2.000×10^{-3}	3.320×10^{-3}	1.8

File #	Conc. (mg/l)	Phosphate (M)	$(dE_{tot}/dt)_0$	W_{exp}
421	20.31	1.200×10^{-6}	3.300×10^{-5}	183.2
423	20.15	2.000×10^{-6}	9.880×10^{-5}	60.3
424	20.47	4.000×10^{-6}	1.004×10^{-3}	6.1
425	20.39	8.000×10^{-6}	2.847×10^{-3}	2.1
426	20.23	1.600×10^{-5}	3.803×10^{-3}	1.6
428	20.15	2.000×10^{-5}	3.889×10^{-3}	1.5
472	20.20	4.000×10^{-5}	1.969×10^{-3}	3.0
473	20.00	1.600×10^{-4}	9.604×10^{-5}	61.1
474	19.90	2.000×10^{-4}	6.949×10^{-5}	83.5

File #	Conc. (mg/l)	Phosphate (M)	$(dE_{tot}/dt)_0$	W_{exp}
461	20.30	2.000×10^{-6}	2.122×10^{-3}	2.8
462	20.26	4.000×10^{-6}	2.773×10^{-3}	2.2
464	20.10	1.200×10^{-5}	7.884×10^{-6}	751.2
465	20.02	1.600×10^{-5}	1.566×10^{-6}	3752.0
466	20.30	2.000×10^{-6}	2.004×10^{-3}	3.0
467	20.26	4.000×10^{-7}	1.152×10^{-4}	52.2
468	20.18	8.000×10^{-7}	5.514×10^{-4}	10.8
469	20.10	1.200×10^{-6}	1.667×10^{-3}	3.6
470	20.02	1.600×10^{-6}	2.056×10^{-3}	2.9

Table A.5: Stability of a hematite suspension as a function of phosphate concentration. In all cases the background ionic strength is 1mM of NaCl. The pH values starting with the top table and working downwards are 3.44, 5.15, 6.55, and 6.97.

File #	Conc. (mg/l)	NaCl (M)	$(dE_{tot}/dt)_0$	W_{exp}
4101	20.23	6.000×10^{-2}	5.373×10^{-3}	1.1
4102	20.31	4.900×10^{-2}	5.046×10^{-3}	1.2
4103	20.39	3.700×10^{-2}	4.649×10^{-3}	1.3
4104	20.47	2.500×10^{-2}	2.472×10^{-3}	2.5
4105	20.51	1.900×10^{-2}	6.640×10^{-4}	9.3
4106	20.55	1.300×10^{-2}	5.275×10^{-5}	117.4

File #	Conc. (mg/l)	NaCl (M)	$(dE_{tot}/dt)_0$	W_{exp}
4107	20.11	4.900×10^{-2}	4.969×10^{-3}	1.2
4108	20.19	3.700×10^{-2}	3.995×10^{-3}	1.5
4109	20.27	2.500×10^{-2}	2.098×10^{-3}	2.9
4110	20.31	1.900×10^{-2}	5.993×10^{-4}	10.1
4111	20.35	1.300×10^{-2}	8.461×10^{-5}	71.8

File #	Conc. (mg/l)	NaCl (M)	$(dE_{tot}/dt)_0$	W_{exp}
496	20.55	1.400×10^{-2}	1.100×10^{-5}	562.8
497	20.47	2.600×10^{-2}	1.211×10^{-3}	5.1
498	20.39	3.800×10^{-2}	3.765×10^{-3}	1.6
499	20.31	4.900×10^{-2}	5.205×10^{-3}	1.2
4100	20.51	2.000×10^{-2}	3.343×10^{-4}	18.5

File #	Conc. (mg/l)	NaCl (M)	$(dE_{tot}/dt)_0$	W_{exp}
492	20.23	6.100×10^{-2}	4.601×10^{-3}	1.3
493	20.39	3.800×10^{-2}	9.715×10^{-4}	6.3
494	20.31	4.900×10^{-2}	4.226×10^{-3}	1.4
495	20.47	2.600×10^{-2}	1.880×10^{-4}	32.7

Table A.6: Stability of a hematite suspension as a function of ionic strength in the presence of phosphate. In all cases the phosphate concentration is 5.0×10^{-4}M. The pH values starting with the top table, are 7.24, 7.85, 9.11, and 10.45.

File #	Conc. (mg/l)	Phthalate (M)	$(dE_{tot}/dt)_0$	W_{exp}
587	17.19	8.000×10^{-6}	2.856×10^{-4}	15.2
588	17.18	1.600×10^{-5}	5.236×10^{-4}	8.3
589	17.16	4.000×10^{-5}	8.894×10^{-4}	4.9
590	16.86	1.800×10^{-6}	3.306×10^{-5}	126.1
591	17.13	8.000×10^{-5}	1.248×10^{-3}	3.4
592	16.54	3.600×10^{-6}	7.510×10^{-5}	53.4
593	17.06	1.600×10^{-4}	2.769×10^{-3}	1.5
594	17.00	2.400×10^{-4}	2.437×10^{-3}	1.7
595	16.93	3.200×10^{-4}	2.872×10^{-3}	1.5
596	16.86	4.000×10^{-4}	2.579×10^{-3}	1.6
597	16.80	4.800×10^{-4}	2.367×10^{-3}	1.7
598	16.67	6.400×10^{-4}	2.161×10^{-3}	1.9
599	16.41	9.600×10^{-4}	1.528×10^{-3}	2.6

File #	Conc. (mg/l)	pH	$(dE_{tot}/dt)_0$	W_{exp}
735	17.10	4.21	9.861×10^{-4}	43.5
736	17.07	4.73	2.817×10^{-3}	15.2
737	17.00	6.00	2.093×10^{-2}	2.0
738	17.00	6.55	2.211×10^{-2}	1.9
739	16.90	7.10	2.299×10^{-2}	1.8
740	16.90	10.45	1.567×10^{-4}	267.2
741	16.00	9.28	1.227×10^{-3}	30.6

File #	Conc. (mg/l)	Oxalate(M)	$(dE_{tot}/dt)_0$	W_{exp}
662	17.19	1.500×10^{-5}	2.299×10^{-4}	18.8
663	17.19	3.000×10^{-5}	7.742×10^{-4}	5.6
664	17.17	6.100×10^{-5}	1.303×10^{-3}	3.3
665	17.14	1.200×10^{-4}	1.562×10^{-3}	2.8
666	17.09	2.400×10^{-4}	2.205×10^{-3}	1.9
667	16.98	4.800×10^{-4}	2.218×10^{-3}	1.9
668	16.86	7.500×10^{-4}	2.124×10^{-3}	2.0
669	16.93	3.100×10^{-3}	2.225×10^{-3}	1.9
670	17.06	1.600×10^{-3}	2.032×10^{-3}	2.1

Table A.7: Stability of a hematite suspension as a function of:

(1) phthalate concentration at pH 6.18±0.06 and background ionic strength 1mM of NaCl (upper table),

(2) pH at constant phthalate concentration of 1×10^{-4}M and background ionic strength 5mM (middle table),

(3) oxalate concentration at pH 6.23±0.03 and background ionic strength 1mM (lower table).

File #	Conc. (mg/l)	PAA (g/l)	$(dE_{tot}/dt)_0$	W_{exp}
541	17.20	2.400×10^{-6}	8.123×10^{-5}	53.4
542	17.19	4.800×10^{-6}	5.858×10^{-4}	7.4
543	17.18	9.700×10^{-6}	1.323×10^{-3}	3.3
544	17.17	1.450×10^{-5}	2.494×10^{-3}	1.7
545	17.17	1.940×10^{-5}	2.852×10^{-3}	1.5
546	17.16	2.420×10^{-5}	2.429×10^{-4}	17.8
547	17.15	2.900×10^{-5}	1.670×10^{-5}	258.2

File #	Conc. (mg/l)	HA (m/l)	$(dE_{tot}/dt)_0$	W_{exp}
560	16.99	2.440×10^{-5}	4.656×10^{-4}	9.1
561	16.99	4.880×10^{-5}	1.645×10^{-3}	2.6
562	16.97	9.760×10^{-5}	1.870×10^{-3}	2.3
563	16.93	2.440×10^{-4}	3.640×10^{-6}	1154.0
564	17.00	1.220×10^{-5}	7.978×10^{-5}	53.1
565	16.95	1.464×10^{-4}	2.262×10^{-5}	186.2
566	16.96	1.220×10^{-4}	6.077×10^{-4}	6.9

File #	Conc. (mg/l)	FA (g/l)	$(dE_{tot}/dt)_0$	W_{exp}
570	16.99	3.560×10^{-5}	9.513×10^{-5}	44.5
571	16.99	7.120×10^{-5}	1.406×10^{-3}	3.0
572	16.98	1.070×10^{-4}	1.964×10^{-3}	2.2
573	16.97	1.420×10^{-4}	1.389×10^{-3}	3.0
575	16.96	1.780×10^{-4}	5.817×10^{-5}	72.5
576	16.95	2.140×10^{-4}	5.295×10^{-6}	795.4

Table A.8: Stability of a hematite suspension as a function of polyelectrolyte concentration. In all cases the background ionic strength is 1mM of NaCl. The upper table is for polyaspartic acid (PAA, molecular weight ~15000), and the pH is 6.80±0.01. The middle table is for humic acid (HA), and the pH is 6.86±0.03. The bottom table is for fulvic acid (FA), and the pH is 6.54±0.04.

File #	Conc. (mg/l)	Sodium (M)	$(dE_{tot}/dt)_0$	W_{exp}
627	17.14	1.000×10^{-2}	9.390×10^{-6}	458.7
628	17.06	2.400×10^{-2}	1.895×10^{-4}	22.5
629	16.86	5.900×10^{-2}	1.651×10^{-3}	2.5
630	16.67	9.300×10^{-2}	2.131×10^{-3}	1.9

File #	Conc. (mg/l)	Calcium (M)	$(dE_{tot}/dt)_0$	W_{exp}
631	17.13	4.000×10^{-4}	8.790×10^{-6}	489.4
632	17.06	8.000×10^{-4}	2.100×10^{-5}	203.2
633	16.93	1.600×10^{-3}	1.479×10^{-4}	28.4
634	16.80	2.300×10^{-3}	7.113×10^{-4}	5.8
635	16.67	3.100×10^{-3}	1.718×10^{-3}	2.4
637	16.53	3.800×10^{-3}	2.300×10^{-3}	1.7

File #	Conc. (mg/l)	Art. SW (M)	$(dE_{tot}/dt)_0$	W_{exp}
636	16.86	1.400×10^{-2}	1.559×10^{-5}	267.3
638	16.76	1.800×10^{-2}	6.080×10^{-5}	67.7

File #	Conc. (mg/l)	pH	$(dE_{tot}/dt)_0$	W_{exp}
743	17.10	4.05	2.226×10^{-4}	19.3
744	17.10	6.15	1.587×10^{-3}	2.7
745	17.10	4.80	6.356×10^{-4}	6.7
746	17.10	5.01	7.302×10^{-4}	5.9
747	17.00	5.84	1.842×10^{-3}	2.3
748	17.00	9.95	5.363×10^{-6}	790.0
749	17.00	9.22	4.041×10^{-5}	104.8
750	17.00	7.90	8.375×10^{-4}	5.1

Table A.9: Stability of a hematite suspension in the presence of polyelectrolytes. The experiments represented in the upper three tables were all performed in the presence of 3.0×10^{-4} g/l of Suwannee river humic acid. The pH values for these three tables are (from top to bottom) 6.25±0.03, 6.35±0.08, and 6.95. The experiment reported in the bottom table was performed in the presence of 1.0×10^{-4} g/l of fulvic acid. The background ionic strength is 5mM of NaCl.

File #	Conc. (mg/l)	C3 (M)	$(dE_{tot}/dt)_0$	W_{exp}
790	11.47	1.000×10^{-3}	5.255×10^{-4}	3.7
791	11.47	2.000×10^{-3}	6.795×10^{-4}	2.8
792	11.47	4.000×10^{-3}	9.838×10^{-4}	2.0
793	11.47	8.000×10^{-3}	1.134×10^{-3}	1.7
794	11.47	1.600×10^{-2}	1.243×10^{-3}	1.6
795	11.47	3.200×10^{-2}	1.375×10^{-3}	1.4
796	11.01	5.500×10^{-2}	1.337×10^{-3}	1.3

File #	Conc. (mg/l)	C8 (M)	$(dE_{tot}/dt)_0$	W_{exp}
6111	33.40	4.700×10^{-6}	1.812×10^{-3}	9.0
6112	33.50	1.000×10^{-5}	1.956×10^{-3}	8.4
780	11.47	1.000×10^{-4}	3.000×10^{-4}	6.4
781	11.47	2.000×10^{-4}	4.749×10^{-4}	4.1
782	11.47	4.000×10^{-4}	8.343×10^{-4}	2.3
783	11.47	8.000×10^{-4}	1.469×10^{-3}	1.3
784	11.47	1.600×10^{-3}	1.264×10^{-3}	1.5
785	11.47	3.200×10^{-3}	9.663×10^{-4}	2.0

File #	Conc. (mg/l)	C10 (M)	$(dE_{tot}/dt)_0$	W_{exp}
771	11.28	4.900×10^{-4}	6.266×10^{-5}	29.8
772	11.47	3.000×10^{-4}	3.565×10^{-4}	5.4
773	11.47	1.500×10^{-4}	8.831×10^{-4}	2.2
774	11.47	1.000×10^{-4}	1.327×10^{-3}	1.5
775	11.07	8.000×10^{-5}	8.496×10^{-4}	2.1
776	11.47	5.000×10^{-5}	6.384×10^{-4}	3.0
779	11.07	1.000×10^{-5}	1.900×10^{-4}	9.5

File #	Conc. (mg/l)	C12 (M)	$(dE_{tot}/dt)_0$	W_{exp}
688	35.80	1.100×10^{-6}	2.768×10^{-3}	6.8
689	35.60	2.300×10^{-6}	4.130×10^{-3}	4.5
690	35.20	4.600×10^{-6}	6.269×10^{-3}	2.9
6102	33.80	1.000×10^{-7}	1.759×10^{-3}	9.5
6104	33.70	5.100×10^{-7}	1.723×10^{-3}	9.7
6106	33.50	1.900×10^{-6}	3.198×10^{-3}	5.1
6107	33.00	5.000×10^{-6}	5.950×10^{-3}	2.7
6108	32.10	9.700×10^{-6}	6.347×10^{-3}	2.4
6115	33.90	1.000×10^{-4}	2.603×10^{-4}	64.7
6116	33.90	4.900×10^{-5}	9.331×10^{-4}	18.1
6118	33.80	2.000×10^{-5}	5.708×10^{-3}	2.9

Table A.10: Stability of a hematite suspension as a function of fatty acid concentration. In all cases the background ionic strength is 0.05M of NaCl. The upper table is for propionic acid (C_3), and the pH is 5.01. The second table is for caprylic acid (C_8), and the pH is 5.17±0.08. The third table is for capric acid (C_{10}), and the pH is 5.15±0.03. The bottom table is for lauric acid (C_{12}), and the pH is 5.18±0.03.

Appendix B

B.0 Derivation of ζ-Potential

To convert mobility to ζ-potential, a plot of reduced ζ-potential, $\tilde{\zeta}$, as a function of reduced mobility, E, at various κa values is often utilized. These quantities are defined as,

$$E = \frac{3\mu}{2\epsilon\epsilon_0}\frac{F}{RT}u \tag{B.1}$$

$$\tilde{\zeta}(E) = \frac{F\zeta}{RT} \tag{B.2}$$

At $25°C$, in aqueous media, the constants can be reduced and the corresponding expressions are,

$$E = 0.739u \tag{B.3}$$

$$\zeta = 25.49\tilde{\zeta}(E) \tag{B.4}$$

where u is in $\mu\text{m} \cdot \text{sec}^{-1}/\text{Volt} \cdot \text{cm}^{-1}$, and ζ is in mV. When $\kappa a \rightarrow 0$, $\tilde{\zeta} \rightarrow E$ and Hückel's equation is obtained. As $\kappa a \rightarrow \infty$, $\tilde{\zeta} \rightarrow 2E/3$, which is known as Smoluchowski's equation for electrophoretic mobility. As a result of this, $\zeta = 18.83u$ when Hückel's equation applies, and $\zeta = 12.56u$ when Smoluchowski's equation applies. For intermediate values of κa, the relationship of $\tilde{\zeta}$ and E is obtained from a computer solution to the problem provided by Wiersema et al. (1966).

For particles of diameter 70nm suspended in ionic strength of 0.05M (Fig. 4.18), κa can be calculated to be 28. Applying Eqs. (B.3), (B.4) and solutions of Wiersema

et al. (Fig .(3.19) of Hunter, 1981), ζ as a function of u can be found, as shown in Table B.1. Following this procedure, the pH dependent mobility, u, can be converted to ζ-potential as a function of pH.

u	E	$\tilde{\zeta}(E)$	ζ
4.0	2.96	2.20	56.1
3.5	2.58	1.95	49.7
3.0	2.22	1.70	43.3
2.5	1.85	1.35	34.4
2.0	1.48	1.10	28.0
1.5	1.11	0.85	21.7
1.0	0.73	0.55	14.0

Table B-1: The derivation of ζ-potential from mobility. The first column gives the mobility, u, in units of $\mu\text{m} \cdot \text{sec}^{-1}/\text{Volt} \cdot \text{cm}^{-1}$. The reduced mobility, E, determined by Eq. (B.3) is given in the second column. The reduced ζ-potential is given in the third column. In the fourth column the ζ-potential is given in mV.